UNIVERSITY OF LATVIA

Faculty of Biology

Vitālijs Borisovs

DOCTORAL THESIS

GENETIC BACKGROUND OF DNA DAMAGE IN MULTIPLE SCLEROSIS AND FREE RADICAL PRODUCTION IN MULTIPLE SCLEROSIS AND TYPE I DIABETES MELLITUS PATIENTS

Promotion to the degree of Doctor of Biology

Molecular Biology

Supervisor: Dr. habil. Biol., Prof. Nikolajs Sjakste

Riga, 2023

The doctoral thesis was carried out in the University of Latvia, at the Faculty of Medicine, Department of Biochemistry from 2017 to 2022.

The research was supported by ERDF grant 1.1.1.1/16/A/016

Form of the thesis: dissertation in biology, subfield – molecular biology.

Supervisor: Dr. habil. Biol., Prof. Nikolajs Sjakste

Reviewers:

1) Dr.med. Šimons Svirskis, Riga Stradins University
2) Dr.biol. Una Riekstiņa, University of Latvia
3) PhD Lada Živkovič, University of Belgrad

The thesis will be defended at the public session of the Doctoral Committee of Biology, University of Latvia at 13:00 (EET), on June 30th, 2023 at the University of Latvia Academic Centre, Jelgavas Str. 1.

The thesis is available at the University of Latvia, Kalpaka blvd. 4.

This thesis is accepted for the commencement of the degree of Doctor of Biology on March 9th, 2023 by the Doctoral Committee of Biology, University of Latvia.

Chairman of the Doctoral Committee _____/*vārds, uzvārds*/
(paraksts)

Secretary of the Doctoral Committee _____/*vārds, uzvārds*/
(paraksts)

ABSTRACT

Multiple sclerosis (MS) and type 1 diabetes (T1D) are both chronic autoimmune diseases. The progression of both diseases shares a common autoimmune nature, but the targeted organs are different. In case of MS autoimmunity directly affects neuronal myelin sheath, gradually diminishing signal transduction into the brain, thus limiting even basic abilities of the patient. In T1D pancreatic cells are targeted, resulting in insulin deficiency and inability to metabolize glucose. Some studies indicate that MS patients have increased chances to develop T1D, thus both diseases might have some common mechanisms. With T1D affecting more people worldwide than MS, it is a relatively well-studied disease when the two are compared. MS on the other hand still have a lot of uncertainties in pathophysiology. MS can be diagnosed by MRI scans of the brain or spinal cord, and interferon-based therapies can be applied to successfully slower the progression. However, MS is only diagnosed when symptoms of different severity occur and there is currently no practical way of identifying MS in its early stages.

The main objective of this study was to test different biochemical and genetical biomarkers and evaluate their association with MS. Whole blood of MS and T1D patients was collected, lymphocytes were isolated, DNA was extracted and a set of biochemical and genetical tests were performed. Significant increase in DNA damage was observed for T1D and MS patients, but levels of nitric oxide metabolites (NOx) were elevated in MS patients, and lower in T1D patients when compared to the healthy subjects. MDA level evaluation showed a significant decrease in the MS study group, which also showed association with NOx level, but no associations with disease modifying therapies (DMTs). Genotyping was performed for the most potent SNPs in DNA repair genes (ATM, PARP1, XPC, XPA and XRCC1). SNPs for potential MS candidate genes (ADAR, GRIA3, ZFAT, CIT, IFNAR2, STARD13, ZFHX4) together with NOS1 and NOS2 SNPs were additionally analyzed by NGS. Statistically significant results were observed for PARP1 and XRCC1 associations with NOx and MDA levels of MS patients. NOS1 SNPs linkage disequilibrium analysis has also shown a promising statistical significance. Additionally, low coverage copy number variation analysis was performed and an insight for future perspective was noted.

KOPSAVILKUMS

Multiplā skleroze (MS) un 1. tipa diabēts (1TD) ir hroniskas autoimūnas slimības. Abu slimību progresēšanai ir kopīgs autoimūns raksturs, bet mērķa orgāni ir atšķirīgi. MS gadījumā autoimunitāte tieši ietekmē neironu mielīna apvalku, pakāpeniski samazinot signāla pārraidi smadzenēs, tādējādi ierobežojot pacienta pamatspējas. 1TD gadījumā tiek mērķētas aizkuņģa dziedzera šūnas, kā rezultātā rodas insulīna deficīts un nespēja metabolizēt glikozi. Daži pētījumi liecina, ka MS pacientiem ir augstāka iespēja attīstīt 1TD, tāpēc abām slimībām var būt daži kopīgi mehānismi. Tā kā 1TD skar vairāk cilvēku visā pasaulē nekā MS, tā ir salīdzinoši labi pētīta slimība, ja salīdzina abas. No otras puses, MS joprojām ir daudz neskaidrību patofizioloģijā. MS var diagnosticēt ar galvas smadzeņu vai muguras smadzeņu MRI skenēšanu, un, lai veiksmīgi palēninātu progresēšanu, var izmantot uz interferonu balstītas terapijas. Tomēr MS tiek diagnosticēta tikai tad, ja parādās dažāda smaguma simptomi, un pašlaik nav praktiskas metodes kā identificēt MS tās agrīnajā stadijā.

Šī pētījuma galvenais mērķis bija pārbaudīt vairākus bioķīmiskos un ģenētiskos biomarķierus to pielietošanai agrīnai diagnostikai. MS un 1TD slimniekiem tika savāktas asinis, izolēti limfocīti, ekstrahēta DNS un veikti bioķīmiskie un ģenētiskie testi. Pētījuma grupā (MS un 1TD pacienti), salīdzinot ar veseliem cilvēkiem, tika novērots ievērojams DNS bojājumu un NO līmeņa pieaugums MS gadījumā, savukārt 1TD pacientiem NO līmeni bija pazemināti. Malondialdehīda (MDA) līmeņa novērtējums uzrādīja būtisku samazinājumu pētījuma grupā, kas varētu būt saistīts ar slimību modificējošu terapiju (DMT) ietekmi. Genotipēšana tika veikta svarīgākajiem viena nukleotīda polimorfismiem (SNP) DNS reparācijas gēnos (ATM, PARP1, XPC, XPA un XRCC1). Rezultātus apstiprināja ar nākamas paaudzes sekvencēšanu (NGS) ar 100% rezultātu atbilstību. Ar NGS analizēja arī SNP potenciālajos MS kandidātgēnos (ADAR, GRIA3, ZFAT, CIT, IFNAR2, STARD13, ZFHX4), kā arī SNP NOS1 un NOS2 gēnos. Statistiski nozīmīgi rezultāti tika novēroti PARP1 un XRCC1 asociācijām ar MS pacientu NOx un MDA līmeniem. NOS1 SNP saiknes nelīdzsvarotības analīze arī parādījusi daudzsološu statistisko nozīmīgumu. Turklāt tika veikta zema pārklājuma kopiju skaita variāciju (CNV) analīze un dots ieskats nākotnes perspektīvā.

TABLE OF CONTENTS

ABBREVIATIONS

4-HNE – 4-hydroxynonenal
AA – Arachidonic acid
AD – Alzheimer's disease
ADAR – adenosine deaminase, RNA-specific
ADP – Adenosine diphosphate
ANOVA –Analysis of variance
AO – Aldehyde oxidase
APC – Antigen presenting cell
ATM – Ataxia-telangiectasia mutated
ATR – ataxia-telangiectasia and Rad3-related
BBB – Blood-brain barrier
BER – Base excision repair
BIR – break-induced repair
CD4 – Cluster of differentiation 4
CIT – citron Rho-interacting serine/threonine kinase
Chr - Chromosome
CNS – Central nervous system
CNV – Copy number variation
DDR – DNA damage response
DMSO – Dimethyl sulfoxide
DMT – Disease modifying therapy
DNA – Deoxyribonucleic acid
DNB – DNA nano ball
dNTP – Deoxynucleoside triphosphate
DSB – Double strand break
dsDNA – Double strand DNA
EDTA – Ethylenediaminetetraacetic acid
EDSS – Expanded Disability Status Scale
EndoIII – Endonuclease III
EPR – Electron paramagnetic resonance
ERAT – End Repair and A-tailing
EtOH – Ethanol
FG - Fingolimod
Fpg – Formidopyrimidine [Fapy] DNA glycosylase
GA - galatiramer acetate
gDNA – Genetic DNA
GG-NER – Global genome NER
GRIA3 – glutamate receptor, ionotropic, *AMPA 3*
GTP – Guanosine triphosphate
H2AX – H2A histone family member X
HHT – 12-l-hydroxy-5,8,10-heptadecatrienoic acid
HMGN15 – non-histone protein HMG14
HR – Homologous recombination
HWE – Heidy-Weinberg equilibrium
IDLs – insertion-deletion loops
IFN – Interferon
IFNAR2 – interferon (α, β and ω) receptor 2
IQR – Interquartile range
LD – Linkage Disequilibrium
M1G – Pyrimidopurin-10(3H-)one
MDA – Malondialdehyde
MG – Methylglyoxal

MMR – Mismatch repair
MRI – Magnetic resonance imaging
MS – Multiple Sclerosis
NAD+ – Nicotinamide adenine dinucleotide
NGS – Next generation sequencing
NER – Nucleotide excision repair
NF – Nuclease free
NO – Nitric oxide
NOS – Nitric oxide synthase
OGG1 – 8-Oxoguanine DNA glycosylase
PARP1 – Poly [ADP-ribose] polymerase 1
PBMC – Peripheral blood mononuclear cell
PCR – Polymerase chain reaction
PD – Parkinson's disease
PE – Pair-End
PPMS – primary progressive MS
PRMS – progressive-relapsing MS
PUFA – Polyunsaturated fatty acid
RAD23B – UV excision repair protein Radiation sensitive 23 homolog B
RCA – Rolling circle amplification
RNA – Ribonucleic acid
ROS – Reactive oxygen species
RRMS – Relapse remitting Multiple Sclerosis
SDSA – Synthesis-dependent strand annealing
SEM – Standard error of the mean
SIRT6 – Sirtuin 6
SNP – Single nucleotide polymorphism
SPMS – Secondary progressive Multiple Sclerosis
SSB – Single strand break
ssDNA – Single strand DNA
START – StAR-related lipid transfer
STARD13 – StAR related lipid transfer domain containing 13
TACE – TNF-alpha converting enzymes
TBA – Thiobarbituric acid
TBARS – Thiobarbituric acid reacting substances
TF – Teriflunomide
TFIIH – Transcription factor II H
TLS – Translesion
TXA_2 – Thromboxane A_2
USP7 – Ubiquitin-specific protein 7
UV–DDB – Ultraviolet-damaged DNA damage-binding protein
UVSSA – UV-stimulated scaffold protein A
XAB2 – XPA-binding protein 1
XPC – Xeroderma Pigmentosum, complementation group C
XRCC1 – X-ray repair cross-complementing protein 1
ZFAT – Zinc finger and AT hook domain containing
ZFHX4 – Zinc finger homeobox 4

INTRODUCTION

Multiple sclerosis (MS) and type 1 diabetes (T1D) are the most frequent diseases from the autoimmune demyelinating and metabolic groups. Statistically MS affects about 2 million people and T1D about 8 million people worldwide. Currently in Latvia about 2000 people are diagnosed with MS and about 5000 people with T1D.

The progression of MS involves different severity symptoms ranging from fatigue to pain, mobility problems and deprivation of cognitive abilities. Even though MS and T1D symptomatically are different, T1D and MS share common chronic and autoimmune nature. Current research indicates various possible reasons for MS, in particular oxidative stress which is also associated with T1D. Some studies assume that autoimmune response and demyelination may come from environmental factors (stress, ecology, nutrition, habits), with additional evidence that patients with MS and T1D are more susceptible to develop additional autoimmune disorders. According to previous studies MS has a certain genetic background whether it is a genetic predisposition or DNA damage. This study focuses on the genetic aspect of MS which is potentially a great starting point to investigate the relation between MS and T1D with respect to oxidative stress. T1D is a better studied disease, with well-described methods of diagnosis and treatment, if compared to MS. Currently known methods of MS diagnosis involve brain MRI scan or spinal cord punctures, but only after the first symptoms occur. It is then for interferon-based therapies to slow down the progression of MS and delay the MS transition into more severe phases.

Importance of this work: There is currently no means to identify MS in its early stages and the pathology is not fully understood. But it is of great importance to uncover which markers are associated with MS. Discovery of molecular and genetic markers associated with MS will allow to expand the understanding of the cause, and in a long-term perspective to delay the progression of the disease, or possibly even prevent it, if timed correctly, thus avoiding complications and increasing the expectancy of life. Similarities in biochemical markers between MS and T1D and genetical data of DNA repair genes in MS might give an insight into the relation between T1D and MS.

Aim of the study: To test different biochemical and genetical biomarkers for their association with autoimmunity with respect to MS and T1D.

Tasks to reach the aim:

1. To evaluate DNA damage in MS and T1D, and oxidized bases in whole blood and lymphocytes of MS patients and compare it to the healthy subjects
2. To evaluate levels of NO in plasma and serum of MS and T1D patients and compare it with the healthy subjects.
3. To evaluate levels of MDA in plasma and serum of MS patients.
4. Investigate the association between each biochemical marker
5. Investigate the association between biochemical markers and patient clinical descriptors
6. Identify possible SNPs in DNA repair genes ATM, PARP1, XPC, XPA, XRCC1 and evaluate their significance.
7. Investigate the association of SNPs with biochemical markers.
8. Evaluate possible CNV with low-coverage NGS, and identify other SNPs that might be relevant to the topic of this study with 30x coverage NGS.

1. LITERATURE REVIEW

1.1. Etiology of Multiple Sclerosis

Multiple Sclerosis (MS) is characterized as a chronic autoimmune neurodegenerative disorder that impacts the central nervous system (CNS). The precise cause of MS is still not clear, however possible mediating factors of MS development are widely described. One of the causes of MS is demyelination caused by the lymphocytes that penetrate blood-brain barrier (BBB) and initiate local inflammation. (Balasa et al., 2021; Tafti et al., 2022).

Women are about twice more susceptible to MS than men. The disease predominantly targets individuals between 20 and 40 years, and more than 2 million people are suffering from MS worldwide. (Coyle, 2021; Huang et al., 2017).

1.2. Mechanism of Multiple Sclerosis

Myelin is the main component of myelin sheath covering the body of nerve cells and supporting the signal transduction from one nerve cell to another (Mallucci et al., 2015). Reduced signal transduction leads to deterioration of nervous system and causes limitation to senso-motoric function of the organism. Depending on which neuron is damaged consequential symptoms will be different and range from impaired memory to general fatigue (Garg and Smith, 2015). Most common symptoms of demyelination (MS in particular) are weakness, painful muscle spasms, fatigue, neuralgia, depression, subtle cognitive difficulties, and seizures (Ghasemi et al., 2017; McGinley et al., 2021).

There is currently little knowledge about the cause of oligodendrocyte apoptosis during demyelination. Some researchers proposed that CD4+ T cells immune response that results in the interaction between APCs (antigen presenting cells) with T lymphocytes is one of the crucial steps in the development of MS (Gandhi et al., 2010; Kasper and Shoemaker, 2010). Upon pathogen binding to toll-like receptors on APCs, the production of interleukins IL-12, IL-23 and IL-4 is initiated. These cytokins induce CD4+T differentiation into three main phenotypes Th1, Th2, or Th17, which then mediate the release of interferon gamma IFNɣ and tumor necrosis factor alpha TNFα necessary for innate and adaptive immune response. The prevailing hypothesis suggests that this process is likely influenced by multiple factors, including the activity of CD4+ and CD8+ T-cells, B-cells, antibody production, the activation of microglia and macrophages, as well as the indirect

effects of proinflammatory cytokines such as interleukin-17, tumor necrosis factor alpha, and nitric oxide (Duffy et al., 2014).

1.3. Progression and evaluation of Multiple Sclerosis

70 to 80% of patients suffer from MS in a relapsing-remitting (RR) way. Relapses trigger new neurological problems or worsen preexisting conditions. In most cases, relapses last for more than 48 hours and develop over a few days or weeks. Remission and clinical stability are maintained between relapses, although residual symptoms may persist (Lane and Yadav, 2020; Tafti et al., 2022).

Within 10 to 15 years of MS onset, 50% of RRMS patients enter a progressive phase of the disease. MS symptoms steadily worsen during this progressive phase, referred to as secondary progressive MS (SPMS). Relapses may continue to occur in patients with SPMS for a long period of time or may be infrequent. Primary progressive MS (PPMS), which represents the third form of MS, is distinguished by a progressively worsening condition right from its onset. PPMS accounts for approximately 15 to 20% of all MS cases.. The fourth type of MS is known as progressive-relapsing (PR) MS: it occurs in 5% of patients and is characterized by gradual degeneration and superimposed relapses (Lane and Yadav, 2020; Tafti et al., 2022).

A clinical diagnosis of MS is still the only means of identifying it (Reich et al., 2018). There is no single test (such as a blood test, an MRI examination, or a CSF study) that is effective in diagnosing MS. Doctors make diagnoses based on patient histories, neurological examinations, and various tests, and then make decisions based on the data. Even though, MRI scanning alone is not enough to diagnose MS, recent advances in this technique have significantly improved the detection of demyelination areas in the brain and spinal cord. Thus, helping to exclude other diseases that might explain MS symptoms (Lane and Yadav, 2020).

1.4. Link between type 1 diabetes and multiple sclerosis

Type 1 diabetes (T1D) and MS both share common chronic and autoimmune nature (Pozzilli et al., 2022). Even though T1D and MS are considered autoimmune diseases specifically targeting different organs, both diseases, as expected, share etiologic and pathologic features (Handel et al., 2009). Studies indicate that patients with MS are more susceptible to developing T1D when compared to the general population (Pozzilli et al., 2022; Tettey et al., 2015). Currently, the co-occurrence of two diseases has not been studied and the mechanism remains unclear. While genetic predisposition is considered significant, the low concordance for MS and T1D in identical twins

and the rising incidence of both diseases suggest the contribution of environmental factors (Tettey et al., 2015).

Autoimmunity is usually described in terms of white blood cells, with T-cells, B-cells and macrophage as key components of immune response (Dong et al., 2016; Ingwersen et al., 2016; Ma et al., 2019; Zacca et al., 2021). Interestingly, erythrocytes might also play important role in pathogenesis of autoimmune diseases. White blood cells make up roughly 1% of total blood volume. The remaining circulatory components are plasma with about 55% of total volume and red blood cells (RBC) which account for about 45% of the total volume (Geiger et al., 2022). Despite the fact that RBC are prevalent in the blood stream, they are usually neglected as a part of immune response, due to the lack of nucleus or internal organelles. The lack of organelles is compensated by the variety of functionally active receptors and transporters in the membrane (Crisp et al., 2016). It also known that RBC participate in the release of key immune response molecules ATP and nitric oxide (NO). In fact, the reports have shown certain abnormalities in levels of these molecules when investigated in the scope of autoimmune diseases (Geiger et al., 2022).

1.5. Lipid peroxidation

Uncontrolled oxidative stress, the mismatch between prooxidants and antioxidants, can cause oxidative damage to cells, tissues, and organs. It is known that lipids are affected by radicals and reactive oxygen species (ROS). ROS production can arise through various mechanisms, involving enzymatic reactions and/or autooxidation of various substances like catecholamines and hydroquinone. Mitochondria, plasma membrane, endoplasmic reticulum, and peroxisomes serve as the primary sources of ROS (Janků et al., 2019; Y. Sun et al., 2020). It is important to note that the liver produces ROS as a response to numerous exogenous impacts, including ionizing radiation, ultraviolet rays, tobacco smoke, pathogen infections, chemicals in the environment, and herbicides/insecticides (Ayala et al., 2014).

Lipid peroxidation is a process that has three steps: initiation, propagation, and termination (Ali et al., 2022; Dodson et al., 2019; Gaschler and Stockwell, 2017). Prooxidants, like the hydroxyl radical, extract an allylic hydrogen atom, leading to the formation of a carbon-centered lipid radical (L•) during the initiation step of lipid peroxidation. In the propagation phase, lipid radicals (L•) are generated, which rapidly combine with oxygen to produce lipid peroxy radicals (LOO•). These radicals then abstract a hydrogen atom from another lipid molecule, resulting in

the formation of lipid hydroperoxide (LOOH). In the termination reaction, a vitamin E radical reacts with another LOO• radical, giving rise to nonradical products. Peroxidation of lipids will lead to a chain of reactions that will result in termination products. (Ali et al., 2022).

A range of products is generated through oxidative reactions involving unsaturated lipids or oxygen. The primary outcomes of lipid peroxidation are lipid hydroperoxides (LOOH). Extensively studied, numerous aldehydes, such as malondialdehyde (MDA), propanal, hexanal, and 4-hydroxynonenal (4-HNE), can be produced during lipid peroxidation. Among the products of lipid peroxidation, MDA is the most mutagenic, whereas 4-HNE is the most toxic (Ali et al., 2022; Saieva et al., 2016).

For many years, since lipid peroxidation of fatty acids can be readily detected using MDA in combination with thiobarbituric acid (TBA), MDA has been used as an inexpensive biomarker for lipid peroxidation (Ito et al., 2019; Mas-Bargues et al., 2021). Upon the reaction of TBA with MDA in the TBA test, a vividly colored chromogen fluorescent red adduct is formed. Originally devised by food chemists to evaluate the autooxidative breakdown of fats and oils, this method has gained prominence. In clinical settings, MDA is widely recognized as one of the most widely used and reliable indicators of oxidative stress, owing to its remarkable reactivity (Giera et al., 2012). Furthermore, its high precision and accuracy makes it a vital component of biomedical research.

The production of arachidonic acid and other polyunsaturated fatty acids (PUFAs) is a significant aspect of MDA generation, occurring through enzymatic or nonenzymatic processes (as depicted in Figure 1). While the enzymatic production of MDA is widely acknowledged, its biological functions and potential dual roles have not been thoroughly investigated. Despite its chemical stability, membrane-permeability (in comparison to ROS), and lower toxicity compared to 4-HNE and methylglyoxal (MG), the precise implications of MDA remain to be explored (Tsikas, 2017). However, there is still limited understanding regarding the nonenzymatic production of MDA, despite its potential significance in clinical contexts. MDA has the ability to form adducts by reacting with various biomolecules under conditions of stress (Tsikas, 2017). Excessive production of MDA has been linked to pathological conditions, further highlighting the need for a comprehensive understanding of its nonenzymatic formation. (Bartoli et al., 2011; Garcia et al., 2013; Li et al., 2012).

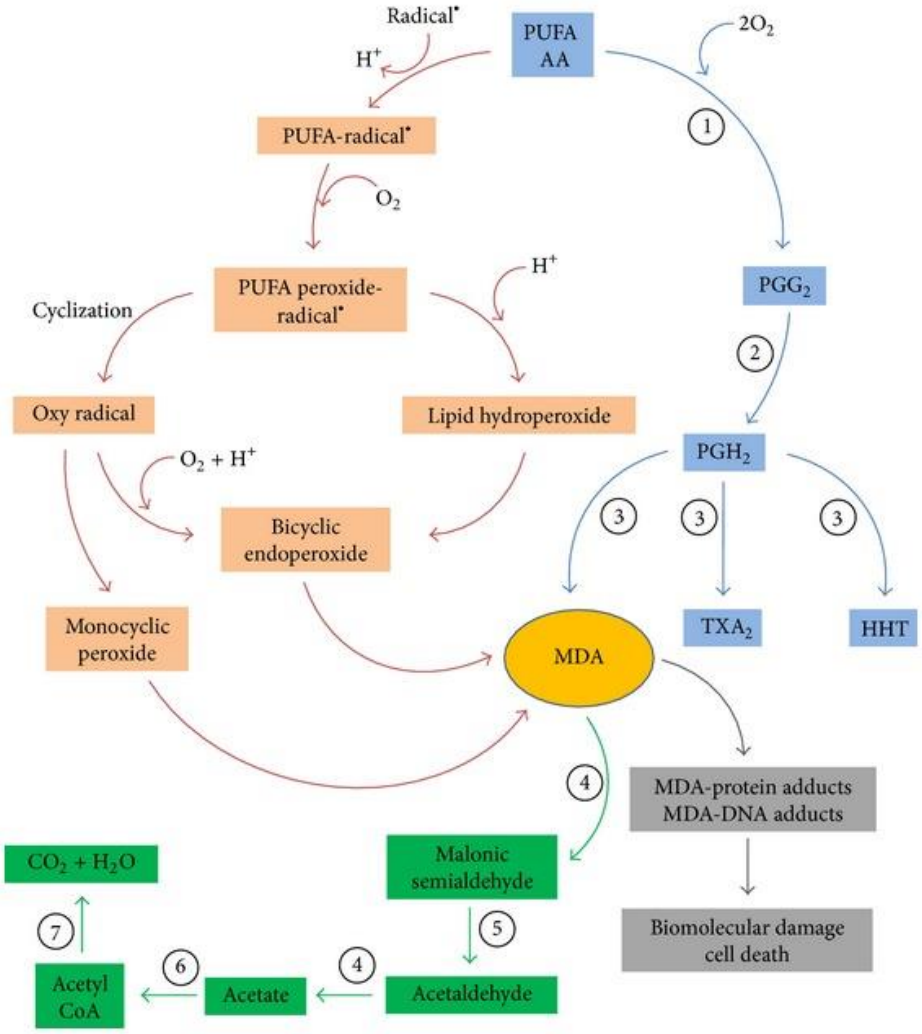

Figure 1. MDA formation and metabolic pathway. AA – arachidonic acid; TXA_2 – thromboxane A_2; HHT – 12-l-hydroxy-5,8,10-heptadecatrienoic acid. 1 to 7 – key enzymes: cyclooxygenases (1); prostacyclin hydroperoxidase (2); thromboxane synthase (3); aldehyde dehydrogenase (4); decarboxylase (5); acetyl CoA synthase (6); tricarboxylic acid cycle (7) (Ayala et al., 2014).

Once MDA has been produced, it can be enzymatically metabolized or can react with proteins or DNA in the cellular and tissular tissues, resulting in the formation of adducts which cause cellular and tissue damage. A recent investigation unveiled a potential biochemical pathway responsible for the metabolism of MDA. This pathway involves the oxidation of MDA by mitochondrial aldehyde dehydrogenases, resulting in the formation of acetaldehyde. Subsequently, acetaldehyde is further oxidized by aldehyde dehydrogenases, leading to the production of carbon dioxide (CO_2) and water (H_2O) (Figure 1) (Ayala et al., 2014).

In the absence of repair mechanisms, MDA-DNA adducts can give rise to various detrimental effects, including the occurrence of mutations such as point mutations and frameshifts, DNA strand breaks, interruption of the cell cycle, and activation of apoptotic pathways (Kay et al., 2019).

1.6. Nitric oxide metabolism

As a messenger molecule, nitric oxide (NO) plays an integral role in physiology as well as in pathophysiology. Exercise, calorie restriction, differentiation of fat cells, and obesity-related inflammation are all affected by NO regulation of mitochondrial function, including biogenesis, fission, and fusion. It is also discussed how NO contributes to neurodegenerative disorders as well as how it plays a role in mitochondrial dysfunction, a topic that has received considerable controversy in the recent past (Knott and Bossy-Wetzel, 2010).

NO, the gas that causes nitrosative stress, plays an important role in many aspects of human health that also include excitotoxicity, protein modification, and other processes that are pathophysiological. The nitric oxide synthase (NOS) in mammals produces NO by breaking down L-arginine into L-citrulline molecules (Akanji et al., 2020; Correa-Aragunde et al., 2018). Three NOS isoforms have been positively identified - endothelial NOS (eNOS), inducible NOS (iNOS), and neuronal NOS (nNOS) (Wang et al., 2020).

eNOS is primarily found in the endothelium of blood vessels, which is where nitric oxide plays an important role in relaxing soft tissues and widening vessels (Heiss et al., 2015). The eNOS is constitutively active, which means that it releases modest amounts of NO at a constant rate over a long period of time in order to fulfil its functions. eNOS is predominantly present in immune cells and glial cells and is activated when pathogens are detected and cytokines are released (Cinelli et al., 2020). In response to pathogens, iNOS has a primary function of mediating cell death through the generation of NO that has toxic levels. Consequently, an increased concentration of NO is produced by iNOS over a short period of time (Cinelli et al., 2020). As a neurotransmitter, NO plays an essential role in cell-to-cell communication and neuronal plasticity and is primarily expressed in central and peripheral neurons. nNOS operates in the same way as eNOS, that is, it is constitutively active. It produces low levels of NO over an extended period of time(Akanji et al., 2020; Cinelli et al., 2020; Wang et al., 2020).

There is no doubt that NO plays an important role in the normal functionality of the human body, but it also has pathophysiological effects on the body. Through various mechanisms, NO

reacts with a wide variety of oxygen species in the cellular environment to produce highly reactive molecules that damage cellular components on a molecular level. In addition, NO is also thought to play an important role in glutamate excitotoxicity in neurons, which occurs when glutamate receptors are overstimulated and calcium ions are too flooded. It has been shown that NO might inhibit glutamate receptors (a subtype of glutamate receptor) by modifying their S-nitrosylation and thus protecting against excitotoxicity (Fairless et al., 2021), but that NO might rather exacerbate neuronal injury that occurs due to excitotoxicity (Baracaldo-Santamaría et al., 2022).

1.7. General background of DNA repair

There are two main types of DNA damage: endogenous and exogenous. During endogenous DNA damage, reactive oxygen species (ROS) and water, which are naturally present in cells, are involved in hydrolytic and oxidative reactions with chemically active DNA. A number of genetic diseases and sporadic cancers are caused by these inherently predisposed interactions between DNA and molecules from its immediate surroundings (Perrone et al., 2016). In contrast to DNA damage originating from within the body, exogenous DNA damage arises when external factors such as physical, chemical, and environmental agents cause harm to the DNA. Alkylating agents, UV and ionizing radiation, and crosslinking agents are among the substances that can induce such damage (Chatterjee and Walker, 2017).

In each human cell replication, replicative polymerases (α and δ) copy over 3×10^9 bases. During DNA replication or repair, however, several other DNA polymerases can produce weaker forms of DNA synthesis. By correcting rare errors that have escaped replication polymerases' proofreading, the mismatch repair pathway contributes more than 100-fold to replication fidelity (Vaisman and Woodgate, 2017).

Despite these circumstances, the accumulation of base substitutions, single base insertions, and deletions persists at a rate of 10^{-6} to 10^{-8} errors per cell per generation (Chatterjee and Walker, 2017). Replication processes can introduce nucleotide insertions and deletions in repetitive sequences, causing replication errors (Chatterjee et al., 2013). Additionally, replicative polymerases can modify the relative and absolute concentrations of dNTPs and rNTPs in the cellular environment, resulting in the incorrect incorporation of uracil in DNA or compromised fidelity (Buckland et al., 2014; Potenski and Klein, 2014).

1.8. Reactive oxygen species and oxidative DNA damage

Oxidative processes, catabolic oxidases, anabolic processes, and peroxisomal metabolism contribute to reactive oxygen species (ROS) in aerobic organisms (Forrester et al., 2018). As low levels of ROS species accumulate in the body, they serve as important cellular messengers that transmit redox signals and trigger immune responses against invading pathogens (Milkovic et al., 2019; Tavassolifar et al., 2020). In excess, ROS species have the potential to induce a wide range of oxidative base lesions and modifications to 2-deoxyribose (Cadet et al., 2012; Cadet and Wagner, 2014; Ravanat et al., 2012).

ROS species most prominently present in the body include superoxide radicals ($\bullet O_2^-$), hydrogen peroxide (H_2O_2), and hydroxyl radicals (•OH) (Tropp, 2012). •OH radicals are the most reactive of these ROS species, and can damage DNA, proteins, and lipids. They are produced by Fenton's reaction of H_2O_2 with Fe^{2+} (Zhao, 2019). These highly reactive radicals engage with the DNA bases by combining with their double bonds, removing hydrogen atoms from the methyl groups, and attacking sugar residues near their double bonds (Greenberg, 2016).

Thymine glycol residues, for example, are formed by attacking the C5/C6 double bonds of thymine with •OH By the same mechanism, the •OH radical formed by H_2O_2 and Fe^{2+} induces guanine and adenine to fragment into formamidopyrimidine (Chatterjee and Walker, 2017).

It is worth mentioning that the saturated imidazole ring 8,8-oxoguanine (8-oxo-G) is another significant oxidative base lesion that holds biological importance, resulting from the hydroxylation of the C-8 residue of guanine.

The oxidation potential of 8-oxo-guanine prevents it from being oxidized into other deleterious secondary DNA lesions because it pairs incorrectly with adenine rather than cytosine (Cadet et al., 2010).

A mammalian cell can undergo an estimated 2300 single strand breaks per hour due to ROS radicals in addition to attacking DNA bases (Chatterjee and Walker, 2017). The repair of DNA backbone breaks is accomplished through either the single strand break repair (SSBR) pathways or the double strand break repair (DSBR) pathways (Abbotts and Wilson, 2017). Adenine, guanine, and cytosine can form mutagens from lipid peroxidation, which involves the oxidation of lipid molecules by hydroxyl radicals (Singh et al., 2019).

1.9. DNA repair genes

1.9.1. Ataxia-telangiectasia mutated (ATM) serine/threonine protein kinase

ATM gene is located on Chr11: 108 223 044-108 369 102; 11q22.3 (Fig. 3), has the size of 146 059 bases and a plus strand orientation ("Gene: ATM (ENSG00000149311) - Summary - Homo_sapiens - Ensembl genome browser 107").

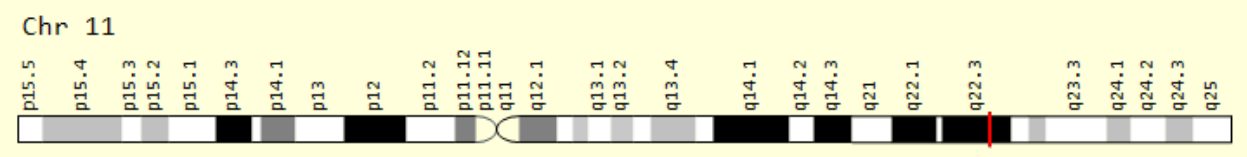

Figure 3. ATM Gene in genomic location: bands according to Ensembl, locations according to GeneLoc (*Gene: ATM (ENSG00000149311) - Summary - Homo_sapiens - Ensembl genome browser 107*).

Neurodegeneration, immunodeficiency, hypogonadism, and a susceptibility to cancer are all characteristics of ataxia-telangiectasia, an autosomal recessive disorder. At the cell level, it is characterized by genomic instability, which is caused by a malfunctioning response to DNA double-strand breaks (DSBs). As a result, the cells become hypersensitive to ionizing radiation (IR) and radioactive compounds, as well as less able to activate the DNA-damage-response system, which involves the cell-cycle checkpoints (Alhmoud et al., 2020). When DSBs occur, a process of autophosphorylation takes place on serine (Ser) 1,981 in order to activate the product of the ATM gene. When a dimer is dissociated, a monomeric form results, causing many enzymes involved in DNA repair and cell-cycle control to be phosphorylated (Campos and Clemente-Blanco, 2020). While ATM is responsible for generating these cascades of signaling events, it is not solely responsible for initiating them. This type of protein also plays a role during the response to agents that stress the DNA replication process as ataxia-telangiectasia and Rad3-related (ATR) protein. Sensor, transducer, and effector molecules support both ATM and ATR in protecting the genome from DNA damage (Luo and Hong, 2020)

1.9.2. Poly (ADP-ribose) polymerase 1 (PARP1)

PARP1 gene is located on Chr1:226 360 210-226 408 154; 1q42.12 (Fig. 4), has the size of 47 403 bases and a minus strand orientation ("Gene: PARP1 (ENSG00000143799) - Summary - Homo_sapiens - GRCh37 Archive browser 107").

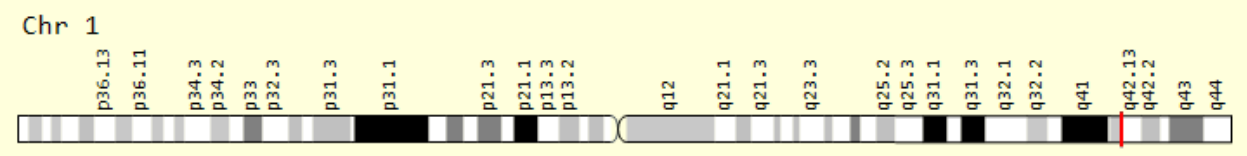

Figure 4. PARP1 Gene in genomic location: bands according to Ensembl ("Gene: PARP1 (ENSG00000143799) - Summary - Homo_sapiens - GRCh37 Archive browser 107")

ADP-ribosylating enzyme Poly (ADP-ribose) Polymerase 1 (PARP1) can activate DNA single-strand and double-strand breaks primarily by binding to ADP-ribosylated ADP. DNA repair depends on the interaction between auto-ribosylation and multiprotein complexes to be activated and assemble (De Vos et al., 2012).

As a result of PARP1's critical role in DNA repair, PARP1 expression is frequently upregulated in cancer cells (Spiegel et al., 2021), and PARP1 null animals are hypersensitive to mutagenic effects of DNA damaging agents (Shall and de Murcia, 2000). Using small molecules to block ADP-ribosylation from PARP1 which is involved in the repair of modified bases can be used to achieve synthetic lethality in cancer treatment (Boehi et al., 2021; Ray Chaudhuri and Nussenzweig, 2017; Spiegel et al., 2021). Furthermore, PARP1 has been shown to play a significant role in the regulation of transcription, in addition to its involvement in DNA repair. PARP1 functions as an enzyme that controls DNA accessibility for RNA polymerase by acting on chromatin remodeling complexes (Eleazer and Fondufe-Mittendorf, 2021; Ke et al., 2019).

1.9.3. Xeroderma Pigmentosum group A (XPA)

XPA gene is located on chr9:97 654 398-97 697 340; 9q22.33 (Fig. 5), has the size of 47 403 bases and a minus strand orientation ("Gene: XPA (ENSG00000136936) - Summary - Homo_sapiens - GRCh37 Archive browser 107").

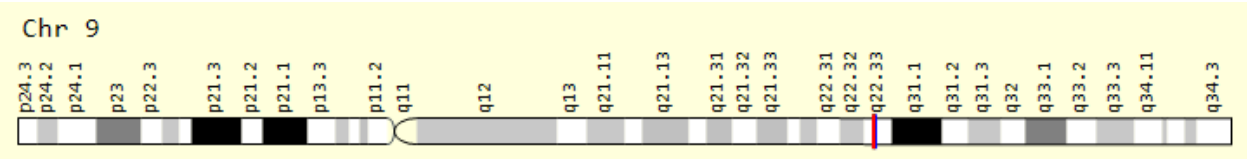

Figure 5. XPA Gene in genomic location: bands according to Ensembl ("Gene: XPA (ENSG00000136936) - Summary - Homo_sapiens - GRCh37 Archive browser 107").

This gene encodes a zinc finger protein that is involved in a special type of DNA repair known as nucleotide excision repair (NER). UV radiation, chemical carcinogens, and certain chemotherapeutic drugs can induce DNA damage, such as UV-induced photoproducts and DNA adducts, which are repaired by the Nucleotide Excision Repair (NER) mechanism. The process of

assembling the NER incision complex at the sites of DNA damage involves the interaction of the encoded protein with DNA as well as multiple NER proteins. The mutation in this gene leads to the skin condition Xeroderma pigmentosum complementation group A (XP-A), which causes hypersensitivity to sunlight and an increased risk of skin cancer ("XPA XPA, DNA damage recognition and repair factor [Homo sapiens (human)] - Gene - NCBI").

XPA has been primarily characterized as a biochemical activity involved in DNA binding. Figure 6A illustrates that the DNA binding domain (residues 98-239) of XPA is responsible for binding both damaged and undamaged DNA strands. Within this domain, there is a minimal DNA binding domain (MDB, residues 98-219) that overlaps with the central globular core domain. (Fadda, 2016; Sugitani et al., 2016). The necessity of XPA in the verification of DNA damage stems from its ability to recognize highly curved DNA structures rather than specific DNA lesions. Moreover, XPA can intervene to halt DNA incision if the NER complex has mistakenly assembled at undamaged DNA locations (Borszéková Pulzová et al., 2020; Kim et al., 2022).

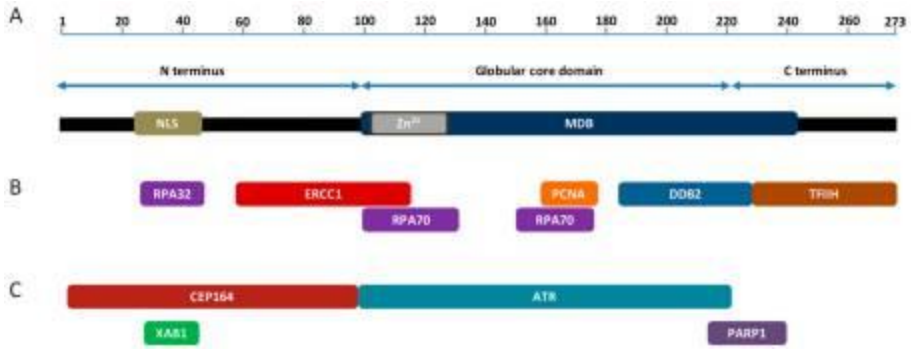

Figure 6. Domains and interacting partners of XPA protein. A - Human XPA protein domain structure. B – NER involved XPA interaction partners. C - Outside NER interaction partners (Borszéková Pulzová et al., 2020).

1.9.4. Xeroderma Pigmentosum group C (XPC)

XPC gene is located on chr3:14,145,147-14,178,621; 3p25.1 (Fig. 7), has the size of 33 475 bases and a minus strand orientation.

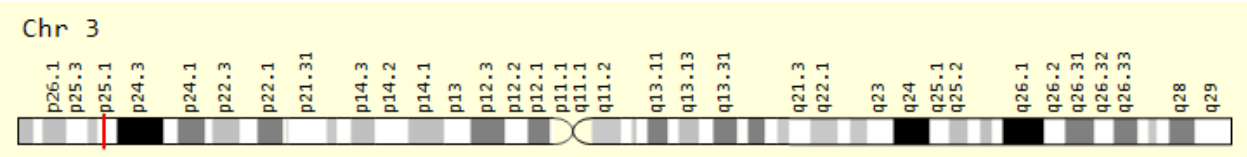

Figure 7. XPC Gene in genomic location: bands according to Ensembl ("Gene: XPC (ENSG00000154767) - Summary - Homo_sapiens - GRCh37 Archive browser 107")

XPC, the gene-encoded protein, is essential in the initial stages of global genome nucleotide excision repair (NER). It performs a critical function in identifying, sensing, and attaching to DNA damage, with a particular affinity for single-stranded DNA rather than double-stranded DNA. Alterations in this gene, as well as other NER components, can lead to a rare autosomal recessive condition called Xeroderma pigmentosum. This disorder is characterized by heightened sensitivity to sunlight and the early onset of carcinomas.

This gene has been found to have a number of alternatively spliced transcript variants ("XPC XPC complex subunit, DNA damage recognition and repair factor [Homo sapiens (human)] - Gene - NCBI").

1.9.5. XRCC1

XRCC1 gene is located on Chr19:43 543 311-43 580 473; 3p25.1 (Fig. 8), has the size of 37 163 bases and a minus strand orientation.

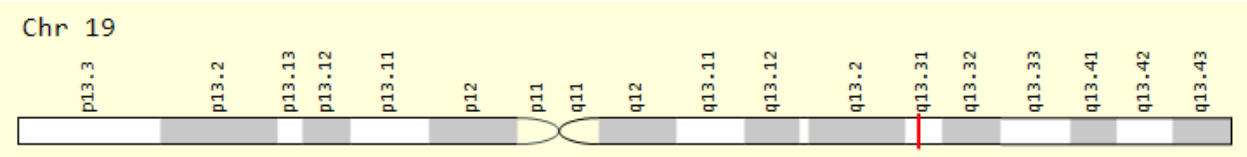

Figure 8. XRCC1 Gene in genomic location: bands according to Ensembl ("Gene: XRCC1 (ENSG00000073050) - Summary - Homo_sapiens - GRCh37 Archive browser 107").

This gene encodes a protein that is responsible for rapidly repairing the single-strand breaks formed in DNA caused by ionizing radiation and alkylating agents when DNA is exposed to these agents. Within the framework of the base excision repair pathway, this protein engages in interactions with DNA ligase III, polymerase beta, and poly(ADP-ribose) polymerase. These interactions are vital for its significant involvement in the base excision repair process. The presence of a rare microsatellite polymorphism of this gene in patients with varying degrees of radiosensitivity seems to be associated with the development of cancer ("XRCC1 X-ray repair cross complementing 1 [Homo sapiens (human)] - Gene - NCBI").

1.9.6. SIRT6

The encoded protein is a member of the sirtuin family of NAD-dependent enzymes, which are essential for various cellular functions including stress resistance, maintenance of genomic stability, regulation of aging processes, and ensuring energy homeostasis.

DNA repair, telomeric chromatin maintenance, inflammation, lipid and glucose metabolism, and DNA repair are some of the functions of this encoded protein. Transcripts encoding different

isoforms can result from alternative splicing (*SIRT6 sirtuin 6 [Homo sapiens (human)] - Gene - NCBI*).

Sirtuins, including those found in yeast, worms, flies, fish, and possibly mammals, are overexpressed or hyperactive in many species (Longo and Kennedy, 2006). Several sirtuins are discovered in mammals, referred to as SIRT1–SIRT7 (Grabowska et al., 2017). In yeast and mammals, Sir2 and SIRT1 both possess ADP-ribosyltransferase (Poulose and Raju, 2015) and protein deacetylase activities. Sirtuins exert their actions via NAD+-dependent enzymatic modification of other proteins (Khoury et al., 2018; Kosciuk et al., 2019; Kratz et al., 2021). Deacetylases like SIRT6 and SIRT4 are more active on deacetylated proteins, such as core histones, while little or no deacetylase activity exists on histone peptides (Klein and Denu, 2020). There appears to be only one type of modification Sir2 performs. Other sirtuins, however, modify a wide array of proteins; for example, SIRT1 influences numerous cellular processes by binding to and/or deacetylating a wide variety of factors (Fang et al., 2019; Lee, 2019).

Among all the sirtuin knockouts, SIRT6 deficiency results in the most striking phenotype from the standpoint of ageing research. When SIRT6 is deficient, cells grow slowly and are more prone to genotoxic damage. A large number of non-clonal chromosomal aberrations can also be observed in SIRT6-deficient cells (Garcia-Venzor and Toiber, 2021).

1.9.7. Potential MS candidate genes

A whole genome research published by Comabella *et al* in 2009 described the association of SNPs with IFN-β therapy response in MS patients (Comabella et al., 2009). Among the top-scoring intragenic SNPs, there are those in the following genes: Zinc finger and AT hook domain containing (ZFAT), glutamate receptor, ionotropic, AMPA 3 (GRIA3), StAR-related lipid transfer (START) domain containing 13 (STARD13), adenosine deaminase, RNA-specific (ADAR), zinc finger homeobox 4 (ZFHX4), interferon (α, β and ω) receptor 2 (IFNAR2) and citron Rho-interacting serine/threonine kinase (CIT) (Bourguiba-Hachemi et al., 2016).

Coding and non-coding RNA transcripts can be modified by A-to-I RNA editing, which converts adenosines into inosines after transcription (Nishikura, 2016). An enzyme named ADAR (adenosine deaminase acting on RNA) catalyzes the reaction, which exists throughout the body but is most prevalent in the brain. By altering codons, adding or removing splice sites, or changing base pairing, ADAR-mediated editing can change the information in RNA molecules post-transcriptionally(Slotkin and Nishikura, 2013). Despite its importance in regulating and

diversifying the transcriptome, ADARs remain unclear in terms of their biological significance. Normal development in mammals necessitates the presence of ADARs. These enzymes exhibit a high level of conservation among vertebrates. Abnormal ADAR activity has been linked to various human diseases, including cancer, neurological disorders, metabolic diseases, viral infections, autoimmune diseases, and more (Song et al., 2022). Mutations in ADAR genes and editing of glutamate receptors, among other mechanisms affecting disease pathologies, have been linked to ADARs, including regulatory roles in microRNA processing recently identified. An improved understanding of ADARs' biological functions may lead to advances in research into many of these diseases(Slotkin and Nishikura, 2013).

The GRIA3 gene is responsible for encoding an AMPA-type glutamate receptor, which is an excitatory neurotransmitter involved in crucial functions such as memory, memory formation, neural development, habit generation, and sensory receptor gating. Activating this receptor excessively can lead to central neurons degenerating and dying. A variety of brain disorders are associated with glutamate receptors in the central nervous system. The damage caused by these conditions leads to the development of several neurodegenerative diseases, including Parkinson's disease, Alzheimer's disease, and amyotrophic lateral sclerosis (Jazireian et al., 2020).

ZFAT (zinc finger protein with AT-hook) is a nuclear protein that contains 18 zinc finger domains. Among vertebrates, ZFAT's amino acid sequence is evolutionarily highly conserved, suggesting that it has a crucial role to play. Binding to the proximal regions of mRNA transcription start sites of specific genes controls the transcription of messenger RNA (mRNA). In addition, ZFAT regulates noncoding RNA transcription at the centromeres by acetylating histones (Ishikura et al., 2021). ZFAT has been shown to play a significant role in various prevalent conditions such as multiple sclerosis, hypertension, and cancer. Additionally, it is involved in crucial processes such as development, primitive hematopoiesis, angiogenesis, immune response, and various types of angiogenesis (Tsunoda and Shirasawa, 2013).

A multidomain protein called citron kinase (CIT) is located near the cleavage furrow and midbody, where it plays an important role in the process of cytokinesis, which is the final step in the process of mitosis. The contractile ring (anillin, actin, myosin, and RhoA) interacts with CIT through an N-terminal kinase domain and numerous C-terminal domains. Multiple organisms have provided experimental evidence suggesting that both the kinase activity and scaffolding functions of CIT are vital for the successful completion of cytokinesis, even though the specific endogenous

substrates have yet to be confirmed. In contrast, when cytokinesis is incomplete, it can result in neurons containing two or more fully developed nuclei (Harding et al., 2016).

The biological effect of IFN-β is achieved through the activation of the JAK-STAT pathway by interacting with its cell surface receptor (IFNAR). The receptor consists of two functional subunits, IFNAR1 and IFNAR2. In both human and mouse, the IFNAR2 genes have the ability to undergo alternative splicing, resulting in the generation of soluble isoforms (sIFNAR2). These soluble isoforms lack the transmembrane and cytoplasmic domains, which have been previously identified and cloned in both human and mouse. Moreover, TNF-alpha converting enzymes (TACE or ADAMS) can cleave IFNAR2 subunits, which release their extracellular and intracellular domains, respectively. Both mechanisms lead to the detection of sIFNAR2 in body fluids, and it has been found that sIFNAR2 is expressed in most mouse tissues at 10-fold higher levels than transmembrane IFNAR2 (Aliaga-Gaspar et al., 2021). Considerable attention has been given to the study of type I interferon responses and their regulation in autoimmune conditions, such as multiple sclerosis. However, limited research has been conducted regarding the role of sIFNAR2 (soluble isoforms of IFNAR2) in these contexts (Samarajiwa et al., 2014).

Initially discovered through its homology to DLC1, STARD13 (DLC2) is frequently deleted in hepatocellular carcinomas. With 58 percent homology to DLC1, STARD13 also shares a SAM-RhoGAP-START domain structure. Several cancers are frequently caused by the deletion of the STARD13 gene located at chromosome 13q12.3. The STARD13 gene shows RhoGTPase activating (RhoGap) activity for RhoA and Cdc42. RhoGap-dependent suppression of HRAS signaling was observed in mouse fibroblasts after STARD13 was introduced. It has been found that STARD13 mRNA is downregulated in primary cancers of the lung, ovary, breast, uterus, and liver (Basak et al., 2018).

There are 12 exons in the ZFHX4 gene, which encodes a transcription factor with 4 homeodomains and 22 zinc fingers. In addition to binding to CHD4, which plays a role in nucleosome remodeling and deacetylation, ZFHX4 also modulates the activity of several genes involved in nucleic acid synthesis. There is a high level of expression of ZFHX4 in the brain, heart, lung, and muscle, and it is responsible for regulating neural differentiation and mesenchymal differentiation. In 8q21.11 deletion syndrome, ZFHX4 is included in the critical region. 8q21.11 deletion syndrome is characterized by intellectual disability, hypotonia, short stature, and a peculiar facial appearance (Fontana et al., 2021).

1.10. Genetic marker choice

SNPs were chosen based on:

- Well-studied SNPs associated with different disease but elucidating the mechanism which is relevant to the topic of this study (DNA repair gene SNPs with recent studies about various DNA genotoxic factors).
- Insufficient overall information and references about the SNP of potentially involved gene (NOS2).
- Genes that are potentially involved in MS, but lacking evidence confirming it (MS candidate genes ADAR, GRIA3, ZFAT, STARD13, ZFHX4, IFNAR2, CIT, SIRT6).

Chosen SNP information is summarized in table 1:

Table 1: Description of the chosen polymorphisms

Marker ID	Genomic coordinates	Gene	Variant	Association	Reference
rs189037	11:108223106	ATM	G > A	Cancer	Mou *et al.*, 2020 He *et al.*, 2019
rs1136410	1:226367601	PARP1	A > G	Cancer	Zhou *et al.*, 2021 Zhao *et al.*, 2020
rs3219090	1:226376990	PARP1	C > T	Cancer	Koleck *et al.*, 2016 Choi *et al.*, 2017
rs1800975	9:97697296	XPA	T > C	Cancer	Zhang *et al.*, 2019 Yuan, Yu and Yu, 2020
rs2228001	3:14145949	XPC	G > T	Cancer	Kaur and Kaur, 2020 Xie *et al.*, 2019
rs1799782	19:43553422	XRCC1	G > A	Cancer	Djansugurova *et al.*, 2020 Özgöz *et al.*, 2019
rs25487	19:43551574	XRCC1	T > C	Cancer	Xie *et al.*, 2021 Pasqualetti *et al.*, 2021
rs1047735	12:117247465	NOS1	G > A	PD	Paul *et al.*, 2016 Polito, Greco and Seripa, 2016
rs3741475	12:117232109	NOS1	G > A	PD CP	Paul *et al.*, 2016 Yu *et al.*, 2018
rs2682826	12:117215033	NOS1	G > A	PD	Redenšek *et al.*, 2019 Santos-Lobato *et al.*, 2018
rs944725	17:27782545	NOS2	C > T	ATDILI SC	Sun *et al.*, 2020 Mnika *et al.*, 2016
rs2248814	17:27773295	NOS2	A > G	PD	Polito, Greco and Seripa, 2016
rs2255929	17:27760941	NOS2	T > A	PD	Hancock *et al.*, 2008 Hancock *et al.*, 2006
rs2229857	1:154601491	ADAR	T > C	HIV MS	Medrano *et al.*, 2017 Bourguiba-Hachemi *et al.*, 2016
rs12557782	X:123243887	GRIA3	G > A	MS	Bourguiba-Hachemi *et al.*, 2016
rs733254	8:134626389	ZFAT	C > A	MS	
rs9527281	13:33249277	STARD13	T > G	MS	
rs11787532	8:76717551	ZFHX4	G > C	MS	
rs2248202	21:33231575	IFNAR2	C > A	MS	
rs350845	19:4174953	SIRT6	A > G	Longevity	Simon *et al.*, 2021
rs7308076	12:119818441	CIT	T > C	MS	Bourguiba-Hachemi *et al.*, 2016

2. MATERIALS AND METHODS

2.1. Ethics

Approval for conducting this study was granted by the Central Medical Ethics Committee of the Republic of Latvia under the reference number 1/17–10-10 on October 10, 2017. Prior to participating in the study, informed consent was obtained from all individuals involved.

2.2.Patients

SNP genotyping was performed on 96 patients as a cohort study. Biochemical analysis (comet assay, detection of NO, levels of nitrates and nitrites, levels of MDA) study group involved 26 volunteers from the doctor's appointment and within the 96-patient collection.

The study group consisted of 96 participants, with 78.1% being females and 21.9% being males, resulting in a female-to-male ratio of approximately 4:1, which aligns with the well-known female predisposition to MS. Among the patients, 43.8% had the RRMS subtype, while 56.2% had progressed to the SPMS stage. The average duration of the RRMS stage within the study group was 13.3 ± 8.2 years. The average duration of MS for the entire group of 96 patients was 29.2 ± 9.3 years. The average age of the participants in the study group was 50.7 ± 10.7 years, with a median value of 51.5 and an interquartile range (IQR) of 16 years. In terms of disease duration specifically for the genotyping study group, the mean value was 21.5 ± 8.9 years, and the IQR was 10.8 years, with an average of 20.0 years. The majority of patients (74.0%) were receiving disease-modifying therapy (DMT), with 34.4% of them undergoing treatment with IFN-based drugs. More detailed information about the study group can be found in Table 2.

Table 2. Demographic and clinical characteristics of patients with MS in study groups

Descriptor	Genotyping	Biochemistry
Sample count	96	26
Sex (N%):		
Females	75 (78.13)	18 (69.23)
Males	21 (21.88)	8 (30.77)
Age of diagnosis, years:		
Mean ± SD	29.23 ± 9.26	29.04 ± 8.32
Median with IQR	29 and 13	29 and 10.5
Age, years		
Mean ± SD	50.73 ± 10.68	48.65 ± 12.43
Median with IQR	51.50 and 16.00	48.50 and 22.75
Disease duration, years:		
Mean ± SD	21.50 ± 8.92	19.62 ± 8.06
Median with IQR	20 and 10.75	19 and 9.5
EDSS:		
Mean ± SD	4.83 ± 1.94	4.63 ± 1.74
Median with IQR	5 and 3.5	4.5 and 3.5
MS type:		
RR	42 (43.75)	12 (46.15)
SP	54 (56.25)	14 (53.85)
RR duration for SP patients:		
Mean ± SD	13.30 ± 8.19	10.36 ± 6.83
Median with IQR	11.5 and 12.25	10 and 7.75
Brain lesions (49 patients):		
Yes	49 (100.00)	17 (100.00)
No	-	-
Spinal cord lesions (49 patients):		
Yes	47 (95.92)	16 (94.12)
No	2 (4.08)	1 (5.88)
DMT:		
Yes	71 (73.96)	18 (69.23)
No	25 (26.04)	8 (30.77)
DMT type:		
No	25 (26.04)	8 (30.77)
IFN	33 (34.38)	9 (34.62)
Glatiramer acetate (GA)	9 (9.38)	2 (7.69)
Mitoxantronum (M)	17 (17.71)	3 (11.54)
Other	12 (12.50)	4 (15.38)

EDSS Expanded Disability Status Scale, IQR interquartile range, RRMS relapse-remitting multiple sclerosis, SPMS secondary progressive multiple sclerosis, DMT disease modifying therapy, IFN interferon, SD standard deviation

60 samples from the 96-sample collection were randomly chosen for NGS CNV analysis and 12 DNA samples for 30x coverage NGS analysis.

Volunteers who expressed their willingness to participate in the study and provided informed consent were included as healthy subjects. These individuals were selected as controls only if there was no documented evidence of any chronic or autoimmune diseases. The control group used for the comet assay and EPR analysis consisted of 22 healthy subjects, comprising 7 males and 15 females aged between 21 and 55 years, with an average age of 30.6 ± 3.2 years. For the control group involved in the assessment of nitric oxide metabolite and MDA, 25 healthy subjects were included, consisting of 4 males and 21 females aged between 20 and 43 years, with an average age of the group being 34.2 ± 1.7 years.

T1D study group involved 71 patients (45 males and 55 females) with the median age of 33 (27 – 44.5) years. T1D control group involved 57 healthy subjects (39 males and 61 female) with the median age of 24 (21 – 31) years. Detailed information about the T1D study group is presented in most recent article Rostoka *et al.*, 2021.

2.3. Collection and processing of blood samples

Venous blood samples were acquired by performing vein puncture and collected using plastic capillaries containing heparin (Microvetter CB 300, Sarstedt, Germany) for EPR spectrometry. For the comet assay, blood was collected in plastic capillaries with EDTA (BD Vacutainer K2E EDTA 10.8 mg, BD-Plymouth, UK).

2.4. Plasma preparation

EDTA-treated tubes (BD Vacutainer K2E EDTA 10.8 mg, BD-Plymouth, UK) were used to collect whole blood, which was then centrifuged at 1500 x g for 10 minutes in a pre-cooled centrifuge. After centrifugation, the supernatant was carefully decanted, divided into 0.5 mL aliquots, and subsequently stored at a temperature of -20°C.

2.5. Serum preparation

EDTA-free tubes were utilized to collect whole blood, which was then allowed to clot at room temperature. The clot was subsequently separated by centrifugation at 1500 x g for 10 minutes using a pre-cooled centrifuge. Following centrifugation, the supernatant was promptly divided into 0.5 mL aliquots and stored at a temperature of -20°C.

2.6. Peripheral blood mononuclear cell (PBMC) isolation.

The isolation procedure followed the standard Hitopaque-1077 protocol provided by Sigma-Aldrich. A 15 mL conical centrifuge tube was used, and 3 mL of Histopaque-1077 was added to it. Carefully, 3 mL of whole blood was layered onto the Histopaque-1077 and centrifuged at room temperature for 30 minutes at 400 x g. After centrifugation, the opaque layer was transferred into a clean conical centrifuge tube using a 1 mL automatic pipette. The cells were washed with 10 mL of PBS and then centrifuged at 250 x g for 10 minutes. The supernatant was discarded, and the cell pellet was resuspended in 5 mL of PBS. This resuspension step was repeated twice, each time followed by centrifugation at 250 x g for 10 minutes. Finally, the cell pellet was resuspended in 0.5 mL of PBS.

2.7. DNA isolation from whole blood

5 mL of whole blood were transferred into the 15 mL conical centrifuge tube, 10 mL of H_2O were added and centrifuged for 10 minutes at 6000 rpm. Supernatant was removed and the same procedure was repeated once more removing the supernatant after the second washing step. Pellet was then resuspended in 3 mL lysis buffer (10 mM TRIS, 0.4M HCl, 0.32 M sucrose, 5 mM $MgCl_2$, 1% Triton-X 100, pH = 7.5), incubated on ice for 10 minutes and then centrifuged for 30 minutes at 6000 rpm. Supernatant was removed and pellet was resuspended in 1.5 mL resuspension buffer (120 mM NaCl, 15 mM EDTA, pH = 8.0). 40 µL Proteinase K, 15 µL RNase and 150 µL 10% SDS were added to the resuspension and mixed thoroughly after the addition of each component. Mixture was then incubated for 2 hours at 56 ^oC. After the incubation 0.6 mL 5M NaCl solution were added, mixed thoroughly, and centrifuged for 10 minutes at 6000 rpm. Supernatant was transferred into the new tube and 1:2 (vol:vol) 96% ice cold EtOH was added. Solution was placed into the -20 ^oC freezer overnight or at least for 1 hour. Solution was then centrifuged for 15 minutes at 6000 rpm and supernatant was removed. Pellet was resuspended in 1 mL 70% EtOH, transferred into the new Eppendorf tube and centrifuged for 10 minutes at 11 000 rpm. Supernatant was removed and pellets were air dried. Pellets were resuspended in 50 mL H_2O.

2.8. The single-cell gel electrophoresis (comet assay)

A volume of 10 µL of fresh blood was combined with 120 µL of 1% low-melting agarose (*Sigma-Aldrich*, Germany) that had been preheated to 37 °C. From this mixture, 100 µL was placed onto a microscope slide pre-coated with 0.5% agarose (type III, *Sigma-Aldrich*, Germany) and

covered with a 24 x 40 mm cover slide (*Biosigma*, Italy). The slides were kept on ice until the agarose solidified. Subsequently, the cell membranes were lysed using a cold lysing solution (2.5 M NaCl, 10 mM Na2EDTA, 10 mM Tris, pH 10 [*AppliChem*, Germany], 1% Triton-X 100, 5% DMSO [*Sigma-Aldrich*, Germany]) for a duration of 1 to 24 hours. Following this, the slides were placed in a horizontal tank filled with fresh electrophoresis buffer (1 mM Na_2EDTA, 300 mM NaOH, pH 13.2) and allowed to sit in darkness for 20 minutes to enable DNA unwinding before electrophoresis (20 minutes at 300 mA, 1 V/cm, and 4 °C). Afterward, the slides were dried for 1 minute, washed twice for 5 minutes with 0.4 M Tris buffer (pH 7.5) for neutralization, and fixed in ice-cold 96% ethanol for 10 minutes. The slides were then dried, stained with ethidium bromide, and examined using a fluorescence microscope (Leica DFC295) equipped with a 515-560 nm excitation filter and a 590 nm barrier filter. The cells were visually classified into 5 classes (A_0-A_4), ranging from class 0 (undamaged with no discernible tail) to class 4 (almost all DNA in tail, with an insignificant head). The DNA damage index (D) in arbitrary units was calculated as follows: $D = A_1 + 2 \times A_2 + 3 \times A_3 + 4 \times A_4$.

2.9. Modified single-cell gel electrophoresis (modified comet assay)

Isolated PBMCs (50 µL) were combined with 100 µL of 1% low-melting agarose (*Sigma-Aldrich*, Germany) that had been preheated to 37 °C. From this mixture, 50 µL was placed onto a microscope slide that had been pre-coated with 0.5% agarose (type III, *Sigma-Aldrich*, Germany) (two samples per slide) and covered with a 24 x 24 mm cover glass (*Corning*, USA). The slides were kept on ice until the agarose solidified. A 10 mM $KBrO_3$ solution was prepared using a 0.1 N $KBrO_3$ stock (*Merck*, Germany). A volume of 50 µL of this solution was applied to the prepared sample slides, covered with a cover glass, and incubated for 5 minutes at room temperature. The slides were then placed into a lysis solution (2.5 M NaCl, 10 mM Na_2EDTA, 10 mM Tris pH 10 [*AppliChem*, Germany], 1% Triton-X 100, 5% DMSO [*Sigma-Aldrich*, Germany]) and left overnight at 4 °C. On the following day, fresh enzyme reaction (ER) buffer was prepared by combining 40 mL of HEPES (*Sigma-Aldrich*, Germany), 0.1 M KCl (*Sigma-Aldrich*, Germany), 0.5 mM EDTA (*Sigma-Aldrich*, Germany), 0.2 mg/mL BSA (*Sigma-Aldrich*, Germany), at pH 8. Dilutions of *Fpg* protein from *E. coli* and *EndoIII* protein from *E. coli* at a 1:3000 ratio in ER buffer were prepared. A volume of 50 µL of each enzyme solution was applied to the samples, followed by incubation at 37 °C for 30 minutes for *Fpg* and 45 minutes for *EndoIII*. After the incubation, the standard alkaline comet assay procedure was followed. The cells were visually

classified into 5 classes (A_0-A_4), ranging from class 0 (undamaged with no discernible tail) to class 4 (almost all DNA in tail with an insignificant head). The DNA damage index (D) in arbitrary units was calculated as follows: $D = A_1 + 2 \times A_2 + 3 \times A3 + 4 \times A_4$.

2.10. Detection of NO

1 mL of fresh blood was combined with 20 mg of diethythiocarbamate (*Sigma-Aldrich*, Germany), stirred, and incubated for 30 minutes. Then, 0.4 mL of the mixture was drawn into an insulin syringe and immediately frozen in liquid nitrogen. The frozen cylinder was extruded from the syringe and placed in a quartz finger Dewar flask (ER 167 FDS-Q, *Bruker*, Karlsruhe, Germany) filled with liquid nitrogen. The concentration of NO was determined by measuring the NO component in the spectrum of Fe-DETC-NO. For quantitative measurements, the height of the nitrogen triplet component (g = 2.031) was measured and compared to the calibration curve. EPR spectra were recorded in liquid nitrogen using the EPR spectrometer Radiopan SE/X2544. The conditions for the EPR measurements were as follows: 25 mW microwave power, 9.24 GHz microwave frequency, 100 kHz modulation frequency, 0.5 mT modulation amplitude, and a receiver gain of 5×10^5.

2.11. Nitrite measurements

Detection of nitrites and nitrates was performed using the chemiluminescence detector Sievers NOA-280i. To prepare the reducing agent, 50 mg of NaI (Sigma-Aldrich, Germany) was dissolved in 0.5 mL of deionized water and mixed with 4.5 mL of glacial acetic acid (Sigma-Aldrich, Germany) to obtain a 5 mL solution. Standard solutions of NO_2^- were prepared by dissolving approximately 69 mg of $NaNO_2$ (Sigma-Aldrich, Germany) in 10 mL of deionized water to create 10 mL of 100 mM NO_2^- solution. From the 100 mM stock solution, 1 μM, 5 μM, 10 μM, and 50 μM NO_2^- standard solutions were prepared by dilution. Triplicates of 50 μL of each standard solution were injected to create a calibration curve before the actual experiment. For the plasma or serum samples, 50 μL of each sample were injected into the reducing agent.

2.12. Nitrate measurements

A 100 mL solution of the reducing agent was prepared by dissolving 0.8 g of VCl_3 (Sigma-Aldrich, Germany) in 1 M HCl (Sigma-Aldrich, Germany) and then filtering it through filter paper. To prevent HCl vapors from entering the NOA, the gas bubbler was filled with 15 mL of 1 M aqueous NaOH solution (Sigma-Aldrich, Germany). The water bath, which was connected to the purge vessel, was set to a temperature of 95°C. Standard stock solutions of NO_3^- were prepared by

dissolving approximately 85 mg of $NaNO_3$ (Sigma-Aldrich, Germany) in 10 mL of deionized water to create a 10 mL solution of 100 mM NO_3^-. From the 100 mM stock solution, 1 µM, 5 µM, 10 µM, and 50 µM NO_3^- standard solutions were prepared by dilution. Triplicates of 50 µL of each standard solution were injected to create a calibration curve prior to the experiment. For the plasma or serum samples, 50 µL of each sample were injected into the reducing agent and NO_3^-. The concentrations of NO_2^- and NO_3^- were determined using the provided "NOA Liquid" software based on the respective calibration curves.

2.13. Nitrite measurement calibration

A series of $NaNO_2$ standard dilutions were prepared. mV values were measured for 1 µM NO_2^-, 5 µM NO_2^-, 10 µM NO_2^- and 50 µM NO_2^-. Calibration curve was constructed (Fig. 9) based on the obtained measurements, and the linear equation (1) was used to calculate the unknown concentrations of MS patient samples.

(1) $$y = 765.53x + 131.17$$

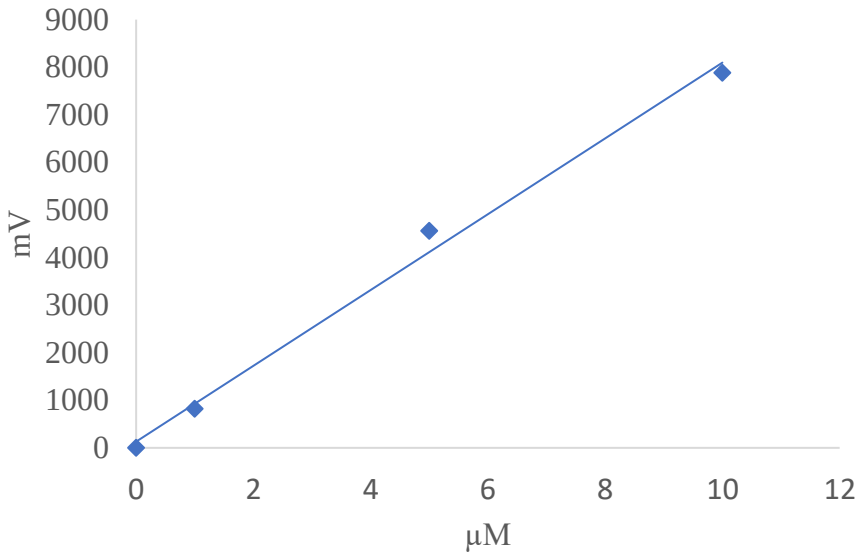

Figure 9. Nitrite measurement calibration curve (R^2 = 0.9931)

2.14. Nitrate measurement calibration

A series of $NaNO_2$ standard dilutions were prepared. mV values were measured for 1 µM NO_3^-, 5 µM NO_3^-, 10 µM NO_3^- and 50 µM NO_3^-. Calibration curve was constructed (Fig. 10) based on the obtained measurements, and the linear equation (2) was used to calculate the unknown concentrations of MS patient samples.

(2) $$y = 1399.1x + 476.4$$

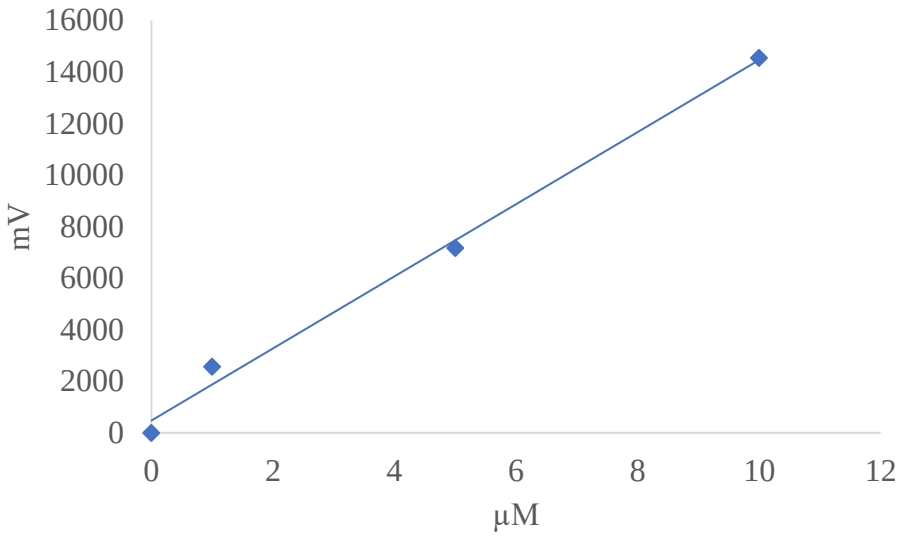

Figure 10. Nitrate measurement calibration curve (R^2 = 0.9934)

2.15. TBARS assay

The Lambda 25 UV-VIS spectrometer (*PerkinElmer*, UK) was used to perform the measurements using single-use cuvettes with a thickness of 1 cm (*Sarstedt*, Germany). To prepare the 4.0 mM TBA standard solution, 57.66 mg of TBA (Sigma-Aldrich, Germany) was dissolved in 100 mL of 99.5% glacial acetic acid (Sigma-Aldrich, Germany). Similarly, the 1 mM MDA standard stock solution was prepared by dissolving 31.35 mg of malondialdehyde tetrabutylammonium salt (*Sigma-Aldrich*, Germany) in 100 mL of 99.5% glacial acetic acid. From the 1 mM stock solution, 0.1 mM, 0.2 mM, 0.4 mM, 0.6 mM, and 0.8 mM standard solutions were prepared through dilution. Each 500 µL of the 4.0 mM TBA standard solution was mixed with the corresponding MDA standard solution, and the mixture was heated for 60 minutes at 95°C in a water bath. The absorption of each sample was then measured at 532 nm to construct the calibration curve. For the plasma or serum samples, 500 µL of the sample were mixed with 500 µL of the 4.0 mM TBA standard solution. The mixture was heated for 60 minutes at 95°C in the

water bath, and the absorption of each sample was measured at 532 nm. The MDA concentration in the plasma or serum samples was calculated based on the calibration curve.

2.16. Statistical analysis

Shapiro – Wilk or Kolmogorov – Smirnov tests were used to determine whether the numerical data follow normal distribution. Method choice was defined by the size of the sample pool: $n < 50$ – Shapiro – Wilk; $n > 50$ – Kolmogorov – Smirnov.

Group-wise comparison was done by parametric t-test if two groups were following normal distribution, and one-way ANOVA test if group count was more than two. For data that was not within the normal distribution Mann-Whitney test was performed for two group comparison, and Kruskal-Wallis test for multiple groups comparison.

Prior to correlation analysis Hardy-Weinberg equilibrium was calculated for each SNP. The biochemical and genetic biomarker correlation was estimated by Pearson r (for data following normal distribution) or Spearman ρ (for data outside the normal distribution) tests.

Statistical analysis was performed using the IBM SPSS Statistics v25.0 software. Heatmaps were prepared with Python3.

2.17. Single Nucleotide Polymorphism (SNP) genotyping

Primer design was performed using the Primer3 software (available online). Genotyping was done by cleaved amplified polymorphic site method. Restriction methods and relevant primer sequences are shown in table 3:

Table 3. Primers for PCR amplification and restriction conditions

Gene ID	Marker ID	Restrictase	Primer	Product size (bp), amplified/restricted
ATM	rs189037	MlsI	F-5' - ACTGTCGTCACTTCCGTCCT-3' R-5' - TGAGGAGAGGGAGGAGTCAA-3'	575/442 + **227** + **215** + 133
PARP1	rs3219090	AgsI	F-5' - GAAAAGACTGTTCCTCCTCGAT-3' R-5' -CTGGAACAGATGCCGTCCAA-3'	689/638 + 381 + 257 + 51
	rs1136410	EciI	F-5' - AAGTTCACGCTACAAGGGTTT-3' R-5' -CTGACCAGCAGGAGGGTTTG-3'	626/626 + 477 + 149
XPA	rs1800975	ApaI	F-5' -AGGTGACCAGGTCGTGAGATA-3' R-5' -GCTTGCACGAGCCAGTCT-3'	514/514 + **267** + **247**
XPC	rs2228001	PvuII	F-5' -GGACGGCTCAGTAAGAAGGG-3' R-5' -AAACGATCAGCGCATTCACG-3'	792/792 + 407 + 385
XRCC1	rs1799782	PvuII	F-5' -CCAAAACCCACCAGTGATCCA-3' R-5' -ATGGGTGTTCATGAGAGGGAAG-3'	622/622 + 376 + 246
	rs25487	PvuII	F-5' -GCTCCTCCAGCCTTTTCTGA-3' R-5' -CTCATGTAGGCTTGCGCC-3'	688/688 + 449 + 239

PCR amplification was performed with DreamTaq polymerase (Fermentas, Vilnius, Lithuania) following a standard PCR protocol with the parameters as provided ThermoFisher): denaturing at 95 ^{o}C for 1 min, annealing at 60 ^{o}C for 30 seconds (all primers had a T_m of around 65 ^{o}C), extension at 72 ^{o}C for 1 minute with a total of 30 cycles, and with the final extension at 72 ^{o}C for 1 minute.

DNA digestion with restriction enzymes was performed according to the enzyme manufacturer protocols (Fermentas, Vilnius, Lithuania).

The analysis of PCR amplification products and enzyme restriction was conducted using gel electrophoresis in an agarose gel ranging from 1% to 5% in concentration. Gels were stained by EtBr and visualized by UV camera. Each single locus genotype was represented by specific band pattern on agarose gel: rs189037 AG – 442 + 227 + 215 + 133 bp, AA – 227 + 215 + 133 bp, GG – 442 + 133 bp; rs1136410 AG – 626 + 477 + 149 bp, AA – 626 bp, GG – 477 + 149 bp; rs3219090 CT – 638 + 381 + 257 + 51 bp, CC – 638 + 51 bp, TT – 381 + 257 + 51 bp; rs1800975 TT – 514 bp, TC – 514 + 267 + 247 bp, CC – 267 + 247 bp; rs2228001 TT – 792 bp, TG – 792 + 407 + 385 bp, GG – 407 + 385 bp; rs1799782 AA – 376 + 246 bp, AG – 622 + 376 + 246 bp, AA – 376 + 246 bp; rs25487 TT – 688 bp, TC – 688 + 449 + 239 bp, CC – 449 + 239 bp. Fragment sizes in bold from Table 1 (**227** + **215** for rs189037 and **267** + **247** for rs1800975) could not be

distinguished on the gel. If a band was visible in the appropriate size region, one would assume that both fragments were observed.

2.18. Next Generation Sequencing

2.18.1. Quality control of gDNA

DNA integrity was verified by Nanodrop (OD_{260}/OD_{280} should be within 1.8 – 2.0 range). gDNA concentration was measured using Qubit dsDNA High Sensitivity kit following the standard protocol: 1 µL of fluorescent dye was added to 199 µL HS buffer (per sample) to create a Master Mix. 199 µL of Master Mix were transferred to a 0.5 µL Qubit tube and 1 µL of gDNA was added. Concentration was then measured using Qubit Fluorometer (Thermo Fisher Scientific, USA) and the gDNA was considered qualified for the library prep if the concentration was ≥ 15 ng/µL.

2.18.2. Library preparation

MGIEasy FS DNA Library Prep Kit was used for library preparation. gDNA was normalized in Nuclease Free (NF) water according to the required input of 200 ng (for complex genome) and a total volume of 14 µL.

4 µL of Frag enzyme were added to 2 µL of Frag buffer and the fragmentation mixture was transferred to the 0.2 mL PCR tube containing 14 µL of normalized gDNA. Fragmentation conditions were selected to target 350 bp fragment size for Pair-End (PE) 150 sequencing approach. Thermocycler was setup according to the standard FS DNA Library prep manual: incubation for 5 minutes at 32 ^{o}C followed by 30 minutes incubation at 65 ^{o}C.

The tube was then briefly centrifuged at 2000 x g to collect the solution at the bottom. 31 µL of TE were then added to the 0.2 mL with the fragmentation reaction product. 50 µL of the mixture were transferred to a new 1.5 mL Eppendorf tube. Size-selection was immediately proceeded.

2.18.3. Size-selection of the fragmentation product

To achieve the desired fragment size for the PE150 approach and with an input of 200 ng gDNA, a two-step size-selection process was necessary, using 30 µL + 10 µL of DNA Clean beads. The DNA Clean beads were removed from the refrigerator and vortexed before being incubated at room temperature for 30 minutes. Subsequently, 30 µL of DNA Clean beads were added to an Eppendorf tube containing the fragmented DNA, followed by vortexing and incubation at room temperature for 5 minutes. The Eppendorf tube was briefly centrifuged at 2000 x g and placed on

a Magnetic Separation Rack for 2-5 minutes, allowing the clear liquid (supernatant) to separate. The supernatant was then carefully transferred to a new centrifuge tube with a volume of 80 µL.

Next, 10 µL of DNA Clean Beads were added to the centrifuge tube containing 80 µL of the supernatant obtained from the previous step. The mixture was thoroughly mixed by pipetting at least 10 times and incubated at room temperature for 5 minutes. After a brief centrifugation at 2000 x g, the tube was placed on a Magnetic Separation Rack. The beads were washed twice with 200 µL of freshly prepared 80% ethanol, and the liquid was discarded each time. The tube was then left open on the Magnetic Separation Rack to air dry until no wetness was observed. Once dry, the centrifuge tube was removed from the Magnetic Separation Rack, and 42 µL of 1x TE buffer were added to elute the DNA. The mixture was again thoroughly mixed by pipetting at least 10 times and incubated at room temperature for 5 minutes. After a brief centrifugation at 2000 x g, the tube was placed on a Magnetic Separation Rack for 2-5 minutes until the liquid became clear. Finally, 40 µL of the clear supernatant were carefully transferred to a new 0.2 mL PCR tube.

2.18.4. End Repair and A-tailing

End Repair and A-tailing (ERAT) mixture was prepared by adding 2.9 µL ERAT Enzyme Mix to 7.1 µL ERAT buffer. 10 µL of ERAT mixture were added to the 0.2 mL PCR tube containing Fragmentation product. 0.2 mL PCR tube was then vortexed, briefly centrifuged and placed into the thermocycler for 30 minutes at 37 ^{o}C followed by the incubation for 15 minutes for 65 ^{o}C.

2.18.5. Adapter Ligation

0.2 mL PCR tube with the ERAT product was centrifuged, and Adapter Ligation was started immediately. 5 µL of MGI adapter were added to the ERAT product, the tube was vortexed and centrifuged briefly. Adapter Ligation Mixture was prepared by adding 1.6 µL of DNA Ligase to 23.4 µL Ligation Buffer. 25 µL of the Adapter Ligation Mixture were added to the adapter containing ERAT product, the tube vortexed and centrifuged briefly. The tube was then placed into the thermocycler and incubated for 30 minutes at 23 ^{o}C.

The 0.2 mL PCR tube containing Adapter Ligation product was centrifuged briefly, 20 µL of 1x TE were added to the total volume of 100 µL, and the mixture was transferred to a new 1.5 mL Eppendorf tube.

2.18.6. Adapter-Ligated DNA Cleanup

To the 1.5 mL tube containing the Adapter Ligation product, 50 µL of DNA Clean Beads were transferred. The mixture was vortexed and incubated at room temperature for 5 minutes. The 1.5 mL Eppendorf tube was then briefly centrifuged at 2000 x g and placed on the Magnetic Separation Rack for 2-5 minutes or until the liquid cleared. The resulting supernatant was carefully transferred to a new 1.5 mL centrifuge tube. After discarding the supernatant, the beads were washed with 200 µL of freshly prepared 80% ethanol. This ethanol washing step was repeated at least twice. Subsequently, the tube was left open on the Magnetic Separation Rack until there was no wetness or reflectiveness observed, allowing it to air dry. The centrifuge tube was then removed from the Magnetic Separation Rack, and 21 µL of 1x TE buffer were added to elute the DNA. The mixture was thoroughly mixed by pipetting at least 10 times and incubated at room temperature for 5 minutes. After another brief centrifugation at 2000 x g, the tube was placed on a Magnetic Separation Rack for 2-5 minutes or until the liquid became clear. Finally, 19 µL of the resulting clear supernatant were carefully transferred to a new 0.2 mL PCR tube.

2.18.7. PCR Amplification

The number of PCR cycles was optimized depending on the gDNA input and the expected yield of PCR product. The optimal number of cycles for 200 ng of gDNA with the corresponding yield of 1 ug of PCR product was chosen to be 8. PCR amplification mix was prepared by adding 6 µL of PCR Primer Mix to 25 µL of PCR Enzyme Mix. 31 µL of PCR amplification mix were transferred to the 0.2 mL PCR tube containing purified Adapter-Ligated product. The thermocycler was pre-set to the following PCR reaction conditions described in table 4:

Table 4. PCR amplification Reaction Conditions

Temperature	Time	Cycles
Heated lid	On	
95 °C	3 min	1 cycle
98 °C	20 s	
60 °C	15 s	8 cycles
72 °C	30 s	
72 °C	10 min	1 cycle
4 °C	Hold	

2.18.8. Cleanup of PCR product

The entire PCR product was transferred to a new 1.5 mL Eppendorf tube. Then, 50 µL of DNA Clean Beads were added to the 1.5 mL tube containing the dsDNA PCR product. The mixture

was vortexed and incubated at room temperature for 5 minutes. After a brief centrifugation at 2000 x g, the tube was placed on the Magnetic Separation Rack for 2-5 minutes or until the liquid became clear. The resulting supernatant was carefully transferred to a new 1.5 mL centrifuge tube. The supernatant was discarded, and the beads were washed with 200 µL of freshly prepared 80% ethanol. This washing step with ethanol was repeated at least twice. The tube was then left open on the Magnetic Separation Rack to air dry until there was no wetness or reflectiveness observed. Next, the centrifuge tube was removed from the Magnetic Separation Rack and 32 µL of 1x TE buffer were added to elute the DNA. The mixture was thoroughly mixed by pipetting at least 10 times and incubated at room temperature for 5 minutes. After another brief centrifugation at 2000 x g, the tube was placed on a Magnetic Separation Rack for 2-5 minutes or until the liquid became clear. Finally, 30 µL of the clear supernatant were carefully transferred to a new 1.5 mL Eppendorf tube.

2.18.9. Quality control of PCR Product

The purified PCR product was quantified using Qubit dsDNA High Sensitivity kit following the standard protocol: 1 µL of fluorescent dye was added to 199 µL HS buffer (per sample) to create a Master Mix. 199 µL of Master Mix were transferred to a 0.5 µL Qubit tube and 1 µL of dsDNA PCR product was added. Fluorescence was measured by benchtop Qubit Fluorometer (Thermo Fisher Scientific, USA).

DNA fragment size was evaluated by the Agilent 4200 TapeStation (Agilent, USA) with D1000 ScreenTape. Reagents were incubated at room temperature for 30 minutes. 3 µL of D1000 Sample Buffer were mixed with 1 µL of D1000 Ladder in the A1 position of the 8-tube strip. 1 µL of dsDNA PCR product were added to 3 µL of D1000 Sample Buffer in A2 position of the same 8-tube strip (or in the separate 96-well Elisa plate depending on the number of samples). Samples were vortexed, centrifuged and placed into the Agilent 4200 TapeStation.

2.18.10. dsDNA circularization

dsDNA circularization required 1 pmol of dsDNA input that was calculated according to the equation (3):

(3) $$Mass\ (ng)\ corresponding\ to\ 1\ pmol\ PCR\ Product = \frac{DNA\ Fragment\ size\ (bp)}{1000\ bp}\ x\ 660\ ng$$

dsDNA input volume corresponding to 1 pmol was then calculated according to the equation (4):

(4) $$dsDNA\ input\ volume\ (uL) = \frac{Mass\ (ng)\ corresponding\ to\ 1\ pmol\ PCR\ product}{dsDNA\ PCR\ product\ concnentration\ (\frac{ng}{\mu L})}$$

2.18.11. dsDNA denaturation

The dsDNA PCR product, amounting to 1 pmol, was moved to a fresh 0.2 mL PCR tube, and 1x TE was added to reach a total volume of 48 µL. Subsequently, the 0.2 mL PCR tube containing the mixture was positioned in the thermocycler, and denaturation was performed at 95°C for a duration of 3 minutes. Once the denaturation step was completed, the 0.2 mL PCR tube holding the denatured product was placed on ice for 2 minutes and then briefly centrifuged.

2.18.12. Single Strand Circularization

Circularization mixture was prepared by adding 0.5 µL of Rapid DNA Ligase to 11.6 µL of Splint buffer. 12.1 µL of the mixture were then transferred to 0.2 mL PCR tube containing denatured product, vortexed and centrifuged briefly. The tube was then placed into the thermocycler and incubated for 30 minutes at 37 ^{o}C.

After the reaction was completed, the tube placed on ice for the next enzymatic digestion step.

2.18.13. Enzymatic digestion

Enzymatic digestion mixture was prepared by adding 2.6 µL of the Digestion Enzyme to 1.4 µL of the Digestion Buffer. 4 µL of the mixture were then transferred to the 0.2 mL PCR tube containing circularized product, vortexed and centrifuged briefly. The tube was then placed into the thermocycler and incubated for 30 minutes at 37 ^{o}C.

The tube was centrifuged briefly, 7.5 µL of the Digestion Stop Buffer were added, vortexed and centrifuged briefly. All solution was then transferred to a new 1.5 mL Eppendorf tube.

2.18.14. Enzymatic Digestion Product Cleanup

A total of 170 µL of DNA Clean Beads were transferred into the 1.5 mL tube containing the Enzymatic digestion product. The mixture was then subjected to vortexing and incubated at room temperature for a duration of 10 minutes. Following this, the 1.5 mL Eppendorf tube was briefly centrifuged at 2000 x g and positioned onto the Magnetic Separation Rack for 2 – 5 minutes, or until the liquid turned clear. The resulting supernatant was cautiously transferred to a fresh 1.5 mL centrifuge tube. The supernatant was meticulously discarded, and the beads were washed with 500 µL of freshly prepared 80% ethanol. The ethanol washing process was repeated at least twice. Subsequently, the tube was placed open on the Magnetic Separation Rack, allowing it to air dry

until there was no longer any wetness or reflectiveness observed. The centrifuge tube was then removed from the Magnetic Separation Rack, and 32 µL of 1x TE buffer were added to facilitate DNA elution. The mixture was thoroughly mixed through pipetting at least 10 times and then incubated at room temperature for 10 minutes. Following this, the tube was briefly centrifuged at 2000 x g and placed back onto the Magnetic Separation Rack for 2 – 5 minutes, or until the liquid became clear. Finally, 30 µL of the resulting supernatant were carefully transferred to a new 1.5 mL Eppendorf tube.

2.18.15. Quality control of Enzymatic Digestion Product

The purified enzymatic digestion product was quantified using Qubit dsDNA High Sensitivity kit following the standard protocol: 1 µL of fluorescent dye was added to 199 µL HS buffer (per sample) to create a Master Mix. 198 µL of Master Mix were transferred to a 0.5 µL Qubit tube and 2 µL of circularized ssDNA enzymatic digestion product were added. Fluorescence was measured by benchtop Qubit Fluorometer (Thermo Fisher Scientific, USA).

2.19. DNB synthesis

Each DNB reaction required 40 fmol of ssDNA library. ssDNA library concentration in ng/µL was converted to fmol/µL according the equation (3):

(3) $$Concentration\ \left(\frac{fmol}{\mu L}\right) = \frac{3030\ x\ Concentration\ (\frac{ng}{\mu L})}{N}$$

where N represents the number of nucleotides (total library length including the adaptor)

ssDNA library input volume (µL) was then calculated according to the following equation (4):

(4) $$ssDNA\ library\ input\ (\mu L) = \frac{40\ fmol}{Library\ concentration\ (\frac{fmol}{\mu L})}$$

DNB Synthesis Reaction Mix for the first step was prepared according to the following table 5:

Table 5. DNB synthesis reaction mix 1

Component	Volume (µL)
ssDNA library	V
Low TE buffer	20 - V
DNB synthesis buffer	20
Total volume	40

V represents variable sample volume that was previously calculated by the equation (4). 0.2 mL PCR tube was then placed into the thermocycler and the reaction was run under the following conditions described in table 6:

Table 6. Primer hybridization reaction conditions

Temperature	Time
Heated lid (105 °C)	On
95 °C	1 min
65 °C	1 min
40 °C	1 min
4 °C	Hold

The 0.2 mL PCR tube with the primer hybridization product was centrifuged briefly and placed on ice for the DNB making next step.

DNB synthesis reaction mix 2 was prepared by adding 4 µL of DNB Synthesis Enzyme Mix II (LC) to 40 µL of DNB Synthesis Enzyme Mix I. 44 µL of the mix were then added to 0.2 mL PCR tube containing DNB Synthesis Step 1 product, vortexed, centrifuged briefly, and placed into the thermocycler for 25 minutes at 30 °C.

20 µL of Stop DNB Reaction buffer were added once the thermocycler temperature has reached 4 °C. RCA reaction product was then gently mixed by pipetting 5 – 8 with the wide bore tip.

2.19.1. DNB quantification

The RCA reaction product was quantified using Qubit dsDNA High Sensitivity kit following the standard protocol: 1 µL of fluorescent dye was added to 199 µL HS buffer (per sample) to create a Master Mix. 192 µL of Master Mix were transferred to a 0.5 µL Qubit tube and 2 µL of RCA reaction product were added. Fluorescence was measured by benchtop Qubit Fluorometer (Thermo Fisher Scientific, USA).

2.19.2. DNB loading

DNBSEQ-G400RS Flow Cell (FCL) was taken out of the -20 °C storage and incubated for at least 60 minutes at room temperature. MGIDL-200H manual loader was used for DNB loading and required 30 µL of DNB per lane on the Flow-Cell. DNB loading mix was prepared in the new 8-tube PCR strip by adding 0.25 µL of Make DNB Enzyme Mix II (LC) to 8 µL of DNB Load Buffer II. The mix was then vortexed and centrifuged to get rid of possible bubbles at the bottom of each tube. 25 µL of DNB were then added to the loading mix and gently mixed 5 – 8 time with wide bore tips. Flow Cell was placed into the sealing gasket and 30 µL of DNB containing loading mix were aspirated with a wide bore tip. The tip was then inserted into the fluidics inlet, detached

from the pipette and DNB flow within the lane was carefully monitored. Once all the DNB was loaded, wide bore tip was removed from the fluidics inlet by counterclockwise rotation. After all lanes were filled with DNBs, the device was left to incubate at room temperature for 30 minutes with the front side upwards.

2.19.3. DNBSEQ-G400RS preparation

DNBSEQ-G400RS was prepared for sequencing starting with the 3-step Maintenance wash:

1. Washing cartridge was filled with 0.1 NaOH solution, placed into the sequencer and Maintenance wash was ran for 25 minutes.
2. Washing cartridge was filled with 1x TWEEN solution, placed into the sequencer and Maintenance wash was ran for 25 minutes.
3. Washing cartridge was filled with MilliQ H_2O, placed into the sequencer and Maintenance wash was ran for 25 minutes.

Additional 55 minutes long Regular wash step with MiliQ H_2O was required and performed before each sequencing run.

2.19.4. DNBSEQ-G400RS sequencing

DNBSEQ-G400RS FCL PE150 sequencing cartridge was removed from – 20 ^{o}C and left to thaw overnight at 4 ^{o}C.

Wells 1 and 2 of the sequencing cartridge were pierced with a sterile 1 mL tip. 2.400 mL of dNTPs Mix were added to well No. 1 followed by the addition of 2.400 mL of the Sequencing Enzyme Mix. 2.100 mL of dNTPs Mix II were added to well No. 2 followed by the addition of 2.100 mL of the Sequencing Enzyme Mix. Pierced holes were sealed with adhesive film provided with the kit, and the cartridge was mixed by shaking vigorously. 500 µL of MDA Enzyme mix were added to the MDA Reagent tube and mixed by inverting 4 – 6 times. Well No. 15 was then pierced by a sterile 1 mL tip and all of the MDA mix was transferred into that well.

Sequencing was run for about 72 hours on the DNBSEQ-G400RS as a PE150 sequencing method with a total of 310 reads (150 cycles for Read 1, 150 cycles for Read 2 and 10 barcode cycles). The expected sequencing depth was 30x for each sample with about 90Gb of data generated from one lane.

2.20. Genotyping and sequencing data statistical analysis

FastQ raw data from DNBSEQ-G400RS sequencer were uploaded to HPC and the automatic QC analysis was performed through the MegaBOLT Whole Genome Sequencing (WGS) pipeline with the built-in enhanced SOAPnuke algorithm. Genome mapping was performed manually by Integrative Genomic Viewer (IGV) v.2.11.9 open-source software (Broad Institute and the Reagent of University of California; available at www.igv.org).

Genotyping and sequencing SNP data statistical analysis was performed using the SNPstats online statistical tool (Catalan Institute of Oncology, Spain; available at www.snpstats.net).

3. RESULTS

3.1. DNA damage

The first step was to evaluate an overall DNA damage in whole blood and isolated peripheral blood mononuclear cells (PBMNC) and validate the difference between the whole blood comet assay approach and PBMNC comet assay approach. The DNA damage comparison was done based on the whole blood and PBMNC comet assay data from the control group and MS patient group.

Comet assay results show an increase in the level of DNA damage in MS patients compared to the control group (Fig. 11), the difference between DNA lesion level in MS patients and healthy subjects were statistically significant - $p = 0.0090$. Similar results were obtained if comet assay was performed on whole blood and peripheral mononuclear blood cells (lymphocytes).

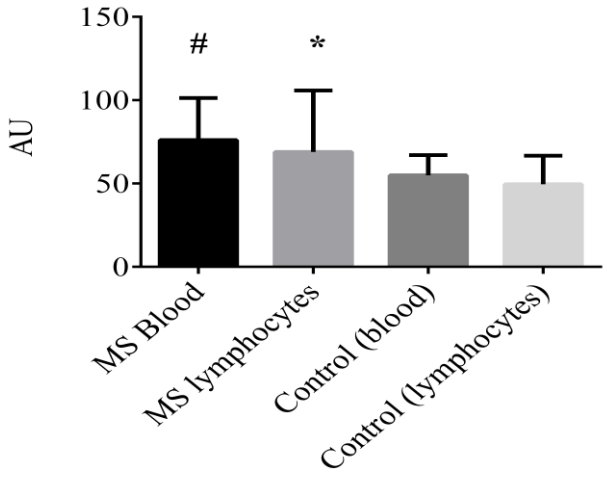

Figure 11. Level of DNA damage (arbitrary units) in whole blood cells and PBMNCs of MS patients (n = 26) and controls (n = 22). Data are presented as mean ± SD (arbitrary units). # and *- $p < 0.05$ of whole blood and PBMNCs of MS group *vs*. control group

3.2. Levels of oxidized DNA bases

Figures 12-1 and 12-4 depict the Comet assay results, revealing an elevated presence of DNA single-strand breaks in individuals diagnosed with MS compared to the healthy control subjects. These findings complement the previous outcomes obtained from the alkaline comet assay. To assess the quantity of oxidized bases, the DNA damage data was subtracted from the enzyme-induced damage data. Notably, the level of oxidized bases appears to be comparable

between the MS group (Figures 12-5 and 12-6) and the control group (Figures 12-3 and 12-4). Although individual variations among patients were notably diverse, the obtained results did not reach statistical significance (p = 0.919).

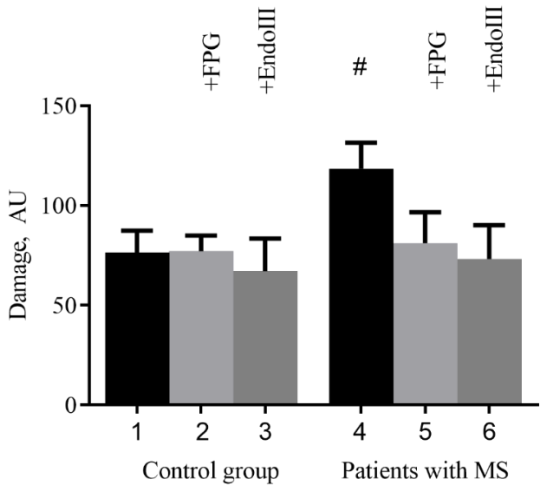

Figure 12. Modified comet assay data showing DNA damage levels and levels of oxidized bases (arbitrary units) in PBMNC of healthy controls (n = 22) and patients with MS (n = 26). 1 – Total DNA damage of healthy subjects; 2 and 3 – levels of oxidized bases in healthy subjects; 4 – total DNA damage of patients with MS; 5 and 6 – levels of oxidized bases in patients with MS. Data are presented as mean ± SEM (arbitrary units). # $p < 0.05$ *vs*. the control group; levels of oxidized bases were not statistically significant (p = 0.9190)

3.3. Nitric oxide production

The next step was to estimate overall levels of NO production in the study group consisting of MS patients and to compare the data with the control group. NO detection was done by Electron Paramagnetic Resonance (EPR).

The level of NO production also appeared to be higher in patients with MS (Fig. 13), and the difference between the control group and the study group was statistically significant $p < 0.0001$.

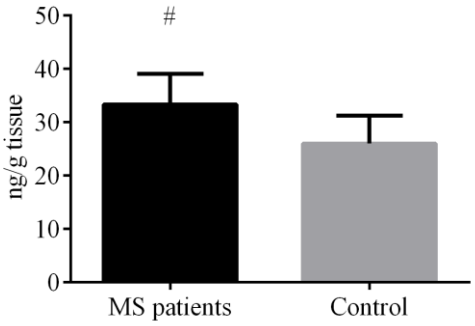

Figure 13. Rate of NO production in the blood of MS patients (n = 26) and healthy controls (n = 22) (ng/g tissue). Data are presented as mean ± SEM (arbitrary units). # - $p < 0.05$ *vs*. control group.

A significant increase in overall DNA damage might have been caused by oxidative stress as one of the primary factors affecting DNA integrity. Elevated levels of NO production give an idea that nitric oxide synthase (NOS) overproduction and accumulation of NO metabolic products might be the case. Thus, a more in-depth analysis was required to confirm these assumptions.

3.4. Nitrite levels in plasma and serum

To the best of our knowledge, there is currently no existing evidence to definitively establish whether determining metabolite concentrations in blood plasma or serum yields more accurate results. In this particular study, we investigated the concentrations of nitrite and nitrate in both plasma and serum samples obtained from patients diagnosed with MS. The results presented in Figure 14 demonstrate that the nitrite concentration in plasma and serum samples from healthy individuals is comparable, measuring at 0.64 ± 0.02 μM (Figure 14; Control group - P) in plasma and 0.65 ± 0.04 μM (Figure 14; Control group - S) in serum. On the contrary, the overall levels of nitrites in plasma and serum samples from patients with MS are significantly higher when compared to those of the healthy subjects. However, it is worth noting that the nitrite concentration in plasma appears to be higher than that in serum, measuring at 1.13 ± 0.05 μM (Figure 14; Patients with MS - P) in plasma and 0.79 ± 0.06 μM (Figure 14; Patients with MS - S) in serum.

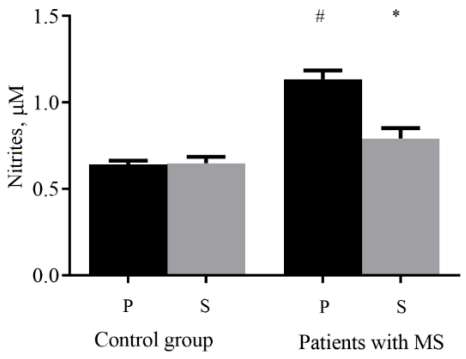

Figure 14. Concentrations of nitrites determined in human blood plasma and serum of patients with MS (n = 26) and healthy subjects (n = 25). P and S – plasma and serum samples correspondingly. Data are presented as mean ± SEM (μM). # and * $p < 0.05$ *vs*. the control group

3.5. Nitrate levels in plasma and serum

A similar pattern can be observed in the concentrations of nitrates (Figure 15), mirroring the trends seen in nitrite concentrations. Specifically, both plasma and serum samples from healthy individuals exhibit comparable levels of nitrates, measuring at 24.98 ± 1.20 μM (Figure 15; Control group - P) in plasma and 25.05 ± 3.44 μM (Figure 15; Control group - S) in serum. In contrast, samples obtained from patients diagnosed with MS demonstrate elevated levels of nitrates in both plasma and serum. Specifically, the concentrations of nitrates in plasma reach 33.67 ± 2.97 μM (Figure 15; Patients with MS - P), while those in serum are measured at 36.30 ± 3.81 μM (Figure 15; Patients with MS - S).

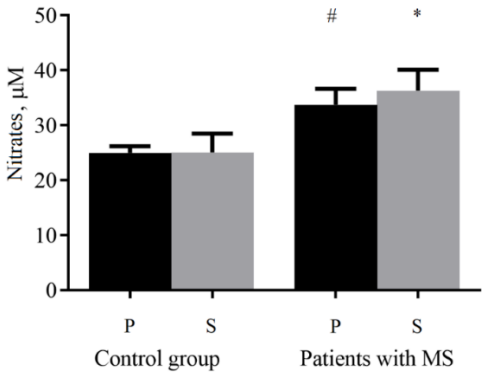

Figure 15. Concentrations of nitrates determined in human blood plasma and serum of patients with MS (n = 26) and healthy subjects (n = 25). P and S – plasma and serum samples. Data are presented as mean ± SEM (μM). # and * $p < 0.05$ *vs*. the control group

3.6. MDA levels in plasma and serum

MDA serves as a widely utilized biomarker for various disorders, including MS. The results presented in Figure 16 demonstrate a notable decrease in MDA levels observed in both plasma and serum samples obtained from patients diagnosed with MS compared to the healthy subjects. Specifically, the control samples in plasma and serum exhibit MDA levels of 5.33 ± 0.19 μM (Figure 16; Control group - P) and 6.07 ± 0.42 μM (Figure 16; Control group - S), respectively. In contrast, the plasma and serum samples from patients with MS display reduced MDA concentrations. Specifically, the MDA levels in plasma measure at 3.78 ± 0.32 μM (Figure 16; Patients with MS - P), while the levels in serum are recorded as 4.95 ± 0.23 μM (Figure 16; Patients with MS - S).

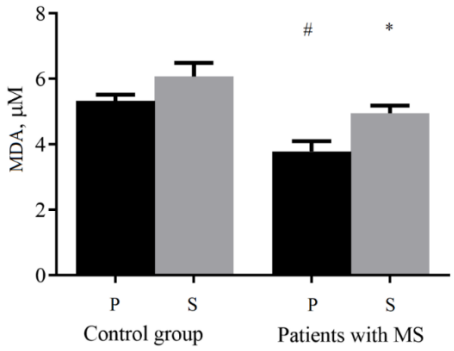

Figure 16. Concentrations of MDA, according to TBARS assay determined in human blood plasma and serum of patients with MS (n = 26) and healthy subjects (n = 25). P and S – plasma and serum samples. Data are presented as mean ± SEM (μM). # and * $p < 0.05$ *vs*. the control group

3.7. DNA damage and nitric oxide metabolites in T1D

DNA damage was previously evaluated by Evita Rostoka and Alise Dekante, and results were previously presented in the thesis by Evita Rostoka.

Method protocols were the same as previously described, but with a larger sample pool consisting of 57 control patients and 71 test subjects for comet assay; 31 control sample and 62 test subjects for serum nitrite measurements; 30 control samples and 69 test subjects for serum nitrate measurements. Results are presented on Figure 17.

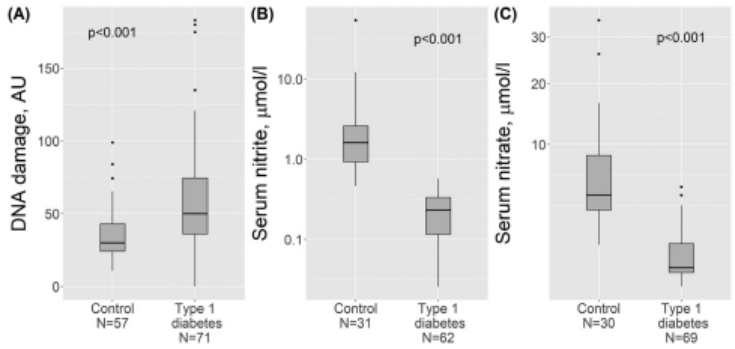

Figure 17. DNA damage, serum nitrite and nitrate concentrations in the leukocytes of healthy subjects and patients with type 1 diabetes. (A) Level of DNA damage in leukocytes expressed in AU. (B) Serum nitrite concentration (log10-transformed y-axis). (C) Serum nitrate concentration (sqrt-transformed y-axis).

All the data appeared to be statistically significant with p values < 0.001. Patients with Type 1 diabetes patients had higher levels of DNA lesions (Figure 17 – A) than the control group, but also high standard error for each group. In case of nitrates and nitrites patients with Type 1 diabetes had lower levels both of nitrites (Figure 17 – B) and nitrates (Figure 17 – C) also with high standard errors in both approaches.

3.8. Associations of DNA damage with nitrite and nitrate levels in T1D

Clinical and demographic factors did not show any significant difference in DNA damage levels. Thus, T1D patient group was divided into three groups based on the levels of DNA damage and correlated with nitric oxide metabolite levels (Fig 18). Spearman correlation analysis demonstrated a medium negative correlation between levels of DNA damage and serum nitrite ($R = -0.335$, $p = 0.008$).

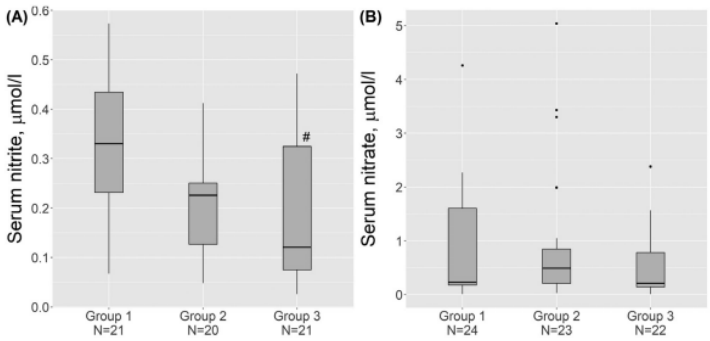

Figure 18. Serum nitrite (A) and serum nitrate (B) concentrations in groups of patients with T1D stratified according to the level of DNA damage. Group 1 – patients with AU 0-39.2, group 2 – patients with AU 39.2-63.7 and groups 3 – patients with AU ≥ 63.7. # - p value < 0.05 between groups 1 and 3.

3.9. Associations between MS biochemical markers

Significant findings emerged from the correlation analysis conducted on the biochemical markers. Particularly noteworthy were the correlations between the levels of NO and serum nitrites, as well as between plasma MDA levels and NO levels. The p-values obtained for these correlations were 0.022 for the relationship between NO and serum nitrite levels, and 0.0049 for the association between NO and plasma MDA levels, respectively. In both cases, a medium reverse correlation was observed, indicated by correlation coefficients ranging from ±0.40 to ±0.60. This implies that an increase in NO levels is accompanied by a decrease in plasma MDA levels, and vice versa. Furthermore, a statistically significant medium reverse correlation was observed between nitrite and nitrate levels in serum, with a p-value of 0.0013 and a correlation coefficient of -0.61. Another significant correlation was found between plasma MDA levels and serum nitrite levels, with a p-value of 0.0026. Additionally, two correlations approached significance, namely the correlations between plasma and serum nitrate levels (p-value of 0.035) and between serum MDA levels and serum nitrate levels (p-value of 0.084). To visualize these correlations, a heatmap was generated and presented in Figure 19.

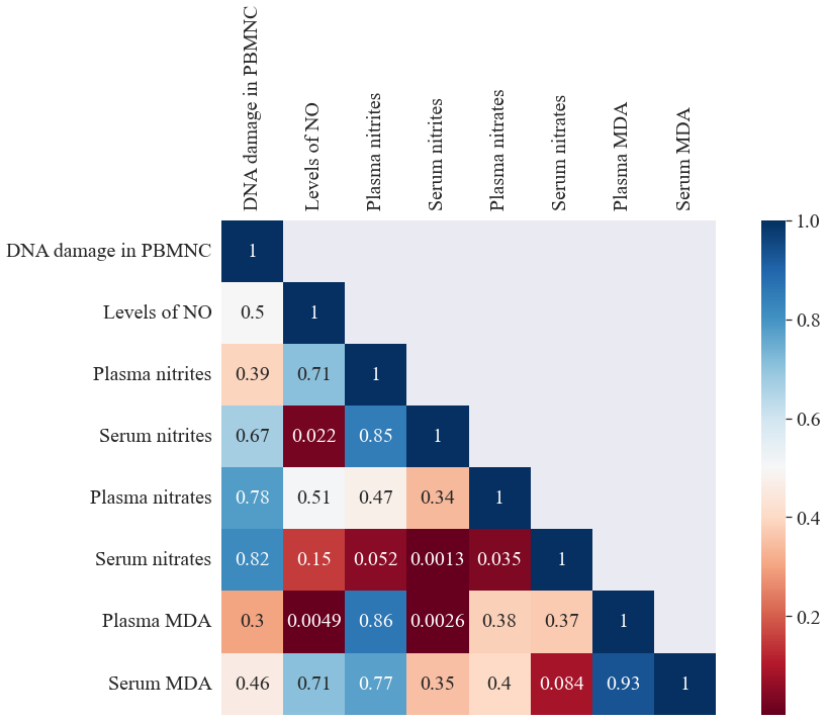

Figure 19. Correlation heatmap between identified biochemical MS markers. Nitrite levels were analyzed by the Spearman correlation test (data were not following normal distribution), other correlations were analyzed by the Pearson test. Numerical values represent p values from dark blue – no correlation to dark red – significant correlation.

3.10. Associations between MS biochemical markers and patient descriptors

DNA damage in lymphocytes (PBMNC), levels of NO, plasma and serum nitrate, nitrite and MDA levels were correlated with demographic and clinical descriptors (gender, age, disease type – RR or SP, disease duration, EDSS score and disease modifying therapies – DMT) of MS patients. The most significant medium correlation with p value 0.027 and $\eta = 0.46$ were observed for serum nitrites that showed higher levels in females (median value of 0.93 μM) when compared to males (median value of 0.56 μM).

Another significant observation ($p = 0.0445$) is the medium reverse correlation ($\rho = -0.41$) between serum nitrites and EDSS score. It seems that with the progression with MS levels of serum nitrite tend to decrease. Additionally, serum nitrate levels showed a close to significant association ($r = -0.37$; $P = 0.066$) with patient age. Results are visualized as a heatmap on figure 20. A more detailed information about each parameter can be found in Appendix A tables A-1 to A-5.

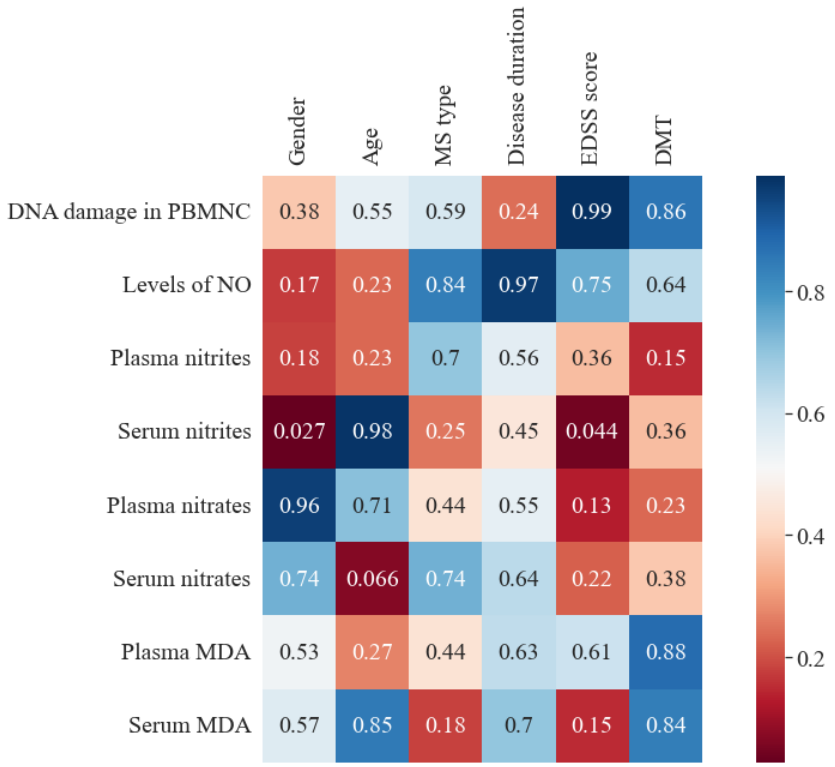

Figure 20. Correlation heatmap between identified biochemical MS markers and patient descriptors. Numerical values represent p values from dark blue – no correlation to dark red – significant correlation. PBMNC – peripheral blood mononuclear cells, MS – multiple sclerosis, MDA – malondialdehyde, DMT – disease modifying therapies, EDSS Expanded Disability Status Scale.

3.11. Genotyping

3.11.1. SNP distribution in the study group

SNP genotyping was performed on seven loci of five DNA repair genes. The current genotyping experiment was conducted as a MS cohort study to investigate if the chosen SNPs in Latvian population follow the same trend observed in NCBI database. The result comparison is summarized in Table 7 and visualized on Figure 21:

Table 7. Reference and alternative allele frequency comparison between NCBI and experimental data

	NCBI Global	NCBI European	Experimental
rs189037			
A	0.48	0.43	0.49
G	0.52	0.57	0.51
rs1136410			
A	0.83	0.84	0.84
G	0.17	0.16	0.16
rs3219090			
T	0.35	0.33	0.28
C	0.65	0.67	0.72
rs1800975			
T	0.33	0.33	0.31
G	0.67	0.67	0.69
rs2228001			
T	0.59	0.58	0.62
G	0.41	0.42	0.38
rs1799782			
G	0.93	0.94	0.92
A	0.07	0.06	0.08
rs25487			
T	0.34	0.36	0.51
C	0.66	0.64	0.49

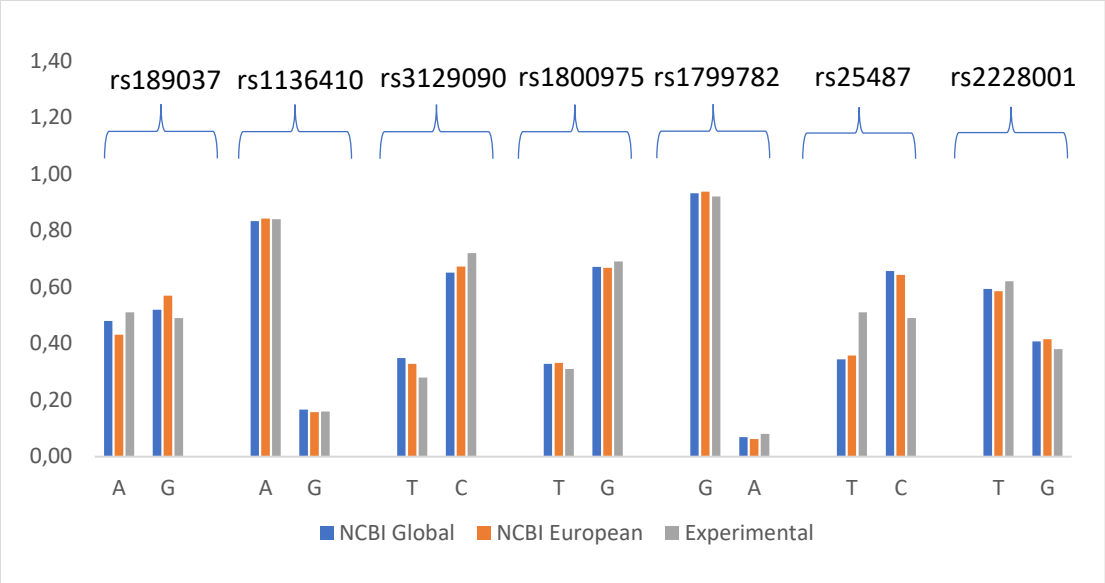

Figure 21. Comparison of SNP frequencies in Latvian population with data from NCBI database

Based on the data from Table 21 and Figure 22, most of the SNP allele frequencies follow the same trend as indicated by NCBI database. Few SNP allele frequencies show slight deviations from the general trend. SNP rs189037 reference allele A frequency (0.51) appear to be higher when compared to NCBI data both from Global (0.48) and European (0.43) data pools. Alternative allele G frequency (0.49), however, is slightly lower than in the European pool (0.57), but is quite close to the Global (0.52) data pool. Similar observation takes place in case of SNP rs3219090, with reference allele T frequency (0.28) being lower than both NCBI (0.35 for Global and 0.28 for European) data pools, and alternative allele C frequency (0.72) being slightly elevated compared to both NCBI (0.65 for Global and 0.67 for European) data pools. SNP rs25487 shows a noticeable deviation from the general trend. With reference allele C being much more frequent in both NCBI (0.49 for Experimental, 0.64 for European and 0.66 for Global) data pools, and alternative allele T being noticeably less frequent with 0.51 for Experimental data, 0.36 for European NCBI data and 0.34 for Global NCBI data. All SNP allele frequencies, except PARP1 rs1136410 A > G, show minor and major differences. This could mean that SNP allele distribution in Latvia population follow a different trend. Control samples are needed to further investigate this phenomenon.

3.11.2. SNP association with MS

One method for assessing the association between the selected SNP and the disease is to examine deviations from Hardy-Weinberg (HW) equilibrium. Tables 8a and 8b provides information on allele frequencies, genotypes, and HW equilibrium. A significant deviation from HW equilibrium was observed for the XRCC1 rs25487 T>C variant (PHW = 0.000213). The results indicate that Latvian MS patients exhibit a higher prevalence of the rare T allele (MAF = 0.66) compared to the data available from NCBI (T = 0.3658 according to 1000Genome and T = 0.357623 according to NCBI European). Since, MS is predominant in females, allele frequencies were compared between male and female groups. Results in tables 8a and 8b indicate that there is no significant difference in allele frequencies between two groups, thus both groups can be used together for further analysis.

Table 8a. MS collection SNP genotyping result

SNP	**MS collection Frequency, % (sample number)**			**Statistical analysis between genders**	
	All samples	**Females**	**Males**	**P_χ**	**V_1**
*ATM rs189037 G>**A***					
MAF	49.48	51.33	42.86	0.33	0.07
AA	28.13 (27)	26.67 (20)	33.33 (7)		
AG	44.79 (43)	44.00 (33)	47.62 (10)	0.07	0.1
GG	27.08 (26)	29.33 (22)	19.05 (4)		
P_{HW}	0.65	0.65	1	-	-
*PARP1 rs1136410 **A**>G*					
MAF	19.02	19.44	17.5	0.78	0.02
AA	69.57 (64)	69.44 (50)	70.00 (14)		
AG	22.83 (21)	22.22 (16)	25.00 (5)	1	0.06
GG	7.60 (7)	8.34 (6)	5.00 (1)		
P_{HW}	2.53 x10-2	0.07	0.92	-	-
*PARP1 rs3219090 **C**>T*					
MAF	31.11	32.67	35	0.55	0.04
CC	51.11 (46)	52.86 (37)	45.00 (9)		
CT	35.56 (32)	34.28 (24)	40.00 (8)	0.77	0.06
TT	13.33 (12)	12.86 (9)	15.00 (3)		
P_{HW}	0.29	0.27	0.69	-	-

MAF minor allele frequency, P_{HW} statistical significance between expected and real genotype distribution according to Hardy-Weinberg equilibrium. Common alleles in bold.

Table 8b. MS collection SNP genotyping result

SNP	MS collection Frequency, % (sample number)			Statistical analysis between genders	
	All samples	**Females**	**Males**	**P_χ**	**V_1**
*XPA rs1800975 T>**C***					
MAF	31.25	32.67	26.19	0.61	0.04
CC	46.88 (45)	45.33 (34)	52.38 (11)		
CT	43.75 (42)	44.00 (33)	42.86 (9)	0.88	0.06
TT	9.38 (9)	10.67 (8)	4.76 (1)		
P_{HW}	0.99	1	0.95	-	-
*XPC rs2228001 G>**T***					
MAF	35.87	33.33	47.06	0.13	0.11
TT	40.22 (37)	45.33 (34)	17.65 (3)		
TG	47.83 (44)	42.67 (32)	70.59 (12)	0.28	0.15
GG	11.96 (11)	12.00 (9)	11.76 (2)		
P_{HW}	0.9	0.91	0.15	-	-
*XRCC1 rs1799782 **G**>A*					
MAF	7.81	6.67	11.9	0.26	0.08
GG	84.38 (81)	86.67 (65)	76.19 (16)		
GA	15.62 (15)	13.33 (10)	23.81 (5)	0.24	0.12
AA	0 (0)	0 (0)	0 (0)		
P_{HW}	0.658	0.74	0.62	-	-
*XRCC1 rs25487 T>**C***					
MAF	54.17	53.33	57.14	0.66	0.03
CC	10.42 (10)	13.33 (10)	0 (0)		
CT	70.83 (68)	66.67 (50)	85.71 (18)	0.17	0.2
TT	18.75 (18)	20.00 (15)	14.29 (3)		
P_{HW}	2.13×10^{-4}	1.40×10^{-2}	1.76×10^{-3}	-	-

MAF minor allele frequency, P_{HW} statistical significance between expected and real genotype distribution according to Hardy-Weinberg equilibrium. Common alleles in bold.

3.11.3. SNP correlation with biochemical markers

The statistical analysis conducted has revealed a significant correlation between the XRCC1 rs25487 T>C SNP and DNA damage in PBMNC, with a p-value of 0.0093. Specifically, patients with the rare homozygous genotype TT demonstrated approximately twice the increase in DNA damage compared to individuals with the CC and CT genotypes. Additionally, the XRCC1 rs25487 SNP exhibited correlations, nearing statistical significance, with levels of NO ($p = 0.079$), serum nitrites ($p = 0.05$), plasma MDA levels ($p = 0.059$), and serum MDA levels ($p = 0.093$).PARP1 rs11364110 A>G SNP indicated a close to significant correlation with plasma

nitrite levels (p = 0.046). Patients with rare GG genotype had a notable increase in nitrite levels in plasma. Results are visualized on figure 22, and a more detailed information can be found in Appendix B tables B-1 to B-8. Interestingly, levels of NO followed a similar trend to DNA damage, being elevated in patients with the T allele present in their genotype. On the other hand, serum nitrite levels tended to be higher when the C allele was present in the genotype. Moreover, plasma MDA levels demonstrated a decrease of approximately 1.5 times if at least one rare T allele was present in the genotype. Regarding serum MDA levels, it appears that the common C allele influenced the increase in MDA levels. Furthermore, another SNP, rs1799782 G>A, within the same XRCC1 gene, exhibited a close to significant correlation with plasma nitrate levels. However, a larger sample pool is required to draw more definitive conclusions, despite the observation of slightly increased nitrate levels in individuals with the common genotype GG.

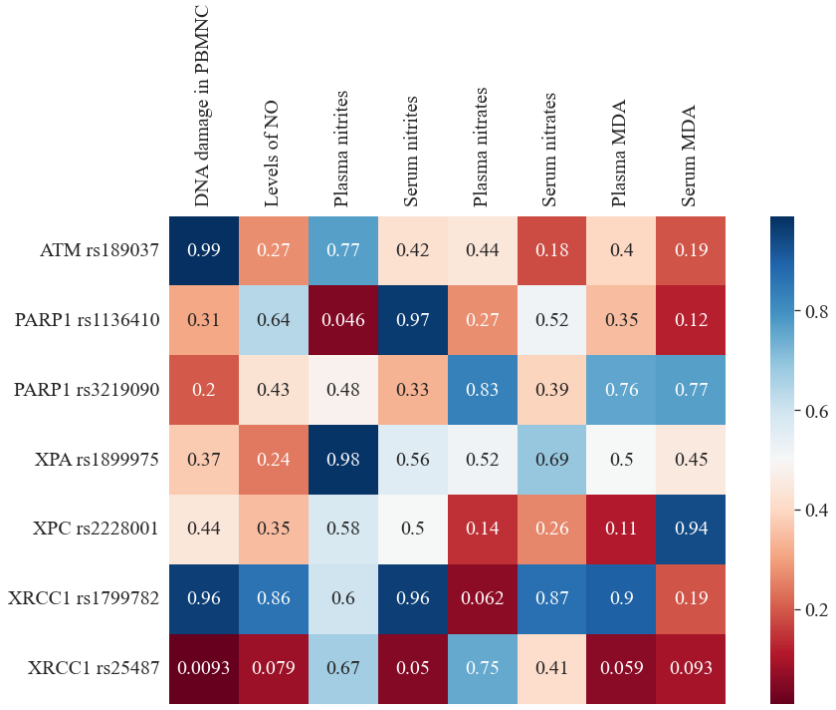

Figure 22. Correlation heatmap between identified biochemical MS markers and SNPs. Numerical values represent p values from dark blue – no correlation to dark red – significant correlation.

3.12. Next Generation Sequencing PCR product quality control

Fragment size of the dsDNA product was evaluated by Agilent 4200 TapeStation system (Figure 23).

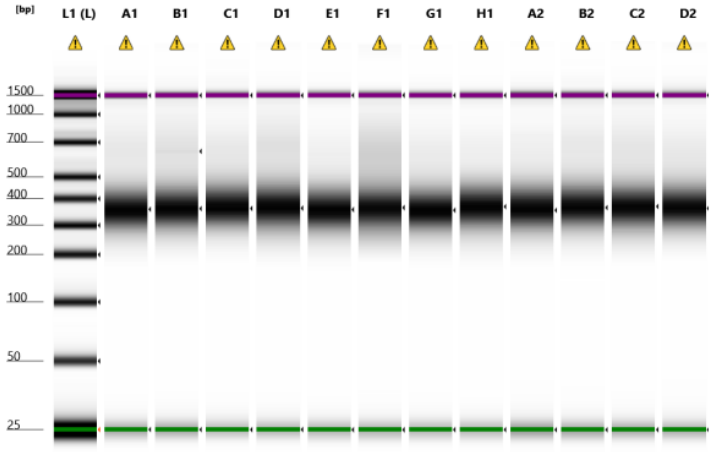

Figure 23. General illustration of dsDNA product quality. L1 – DNA ladder

Detailed information regarding the exact fragment size and the degree of sample purification was obtained from electropherogram for each sample (Figure 24).

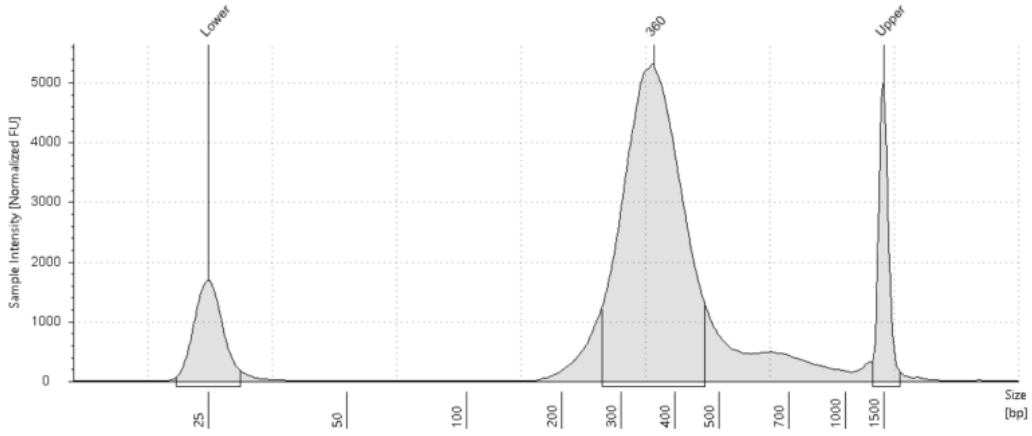

Figure 24. An example of electropherogram for sample A1

Agilent 4200 TapeStation analysis has shown that all samples have the consistent and uniform fragment size of about 360 bp. Samples were purified to a satisfactory degree and were suitable for PE150 sequencing approach.

3.13. Low coverage Copy Number Variation (CNV) analysis

To get an insight of NGS results for MS patients 60 MS samples were analyzed in a pool. Each sample had approximately 1x to 2x sequencing depth. Low quality sequence filtering, alignment and copy number variation detection were performed on these samples. Sequencing results are presented as a heatmap (Figure 25).

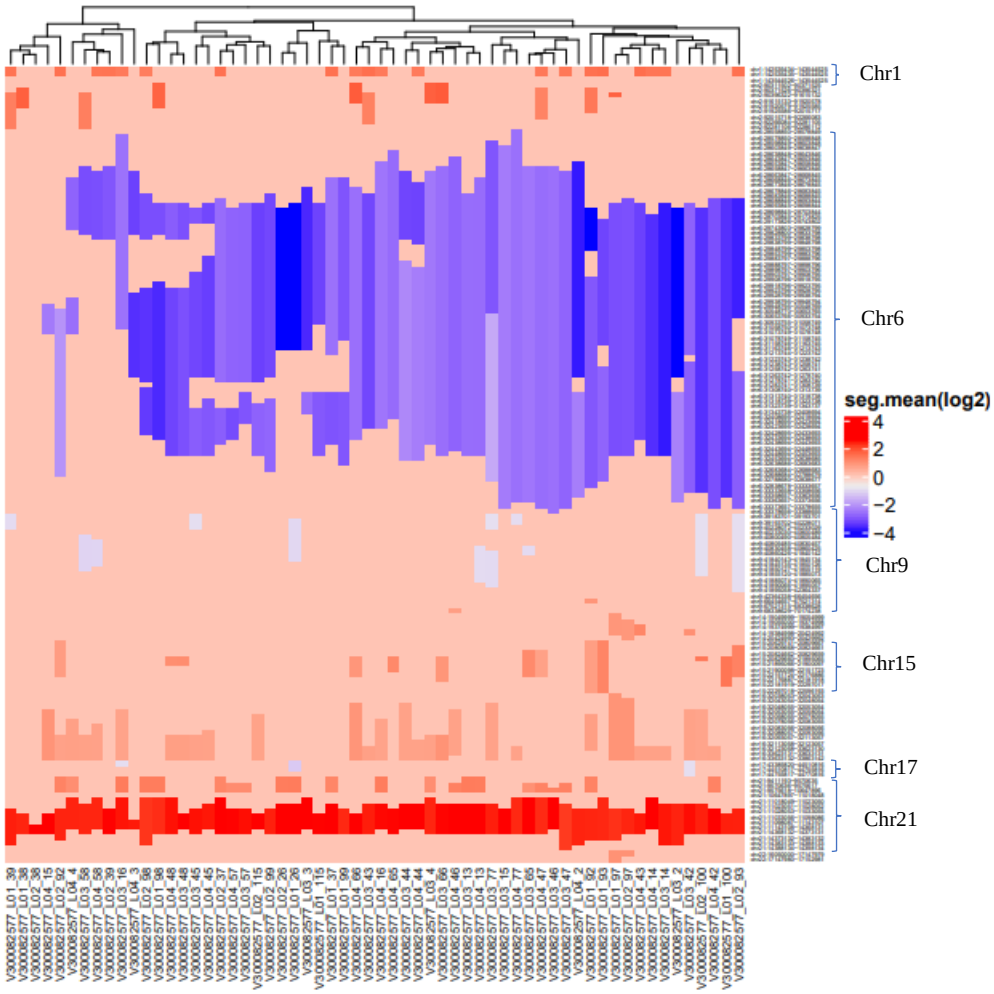

Figure 25. Heatmap representing the NGS CNV data of 60 low coverage MS samples

Considering the limitations of low coverage data, fragments up to the size of 1Mb were mainly looked at. Large fragment variations were mainly found in chromosomal regions of Chr1 (142535434 – 143544526), Chr6 (28558850 – 33388655), Chr9 (39183701 – 70174238), Chr15

(20629741 – 22297018), Chr17 (43385820 – 44770816) and Chr21 (9411193 – 14398134) (Figure 25).

Genomic data of 2 normal (high coverage) Latvians were randomly selected and 2x/5x data were extracted, same parameters were used as for other 60 samples. Both control samples were extrapolated together with 60 samples of the study group. Result is presented as heatmap on Figure 26.

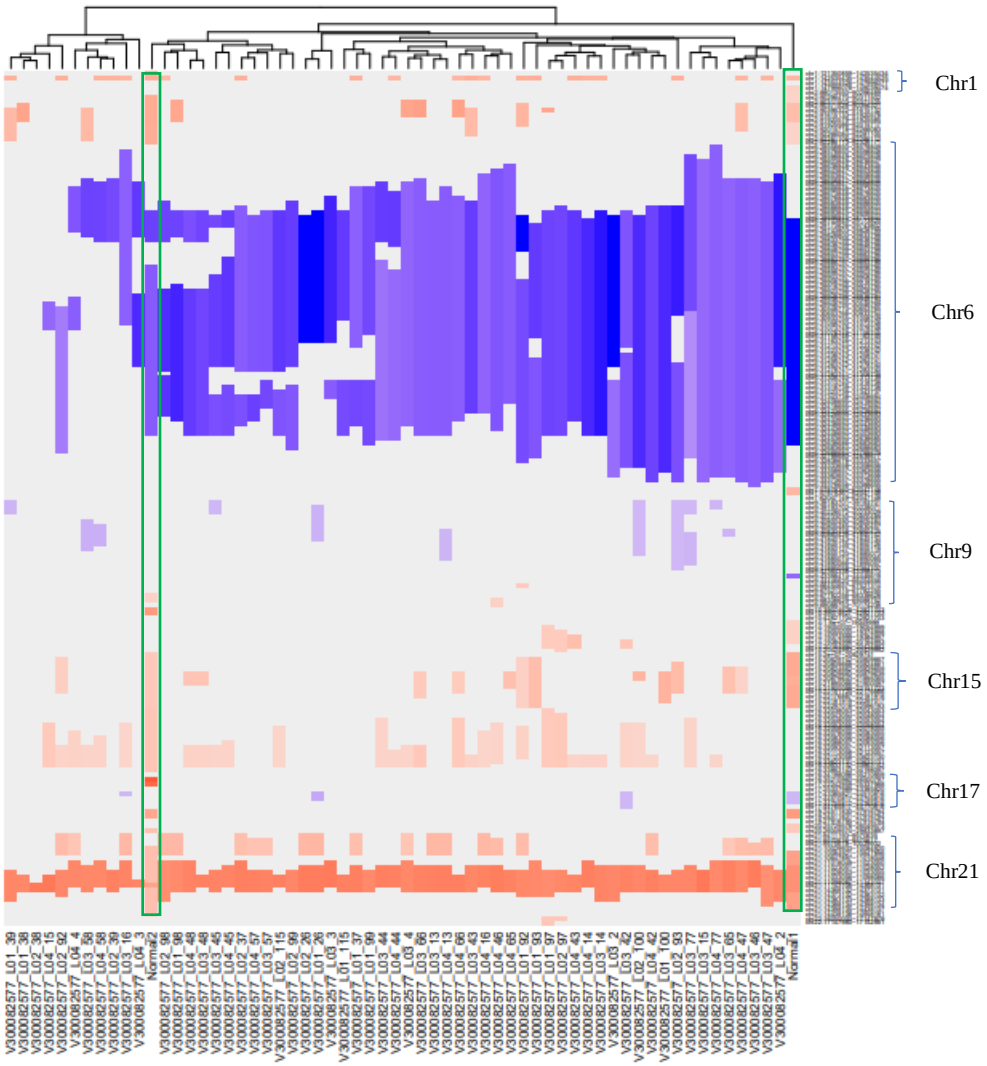

Figure 26. 60 MS sample and 2 healthy control CNV result extrapolated together in a heatmap. Green boxes – high coverage sample regions.

Homologues deletion of Chr6 and amplification of Chr21 were also present in 2 normal samples. This indicates that these occurrences might not be a feature of MS. Particularly low coverage fragments create an illusion of homozygous deletion in Chr6 region, but due to their low

consistency with reference genome, might as well not be considered. There is a noticeable loss of heterozygosity in Chr9: 39183701-42364337 region for 11 samples out of 60, which leads to an assumption that this region might be connected to the development of MS.

3.14. Next Generation Sequencing for SNP identification

Whole Genome Sequencing for 12 human DNA samples was performed to confirm the identity to genotyping result and, thus, possible use to check additional SNPs. Each sample was sequenced with a 30x coverage and about 80Gb of data. Data analysis was performed by MGI HPC with the established WGS pipeline. Mapping was done by the open source IGV software.

Allele frequencies were calculated for each sequenced SNP and summarized in Tables 9a and 9b.

Table 9a. Repair gene allele and genotype frequencies

Allele/Genotype	**All subjects (n = 12)**	**Sex: F (n = 8)**	**Sex: M (n = 4)**
ATM rs189037	**Frequency (sample number)**		
A	0.50 (12)	0.50 (8)	0.50 (4)
G	0.50 (12)	0.50 (8)	0.50 (4)
AA	0.33 (4)	0.25 (2)	0.50 (2)
GA	0.33 (4)	0.50 (4)	0.00
GG	0.33 (4)	0.25 (2)	0.50 (2)
PARP1 rs1136410			
A	0.83 (20)	0.88 (14)	0.75 (6)
G	0.17 (4)	0.12 (2)	0.25 (2)
AA	0.75 (9)	0.75 (6)	0.75 (3)
AG	0.17 (2)	0.25 (2)	0.00
GG	0.08 (1)	0.00	0.25 (1)
PARP1 rs3219090			
T	0.71 (17)	0.69 (11)	0.75 (6)
C	0.29 (7)	0.31 (5)	0.25 (2)
CC	0.17 (2)	0.12 (1)	0.25 (1)
CT	0.25 (3)	0.38 (3)	0.00
TT	0.58 (7)	0.50 (4)	0.75 (3)
XPC rs2228001			
T	0.62 (15)	0.62 (10)	0.62 (5)
G	0.38 (9)	0.38 (6)	0.38 (3)
TT	0.17 (2)	0.12 (1)	0.25 (1)
TG	0.42 (5)	0.5 (4)	0.25 (1)
GG	0.42 (5)	0.38 (3)	0.50 (2)

Table 9b. Repair gene allele and genotype frequencies

Allele/Genotype	**All subjects (n = 12)**	**Sex: F (n = 8)**	**Sex: M (n = 4)**
XPA rs1800975	**Frequency (sample number)**		
T	0.33 (8)	0.44 (7)	0.12 (1)
C	0.67 (16)	0.56 (9)	0.88 (7)
CC	0.42 (5)	0.25 (2)	0.75 (3)
CT	0.50 (6)	0.62 (5)	0.25 (1)
TT	0.08 (1)	0.12 (1)	0.00
XRCC1 rs1799782			
G	0.92 (22)	0.94 (15)	0.88 (7)
A	0.08 (2)	0.06 (1)	0.12 (1)
GA	0.17 (2)	0.12 (1)	0.25 (1)
GG	0.83 (10)	0.88 (7)	0.75 (3)
XRCC1 rs25487			
T	0.50 (12)	0.44 (7)	0.62 (5)
C	0.50 (12)	0.56 (9)	0.38 (3)
CC	0.17 (2)	0.12 (1)	0.25 (1)
TC	0.67 (8)	0.62 (5)	0.75 (3)
TT	0.17 (2)	0.25 (2)	0

NGS sample group, consisting of 8 female and 4 male subjects, was too small to make any statistical conclusions. However, allele frequencies should be in the same ballpark as the genotyping data. Figure 27 summarizes the comparison of NGS allele frequencies with genotyping data.

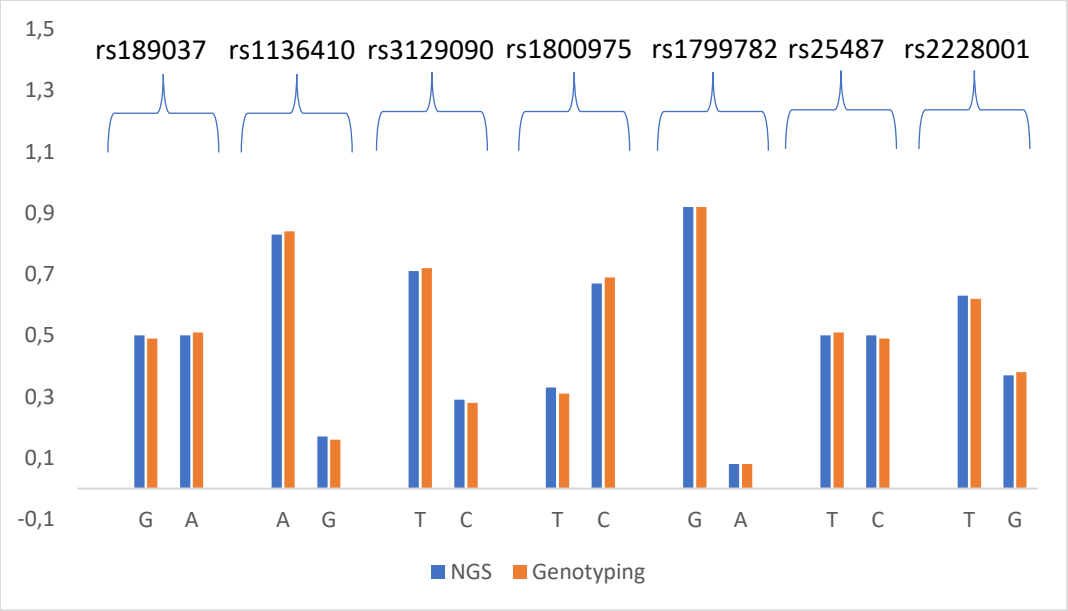

Figure 27. Allele frequency comparison between NGS and genotyping data.

Due to the difference in sample pools, with NGS having a significantly lower patient count, there are dissimilarities in numerical values. However, all frequencies seem to follow the same pattern in both methods.

3.15. MS candidate gene SNPs

Next Generation Sequencing was performed as a cohort analysis for 12 randomly chosen MS patients from the genotyping group. Similarly, to the genotyping predominantly female patients were in the study group (66.67 % of females and 33.33 % of males) as shown in Table 21.

Seven SNPs of MS-related genes rs2229857 (ADAR), rs12557782 (GRIA3), rs733254 (ZFAT), rs9527281 (STARD13), rs11787532 (ZFHX4), rs2248202 (IFNAR2) and rs7308076 (CIT) were chosen based on previous reports about positive association with IFN-β treatments (Bourguiba-Hachemi et al., 2016). Additionally, SNP rs350845 of another DNA repair gene SIRT6, responsible for aging, was identified. Allele frequencies are summarized in Tables 10a and 10b. The comparison with NCBI was also performed for all the chosen SNPs.

Table 10a. Allele and genotype frequencies of MS-candidate gene SNPs

Allele/Genotype	**All subjects (n = 12)**	**Sex: F (n = 8)**	**Sex: M (n = 4)**
ADAR rs2229857	**Frequency (sample number)**		
C	0.62 (15)	0.56 (9)	0.75 (6)
T	0.38 (9)	0.44 (7)	0.25 (2)
CC	0.33 (4)	0.25 (2)	0.5 (2)
CT	0.58 (7)	0.62 (5)	0.5 (2)
TT	0.08 (1)	0.12 (1)	0
GRIA3 rs12557782			
A	0.71 (17)	0.69 (11)	0.75 (6)
G	0.29 (7)	0.31 (5)	0.25 (5)
AA	0.5 (6)	0.38 (3)	0.75 (3)
AG	0.42 (5)	0.62 (5)	0
GG	0.08 (1)	0	0.25 (1)
ZFAT rs733254			
C	0.75 (18)	0.69 (11)	0.88 (7)
A	0.25 (6)	0.31 (5)	0.12 (1)
AA	0.08 (1)	0.12 (1)	0
CA	0.33 (4)	0.38 (3)	0.25 (1)
CC	0.58 (7)	0.5 (4)	0.75 (3)
STARD13 rs9527281			
T	0.67 (16)	0.69 (11)	0.62 (5)
G	0.33 (8)	0.31 (5)	0.38 (3)
GG	0.17 (2)	0.12 (1)	0.25 (1)
TG	0.33 (4)	0.38 (3)	0.25 (1)
TT	0.50 (6)	0.50 (4)	0.50 (2)

Table 10b. Allele and genotype frequencies of MS-candidate gene SNPs

Allele/Genotype	All subjects (n = 12)	Sex: F (n = 8)	Sex: M (n = 4)
ZFHX4 rs11787532			
G	0.83 (20)	0.94 (15)	0.62 (5)
C	0.17 (4)	0.06 (1)	0.38 (3)
GC	0.33 (4)	0.12 (1)	0.75 (3)
GG	0.67 (8)	0.88 (7)	0.25 (1)
IFNAR2 rs2248202			
A	0.88 (21)	0.88 (14)	0.88 (7)
C	0.12 (3)	0.12 (2)	0.12 (1)
AA	0.75 (9)	0.75 (6)	0.75 (3)
AC	0.25 (3)	0.25 (2)	0.25 (1)
SIRT6 rs350845			
G	0.83 (20)	0.88 (14)	0.75 (6)
A	0.17 (4)	0.12 (2)	0.25 (2)
GA	0.33 (4)	0.25 (2)	0.50 (2)
GG	0.67 (8)	0.75 (6)	0.50 (2)
CIT rs7308076			
C	0.58 (14)	0.44 (7)	0.88 (7)
T	0.42 (10)	0.56 (9)	0.12 (1)
CC	0.42 (5)	0.25 (2)	0.75 (3)
CT	0.33 (4)	0.38 (3)	0.25 (1)
TT	0.25 (3)	0.38 (3)	0

All SNP allele frequencies follow the similar trend with reference allele being prevalent over alternative allele both in female and male subjects. The only exception is rs7308076 in CIT with alleles C and T total frequencies following the same trend (0.58 and 0.42 respectively), but with a dominance of allele C (0.88). ADAR gene SNP rs2229857 and ZFAT gene SNP rs733254 manifested the presence of rare genotypes TT (0.12 for ADAR rs2229857) and AA (0.12 for ZFAT rs733254) also exclusively in female patients. The similar picture is observed in CIT gene SNP rs7308076. The rare genotype TT (0.38) was found present exclusively in female patients. Rare genotype GG in STARD13 SNP rs9527281 was observed in both patient groups (0.12 for females and 0.25 for males). GRIA3 gene SNP rs12557782 presented a different picture of a rare genotype GG (0.25) found only in male subjects.

Allele frequencies for the chosen SNPs of MS-related genes were compared with the NCBI data. The result comparison is summarized in Table 11 and visualized on Figure 28:

Table 11. The comparison of MS-candidate gene SNPs experimental data with NCBI database

	NCBI Global	NCBI European	Experimental
ADAR rs2229857			
C	0.69	0.7	0.62
T	0.31	0.3	0.38
GRIA3 rs12557782			
A	0.59	0.59	0.71
G	0.41	0.41	0.29
ZFAT rs733254			
C	0.73	0.74	0.75
A	0.27	0.26	0.25
STARD13 rs9527281			
T	0.66	0.66	0.67
G	0.34	0.34	0.33
ZFHX4 rs11787532			
G	0.91	0.89	0.83
C	0.09	0.11	0.17
IFNAR2 rs2248202			
A	0.68	0.67	0.88
C	0.32	0.33	0.12
SIRT6 rs350845			
G	0.88	0.89	0.83
A	0.12	0.11	0.17
CIT rs7308076			
C	0.6	0.62	0.58
T	0.4	0.38	0.42

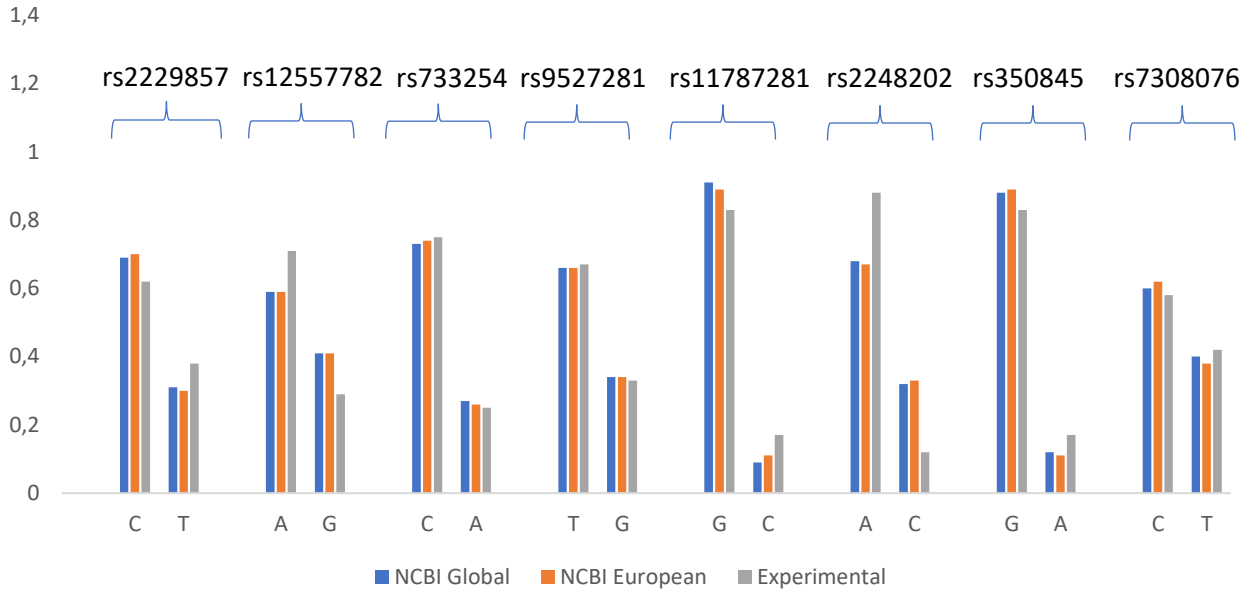

Figure 28. Visual presentation of allele frequency comparison between NGS experimental data and NCBI database.

Based on the numerical values in Table 25 and visual representation on Figure 27, most of the SNP allele frequencies correspond to the data available in NCBI database. The most obvious outliers in this case are rs2229857 with the slightly higher frequency of alternative allele T (0.38) in the experimental data; rs12557782 with the significant frequency increase of reference allele A (0.71) and frequency decrease of alternate allele G (0.29); rs2248202 with a huge increase in reference allele A frequency (0.88) and decrease in alternate allele C frequency (0.12).

3.16. Nitric Oxide Synthase (NOS) related genes

Patients with MS had elevated levels of nitrites and nitrates in the blood. Cumulatively that means an overall high levels of nitric oxide. This observation raises a question about NOS activity and possible mutations. The primary genes for NO metabolism regulation NOS1 and NOS2 were chosen as objects of interest. Six SNPs (three for each gene) were identified and evaluated. Allele frequencies summarized in Table 12.

Table 12. Allele and genotype frequencies for NOS1 and NOS2 genes SNPs

Allele/Genotype	**All subjects (n = 12)**	**Sex: F (n = 8)**	**Sex: M (n = 4)**
NOS1 rs1047735	**Frequency (sample number)**		
G	0.62 (15)	0.69 (11)	0.50 (4)
A	0.38 (9)	0.31 (5)	0.50 (4)
AA	0.08 (1)	0.12 (1)	0
GA	0.58 (7)	0.38 (3)	1 (4)
GG	0.33 (4)	0.5 (4)	0
NOS1 rs3741475			
G	0.62 (15)	0.69 (11)	0.50 (4)
A	0.38 (9)	0.31 (5)	0.50 (4)
AA	0.08 (1)	0.12 (1)	0
GA	0.58 (7)	0.38 (3)	1 (4)
GG	0.33 (4)	0.50 (4)	0
NOS1 rs2682826			
G	0.58 (14)	0.62 (10)	0.50 (4)
A	0.42 (10)	0.38 (6)	0.50 (4)
AA	0.08 (1)	0.12 (1)	0
GA	0.67 (8)	0.5 (4)	1 (4)
GG	0.25 (3)	0.38 (3)	0
NOS2 rs944725			
C	0.58 (14)	0.62 (10)	0.50 (4)
T	0.42 (10)	0.38 (6)	0.50 (4)
CC	0.33 (4)	0.38 (3)	0.25 (1)
CT	0.50 (6)	0.50 (4)	0.5 (2)
TT	0.17 (2)	0.12 (1)	0.25 (1)
NOS2 rs2248814			
G	0.58 (14)	0.56 (9)	0.62 (5)
A	0.42 (10)	0.44 (7)	0.38 (3)
AA	0.25 (3)	0.25 (2)	0.25 (1)
GA	0.33 (4)	0.38 (3)	0.25 (1)
GG	0.42 (5)	0.38 (3)	0.50 (2)
NOS2 rs2255929			
T	0.58 (14)	0.62 (10)	0.50 (4)
A	0.42 (10)	0.38 (6)	0.50 (4)
AA	0.17 (2)	0.12 (1)	0.25 (1)
TA	0.50 (6)	0.50 (4)	0.50 (2)
TT	0.33 (4)	0.38 (3)	0.25 (1)

All three NOS1 SNPs have shown similar numerical values for allele frequencies with reference allele G dominating over alternative allele A in general and in female subjects. Rare Genotypes AA were present only in female subjects. In case of NOS2 SNPs the similar picture was observed. With allele frequencies distributed in the favor of reference allele C for rs944725 (0.58), G for rs2248814 (0.58) and T for rs2255929 (0.58). Rare genotypes, however, were distributed both in female and male study groups.

Table 13. NOS1 and NOS2 SNPs allele frequencies in comparison with NCBI

	NCBI Global	**NCBI European**	**Experimental**
NOS1 rs1047735			
G	0.69	0.69	0.62
A	0.31	0.31	0.38
NOS1 rs3741475			
G	0.78	0.78	0.62
A	0.22	0.22	0.38
NOS1 rs2682826			
G	0.73	0.72	0.58
A	0.27	0.28	0.42
NOS2 rs944725			
C	0.6	0.61	0.58
T	0.4	0.39	0.42
NOS2 rs2248814			
G	0.59	0.58	0.58
A	0.41	0.42	0.42
NOS2 rs2255929			
T	0.54	0.56	0.58
A	0.46	0.44	0.42

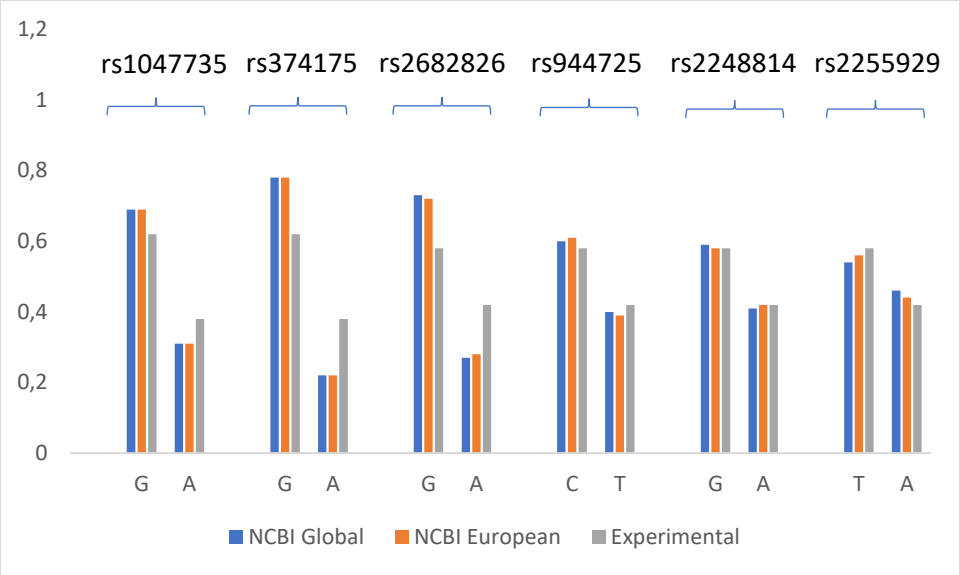

Figure 29. NOS1 and NOS2 SNPs allele frequencies in comparison with NCBI

Allele frequencies for NOS1 and NOS2 SNPs were compared with NCBI database (Table 13 and Figure 29). NOS1 SNPs rs1047735, rs374175 and rs2682826 show dissimilarities with NCBI data.

3.17. Linkage disequilibrium

A correlation between the variances within the same chromosome showing whether the population-wise association happens more often for the linked variances than unlinked. Linkage disequilibrium for rs1047735, rs3741475, rs2682826 and rs7308076 is presented on Figure 28.

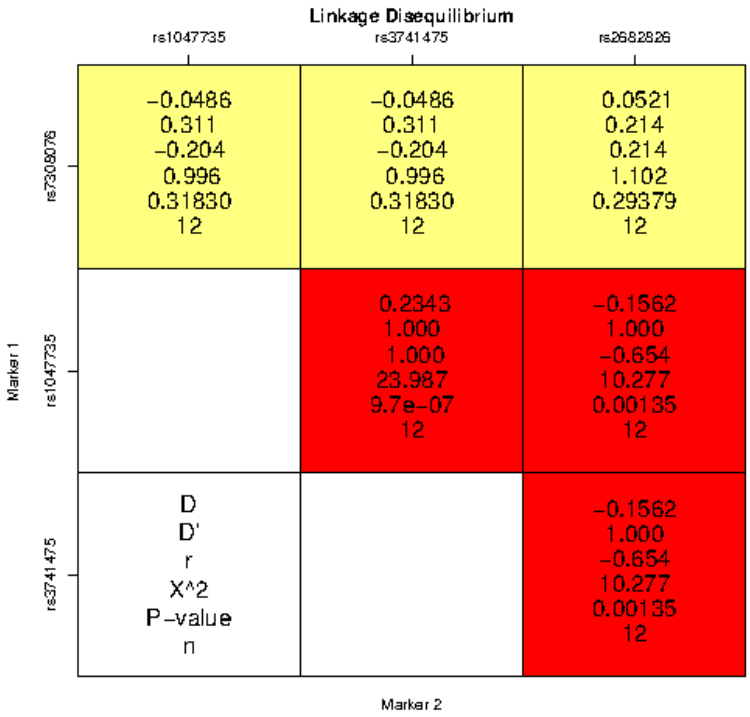

Figure 30. Linkage disequilibrium map for SNPs located on Chromosome 12.

Red color on the heat map (Figure 30) indicates a strong association, that is confirmed by the given p-values 9.7×10^{-7} for rs1047735 and rs3741475; 0.00135 for rs1047735 and rs2682826; 0.00135 for rs3741475 and rs2682826. Based on the LD plot and D values, all the NOS1 SNPs are not in equilibrium and have a strong association with population if linked together over each SNP individually. CIT gene SNP rs7308076 is not associated in linkage with any of the NOS1 SNPs even though they are located within the same chromosome.

4. DISCUSSION

Research on DNA repair is hindered by the different lifespans and sensitivity to mutagens of other populations of white blood cells. PBMNC purification might, however, cause damage by itself (reviewed in Collins *et al.,* 2014). According to our results and those published previously (Menezes et al., 2017; Polachini et al., 2016), trials with the "comet assay" give reproducible results. Our results indicated the increase in levels of DNA damage in both autoimmune cases – MS and T1D. Elevated levels of DNA damage are often tied to oxidative stress and according to recent studies autoimmune diseases and neurodegeneration fully comply to this trend (Pessina et al., 2021; Souliotis et al., 2019; Stratigopoulou et al., 2020). Some theories assume that DNA damage is linked to nitric oxide production (Jaiswal et al., 2001; Yeo et al., 2021). In our study no evidence was found to support the association between DNA damage and other markers or patient descriptors in case of MS. However, T1D patients with higher DNA damage levels had lower levels of serum nitrite. At this point one might assume that nitric oxide regulates the DNA repair in autoimmune disease, but it is not specific for neurodegeneration. Perhaps, additional investigation with larger sample pools and other disease might answer this question. To fully understand the role of oxidative stress in autoimmune diseases levels of oxidized bases should be investigated. Currently the information on this topic is rather scarce. And, unfortunately, in our study levels of oxidized bases did not have any significant difference between MS study group and control group.

Several studies have shown that NO plays an important role in the pathogenesis of MS, with inducible NO synthase (iNOS) being overactive in glia cases and mitochondria damage preceding demyelination (Lan et al., 2018; Mancini et al., 2018). Because of nitric oxide metabolite dilution in the brain, the level of nitric oxide metabolites is not always elevated. (Haghikia *et al.,* 2015). MS patients are still frequently reported to have higher levels of nitrates and nitrites in their blood serum (Fominykh et al., 2016). Our findings also support this theory with MS patients having higher levels of nitrites and nitrates both in plasma and serum. Nitric oxide itself is considered to be difficult to measure. The most common work-around is to measure nitrates and nitrites separately and evaluate a total amount of NO as a sum of both ions (Wu et al., 2013). We have managed to investigate levels of NO by EPR for MS patients. The result indicated the increase of NO in case of MS, but also there was a significant positive correlation with serum nitrites. Therefore, in case of T1D that showed decreased nitrite and nitrate levels, overall, NO

levels are expected to be lower as well. Recent study also proves the fact that T1D patients have reduced levels of NO with the increase only in cases of diabetic nephropathy and kidney disfunction (Sokolovska et al., 2020). Both plasma and serum continue to be utilized for the measurement of nitrites and nitrates using diverse analytical methods.

However, analytical investigation used to be challenging due to the presence of various interfering components (Tsikas, 2012). The chemiluminescence detection method that we used in this study has proven to facilitate the detection excluding a lot of interfering factors (Nagababu and Rifkind, 2007). The only setback here is the necessity to remove plasma and serum proteins. Plasma protein content is higher by 3 – 5 g/L than serum protein content (*Blood Proteins - an overview | ScienceDirect Topics*). This observation could potentially account for the positive correlations observed between serum nitrites and nitrates with other parameters, while no correlation was found for plasma measurements. Our results also indicate that nitrate and nitrite serum measurements might be more informative. Additionally, a correlation has been previously found between NO metabolites and clinical activity (Ljubisavljevic et al., 2014) and severity of the disease as measured by the Expanded Disability Status Scale (EDSS) in some studies (Kallaur et al., 2017). Our findings support this theory and have also showed correlations of serum nitrates with gender and EDSS score of patients. With females having a higher susceptibility to MS, it makes sense that some (if not all) biomarker should be different between two gender groups. The most obvious way to prove this point would be the biomarker comparison between males and females. Unfortunately, the limiting aspect of this study is relatively small study group size, which results in a low female to male ratio, thus making it impossible to observe any statistical significance. Additionally, biochemical markers chosen for this study are influenced by various environmental and dietary factors that are near to impossible to take into account.

Higher disability score would mean the more severe progression of MS, so if any of the biochemical markers, like nitrate levels in our case, correlate with EDSS score, that would provide a valid point to assume that the given biomarker might be associated with the course of the disease progression. In our case, serum nitrate levels had a reverse correlation with EDSS score, meaning that patients with more severe cases of MS are expected to have decreased nitrate levels. Once again due to the previously described limitations of this study it is currently hard to tell whether this correlation is accidental or consequential.

In addition to the development of the pathology, increased NO and its metabolites can sometimes occur as a side effect of treatment. Experimental studies have shown that interferons increase iNOS activity (Lubina-Dąbrowska et al., 2017). A previous study by Niedziela et al., (2016) reported higher levels of NO metabolites in MS patients undergoing interferon therapy. Considering that the majority of MS patients in our study were also treated with interferons, it is plausible that this treatment could be responsible for the observed increase in NO production. However, the correlation analysis results did not indicate any significant association between NO, nitrites, and nitrates with disease-modifying therapy (DMT). The association between plasma nitrites and DMT had the lowest p value of 0.15. That is not even close to being significant, however, based on the limitation of this study in this aspect, namely, relatively small sample pool and the fact that not every patient was undergoing any DMT, we can speculate that with the increase of study group DMT effect on nitrite levels might produce some interesting data.

Using three different drugs to treat MS, (Adamczyk et al., 2017) assessed the levels of MDA in serum of newly diagnosed (untreated) patients. The research findings revealed that individuals newly diagnosed with RRMS exhibited the highest levels of MDA in their serum. MDA levels in serum of drug-treated patients are lower than those in control samples, but they are still higher than those in control samples. In contrast to previous research performed by (Saif Eldeen et al., 2019), lower MDA levels contradict the finding that patients with MS have increased serum MDA levels. In contrast, (Noroozi et al., 2017) found that patients' serum MDA decreased significantly after treatment with IFN-β 1a. In the present study MDA levels of patients with MS were significantly lower when compared to healthy control group. We did not find any associations of MDA levels with DMT or patient descriptors, however serum MDA levels are close to significance when correlated with serum nitrates. So far there are no studies proving an association between NOx and MDA in other cases (Antwi-Boasiako et al., 2020; Soydinç et al., 2007). A rather ancient study by Violi et al., 1999 is by far the only theory explaining the reverse correlation between NO metabolite levels and MDA levels. In our case, the medium reverse correlation was observed between NO levels, serum nitrate and nitrite levels and MDA levels. Based on the evidence that NO can also act as an antioxidant in lipid peroxidation, one might speculate that the overproduction of NO, and thus higher level of its metabolites (which is the proven case in this MS study), will result in the lowered levels of MDA. Following this logic, in case of T1D with the decrease in nitrite and nitrate levels, levels of MDA are expected to be elevated. However, both nitric oxide metabolite and

MDA levels are highly dependent on the dietary antioxidant intake and lifestyle in general, so, assumingly, incredibly large study group would be required to minimize the deviation of each ample from one another. Additional investigation is required of the T1D case in terms of MDA and nitric oxide metabolites, but if confirmed that might be a proven characteristic for MS and novel evidence of NO regulating lipid peroxidation.

CNV analysis have shown abnormalities in specific chromosomal regions of Chr1, Chr6, Chr9, Chr15, Chr17, and Chr21. Previous studies indicate the connection between PARP1 rs3219090 and *Malignant Melanoma* in Spanish population (Chillet *et al*., 2013). Since, PARP1 gene and related SNPs are located on the Chr1, one might assume that the previously mentioned deviation is not due to the smaller sample pool, but, in fact, there might be a direct connection with the progression of MS via DNA repair pathway which PARP1 is involved in. Genotyping data statistical analysis of this PARP1 rs3219090 SNP, however, did not show any significant result, that could mean that the difference from NCBI is due to the general difference of Latvian population. There are multiple gene SNPs described in terms of their relevance to MS (International Multiple Sclerosis Genetics Consortium, 2019). However, not so many proven evidence of the involvement of the DNA repair genes chosen for this study. Conducted CNV analysis cannot give any trustworthy results due to the limitations of having low-coverage sequencing data. However, abnormalities in certain chromosomal regions give an idea where to look deeper. For example, abnormalities in Chr6 region, even though also present in control samples, might indicate the relation to a well-described human leukocyte antigen (HLA) gene cluster on chromosome 6p21 (Patsopoulos, 2018).

XRCC1 gene SNP rs25487 indicated a significant deviation from HWE. Previously, XRCC1 rs25487 was found to be associated with a decreased likelihood of minor treatment response in esophageal cancer and an increased risk of high-grade side effects in head and neck cancer. (Gong et al., 2021). Given the observed elevated levels of DNA damage in leukocytes of MS patients, there appears to be a plausible connection between this SNP and DNA lesions in the context of MS. Correlating XRCC1 rs25487 with DNA damage have shown the most significant result, confirming that DNA damage in MS is indeed associated with this SNP. Interestingly, XRCC1 rs25487 also indicated close to significant correlation with nitric oxide levels, serum nitrites and MDA both in plasma in serum. There are no studies proving this point, so further investigation is required. The speculation here might start with the fact that NO may act as an antioxidant in lipid

peroxidation. The main question then would be how is that associated with DNA repair gene XRCC1? It is currently unclear whether the mutation in XRCC1 gene causes fluctuations in nitric oxide levels or nitric oxide is the one inducing genotoxicity and causing point mutations. A study by Kim, (2017) indicated that nitric oxide indeed has a mutagenic potency and capable of producing point mutations in certain genes. One mentioned example, that might be relevant to our MS case, described the mutagenic potency of NO produced by interferon gamma (IFN-ɣ) activated macrophages. With this being said, one might assume that NO might be the reason behind XRCC1 mutation. As expected, XRCC1 being a DNA repair gene, shows its SNP rs25487 association with levels of DNA damage in lymphocytes. Rare genotype TT, in our case, has shown to correlate with DNA lesions in MS patients, so at this point one might speculate that the C:T point mutation in XRCC1 might be causes by the mutagenic properties of NO, thus disrupting the XRCC1 DNA repair pathway resulting in more evident DNA damage. Once again, DNA lesion are influenced by even more environmental factor than NO, so additional and more specific investigation is required with the large sample pool.

According to the study conducted by Hachemi *et al*. (2016), none of the ADAR, STARD13, ZFHX4, IFNAR2 and CIT genes SNPs have shown any positive association with MS. However, the study has no data about GRIA3 located on the ChrX (Bourguiba-Hachemi et al., 2016). NGS results in our study had quite a few samples, but had a 100% concordance with larger genotyping data pool. Based on this some assumptions can be made from the 30x coverage. Jazireian *et al*. (2020), conducted a study showing that GRIA3 gene rs12557782 SNP did not show any correlation with interferon therapy. Current evidence regarding the rs12557782 is rather scarce, but based on the fact that GRIA3 gene is located on ChrX, one might assume that this gene might be somehow connected to the progression of MS. Genes on X chromosome seem a promising point for further analysis of MS. Considering the fact, that females with T1D are more prone to develop more severe complication than males, infertility is mostly described as an example of this observation (Yi et al., 2021), X chromosome gene analysis might also give some useful insight on this topic.

Considering the fact that NOS1 gene regulates Nitric Oxide Synthase activity and expression, and patients with MS had significantly increased levels of nitrates in nitrites in their serum and plasma, it rather safe to assume that the chosen SNPs rs1047735, rs3741475, rs2682826 are indeed associated with the NO increase in MS patients. Some abnormalities were found during the CNV analysis on Chr17 which is the location of NOS2 gene, nevertheless, no other evidence was found

to confirm the significance of this gene SNPs. Thus, no conclusions can be drawn regarding the chosen NOS2 gene SNPs association with the progression of MS.

Summarizing future prospects of this study one can say that it is of great importance to increase the size of the MS study group. Of course, it would also extremely helpful to sequence more sample with 30x coverage NGS, however, even though this method produces the most informative result, it is also expensive. Since this study provided an insight into the link between MS and T1D, it is necessary to perform additional in-depth studied of this question. For example, since HLA is seemingly involved in the course of both diseases, HLA typing might be the next step to advance findings. Regarding the nitric oxide which, apparently, plays an important role in the pathogenesis of both diseases, even though, as it seems, in a different manner, it is worth to investigate even further. The presence of oxidized bases in MS case has not yet been proven within this study, so one could repeat the experiment with larger sample group, and since, both MS and T1D have shown a similar trend in levels of DNA lesions, it might be worth to do the same for T1D patients.

As for the genetic part of the study, in our opinion XRCC1 gene has proven its association with MS, so the same gene might be considered for the investigation in terms of T1D. With NO metabolite levels being different in MS and T1D cases, and NOS1 gene SNPs showing a promising data in NGS analysis, it would be wise to check the same SNPs for T1D. Alternatively, genes that regulate lipid peroxidation are also worth to consider for investigation, perhaps, it will give a more clear evidence regarding the MDA levels in MS, of course, MDA levels would be also interesting to investigate with respect to T1D.

5. CONCLUSIONS

- Single-strand DNA break levels are significantly increased in MS and T1D patients compared to healthy controls both in whole blood and isolated peripheral blood mononuclear cells. Levels of oxidized bases in MS case, however, did not show any difference between the study group and the control group.
- Nitric oxide production in blood is significantly increased in MS and T1D patients compared to controls. Nitrite and nitrate levels also show a significant increase in the MS study group, but decreases in the T1D study group when compared to healthy control.
- Compared to healthy subjects, patients with MS have decreased MDA levels both in plasma and serum samples.
- There are significant correlations between levels of NO and serum nitrites; level of NO and plasma MDA; serum nitrites and serum nitrates; plasma nitrites and plasma MDA
- Plasma nitrite levels of MS patients are associated with gender, and serum nitrites are associated with EDSS score.
- XRCC1 gene SNP rs25487 show an association with MS based on the HWE analysis, however, further investigation is required.
- XRCC1 gene SNP rs25487 is associated with DNA damage and with levels of NOx. C allele of this gene and TT genotype are associated with plasma and serum MDA levels.
- Based on the NGS data Chr9 region is the most potent for future studies, NOS1 gene SNPs rs1047735, rs3741475, rs2682826 are potentially associated with MS, and GRIA3 rs12557782 SNP on ChrX is a promising subject for investigation.

6. THESIS

- DNA damage caused by single-strand breaks, together with PARP1 rs3219090 and XRCC1 rs25487 SNPs, show a strong association with MS

- MS patients have elevated levels of nitric oxide which might have a positive correlation with NOS1 gene SNPs associated with MS

- MS patients having lower levels of MDA than healthy subjects seem controversial, but might be associated with NO antioxidant properties

- T1D and MS show a similar trend of increased levels of DNA lesions, but different pattern in case of NO metabolites

7. PUBLICATIONS

1. **Borisovs V.**, Ļeonova E., Baumane L., Kalniņa J., Mjagkova N., Sjakste N. Blood levels of nitric oxide and DNA breaks assayed in whole blood and isolated peripheral blood mononucleated cells in patients with multiple sclerosis. Mutat Res Genet Toxicol Environ Mutagen. 2019 Jul;843:90-94. doi: 10.1016/j.mrgentox.2018.11.008. Epub 2018 Nov 23. PMID: 31421744.

2. **Borisovs V.**, Bodrenko J., Kalnina J., Sjakste N. Nitrosative stress parameters and the level of oxidized DNA bases in patients with multiple sclerosis. Metab Brain Dis. 2021 Oct;36(7):1935-1941. doi: 10.1007/s11011-021-00786-5. Epub 2021 Aug 21. PMID: 34417942.

3. Rostoka E., Salna I., Dekante A., Pahirko L., **Borisovs V.**, Celma L., Valeinis J., Sjakste N., Sokolovska J. DNA damage in leukocytes and serum nitrite concentration are negatively associated in type 1 diabetes. Mutagenesis. 2021 Jul 7;36(3):213-222. doi: 10.1093/mutage/geab015. PMID: 34008029.

4. **Borisovs V.**, Paramonova N., Sjakste N., Investigating the Correlation between Genetic and Biochemical Markers in Multiple Sclerosis – submitted

8. APPROBATION OF RESEARCH

1. V. Borisovs, E. Ļeonova, J. Kalniņa, N. Mjagkova, N. Sjakste. *Background level of DNA damage determined in whole blood and lymphocytes of multiple sclerosis patients,* The 76th Conference of the University of Latvia, Riga, Latvia. 2018. Poster presentation.

2. V. Borisovs, E. Leonova, J. Kalnina, N. Mjagkova, N. Sjakste. *DNA oxidative damage determined in whole blood and lymphocytes of patients with multiple sclerosis*, 46th EEMGS/30th GUM meeting, Potsdam, Germany. 2018. Poster presentation.

3. V. Borisovs, E. Ļeonova, J. Kalniņa, N. Mjagkova, N. Sjakste. *DNA damage levels determined in whole lood and lymphocytes of patients with multiple sclerosis*, 56th International scientific student conference, Novosibirsk, Russia. 2018. Poster presentation.

4. J. Sokolovska, K. Ošiņa, V. Borisovs, L. Baumane, A. Dekante, L. Pahirko, J. Valeinis, V. Rovīte, V. Pīrāgs, N. Sjakste. Nitric oxide metabolism and DNA breakage in autoimmune diseases, 13th International Comet Assay Workshop, Pushchino, Russia. 2019. Poster presentation.

5. K. Ošiņa, N. Paramonova, J. Kalniņa, V. Borisovs, N. Sjakste. Proteosomal protein Gene Expression and DNA Integrity in Multiple Sclerosis, 13th International Comet Assay Workshop, Pushchino, Russia. 2019. Poster presentation.

6. J. Bodrenko, V. Borisovs, E. Ļeonova, J. Kalniņa, N. Paramonova, N. Sjakste. *Products of DNA oxidative stress damage as biomarkers for diagnosis of early stages of multiple sclerosis*, The 62nd international scientific conference of Daugavpils university, Daugavpils, Latvia. 2020. Online.

7. V. Borisovs, J. Bodrenko, E. Ļeonova, J. Kalniņa, N. Paramonova, N. Sjakste. *Potential biomarkers for early diagnosis of multiple sclerosis,* The 78th Conference of the University of Latvia, Riga, Latvia. 2020. Poster presentation. Abstract book.

8. V. Borisovs, J. Bodrenko, E. Leonova, I. Trapina, N. Paramonova, N. Sjakste. *The MS puzzle: piecing together biochemical and genetic biomarkers*, 7th Venusberg Meeting on Neuroinflammation, Belval, Luxembourg. 2023. Poster presentation. Abstract book.

9. ACKNOWLEDGEMENTS

This research was supported by the European Regional Development Fund under the project “Determination of proteasome-related genetic, epigenetic and clinical markers for multiple sclerosis” (Project No. 1.1.1.1/16/A/016).

I would like to thank all study participants for their contribution and a special thanks to the medical staff of Latvian Maritime Medicine Centre for organizing patient recruitment and providing biological material.

I would like to express my deepest gratitude to my supervisor Prof. Nikolajs Sjakste for his support and experience. I am also grateful to my colleagues in the University of Latvia for their contribution, practical suggestions, productive collaborations and support with special gratitude to Elīna Ļeonova, Ilva Trapiņa, Natālija Paramonova, Evita Rostoka and Jeļizaveta Sokolovska.

I would also like to thank Latvia MGI Tech for the opportunity to use their platform for this research and invaluable help form their bioinformatics team.

Finally, I would like to thank my wife, family, and friends for their patience, understanding and support.

REFERENCES

1. Abbotts, R., Wilson, D.M., 2017. Coordination of DNA Single Strand Break Repair. Free Radic Biol Med 107, 228–244. https://doi.org/10.1016/j.freeradbiomed.2016.11.039
2. Adamczyk, B., Wawrzyniak, S., Kasperczyk, S., Adamczyk-Sowa, M., 2017. The Evaluation of Oxidative Stress Parameters in Serum Patients with Relapsing-Remitting Multiple Sclerosis Treated with II-Line Immunomodulatory Therapy. Oxid Med Cell Longev 2017, 9625806. https://doi.org/10.1155/2017/9625806
3. Akanji, M.A., Adeyanju, A.A., Rotimi, D., Adeyemi, O.S., 2020. Nitric Oxide Balance in Health and Diseases: Implications for New Treatment Strategies. The Open Biochemistry Journal 14. https://doi.org/10.2174/1874091X02014010025
4. Alhmoud, J.F., Woolley, J.F., Al Moustafa, A.-E., Malki, M.I., 2020. DNA Damage/Repair Management in Cancers. Cancers (Basel) 12, 1050. https://doi.org/10.3390/cancers12041050
5. Ali, J., Aziz, Md.A., Rashid, Md.M.O., Basher, M.A., Islam, M.S., 2022. Propagation of age-related diseases due to the changes of lipid peroxide and antioxidant levels in elderly people: A narrative review. Health Sci Rep 5, e650. https://doi.org/10.1002/hsr2.650
6. Aliaga-Gaspar, P., Hurtado-Guerrero, I., Ciano-Petersen, N.L., Urbaneja, P., Brichette-Mieg, I., Reyes, V., Rodriguez-Bada, J.L., Alvarez-Lafuente, R., Arroyo, R., Quintana, E., Ramió-Torrentà, L., Alonso, A., Leyva, L., Fernández, O., Oliver-Martos, B., 2021. Soluble Receptor Isoform of IFN-Beta (sIFNAR2) in Multiple Sclerosis Patients and Their Association With the Clinical Response to IFN-Beta Treatment. Front Immunol 12, 778204. https://doi.org/10.3389/fimmu.2021.778204
7. Antwi-Boasiako, C., Dankwah, G.B., Aryee, R., Hayfron-Benjamin, C., Aboagye, G., Campbell, A.D., 2020. Correlation of lipid peroxidation and nitric oxide metabolites, trace elements, and antioxidant enzymes in patients with sickle cell disease. Journal of Clinical Laboratory Analysis 34, e23294. https://doi.org/10.1002/jcla.23294
8. Ayala, A., Muñoz, M.F., Argüelles, S., 2014. Lipid Peroxidation: Production, Metabolism, and Signaling Mechanisms of Malondialdehyde and 4-Hydroxy-2-Nonenal. Oxid Med Cell Longev 2014, 360438. https://doi.org/10.1155/2014/360438
9. Balasa, R., Barcutean, L., Mosora, O., Manu, D., 2021. Reviewing the Significance of Blood–Brain Barrier Disruption in Multiple Sclerosis Pathology and Treatment. Int J Mol Sci 22, 8370. https://doi.org/10.3390/ijms22168370
10. Baracaldo-Santamaría, D., Ariza-Salamanca, D.F., Corrales-Hernández, M.G., Pachón-Londoño, M.J., Hernandez-Duarte, I., Calderon-Ospina, C.-A., 2022. Revisiting Excitotoxicity in Traumatic Brain Injury: From Bench to Bedside. Pharmaceutics 14, 152. https://doi.org/10.3390/pharmaceutics14010152
11. Bartoli, M.L., Novelli, F., Costa, F., Malagrinò, L., Melosini, L., Bacci, E., Cianchetti, S., Dente, F.L., Di Franco, A., Vagaggini, B., Paggiaro, P.L., 2011. Malondialdehyde in exhaled breath condensate as a marker of oxidative stress in different pulmonary diseases. Mediators Inflamm 2011, 891752. https://doi.org/10.1155/2011/891752
12. Basak, P., Leslie, H., Dillon, R.L., Muller, W.J., Raouf, A., Mowat, M.R.A., 2018. In vivo evidence supporting a metastasis suppressor role for Stard13 (Dlc2) in ErbB2 (Neu) oncogene induced mouse mammary tumors. Genes Chromosomes Cancer 57, 182–191. https://doi.org/10.1002/gcc.22519

13. Blood Proteins - an overview | ScienceDirect Topics [WWW Document], n.d. URL https://www.sciencedirect.com/topics/biochemistry-genetics-and-molecular-biology/blood-proteins (accessed 11.30.22).
14. Boehi, F., Manetsch, P., Hottiger, M.O., 2021. Interplay between ADP-ribosyltransferases and essential cell signaling pathways controls cellular responses. Cell Discov 7, 1–22. https://doi.org/10.1038/s41421-021-00323-9
15. Borszéková Pulzová, L., Ward, T.A., Chovanec, M., 2020. XPA: DNA Repair Protein of Significant Clinical Importance. Int J Mol Sci 21, 2182. https://doi.org/10.3390/ijms21062182
16. Bourguiba-Hachemi, S., Ashkanani, T.K., Kadhem, F.J., Almawi, W.Y., Alroughani, R., Fathallah, M.D., 2016. ZFAT gene variant association with multiple sclerosis in the Arabian Gulf population: A genetic basis for gender-associated susceptibility. Mol Med Rep 14, 3543–3550. https://doi.org/10.3892/mmr.2016.5692
17. Buckland, R.J., Watt, D.L., Chittoor, B., Nilsson, A.K., Kunkel, T.A., Chabes, A., 2014. Increased and imbalanced dNTP pools symmetrically promote both leading and lagging strand replication infidelity. PLoS Genet 10, e1004846. https://doi.org/10.1371/journal.pgen.1004846
18. Cadet, J., Douki, T., Ravanat, J.-L., 2010. Oxidatively generated base damage to cellular DNA. Free Radic Biol Med 49, 9–21. https://doi.org/10.1016/j.freeradbiomed.2010.03.025
19. Cadet, J., Ravanat, J.-L., TavernaPorro, M., Menoni, H., Angelov, D., 2012. Oxidatively generated complex DNA damage: tandem and clustered lesions. Cancer Lett 327, 5–15. https://doi.org/10.1016/j.canlet.2012.04.005
20. Cadet, J., Wagner, J.R., 2014. Oxidatively generated base damage to cellular DNA by hydroxyl radical and one-electron oxidants: similarities and differences. Arch Biochem Biophys 557, 47–54. https://doi.org/10.1016/j.abb.2014.05.001
21. Campos, A., Clemente-Blanco, A., 2020. Cell Cycle and DNA Repair Regulation in the Damage Response: Protein Phosphatases Take Over the Reins. Int J Mol Sci 21, 446. https://doi.org/10.3390/ijms21020446
22. Chatterjee, N., Santillan, B.A., Wilson, J.H., 2013. Microsatellite Repeats: Canaries in the Coalmine, in: Mittelman, D. (Ed.), Stress-Induced Mutagenesis. Springer, New York, NY, pp. 119–150. https://doi.org/10.1007/978-1-4614-6280-4_7
23. Chatterjee, N., Walker, G.C., 2017. Mechanisms of DNA damage, repair and mutagenesis. Environ Mol Mutagen 58, 235–263. https://doi.org/10.1002/em.22087
24. Choi, J., Xu, M., Makowski, M.M., Zhang, T., Law, M.H., Kovacs, M.A., Granzhan, A., Kim, W.J., Parikh, H., Gartside, M., Trent, J.M., Teulade-Fichou, M.-P., Iles, M.M., Newton-Bishop, J.A., Bishop, D.T., MacGregor, S., Hayward, N.K., Vermeulen, M., Brown, K.M., 2017. A common intronic variant of PARP1 confers melanoma risk and mediates melanocyte growth via regulation of MITF. Nat Genet 49, 1326–1335. https://doi.org/10.1038/ng.3927
25. Cinelli, M.A., Do, H.T., Miley, G.P., Silverman, R.B., 2020. Inducible Nitric Oxide Synthase: Regulation, Structure, and Inhibition. Med Res Rev 40, 158–189. https://doi.org/10.1002/med.21599
26. Collins, A., Koppen, G., Valdiglesias, V., Dusinska, M., Kruszewski, M., Møller, P., Rojas, E., Dhawan, A., Benzie, I., Coskun, E., Moretti, M., Speit, G., Bonassi, S., 2014. The comet assay as a tool for human biomonitoring studies: The ComNet Project. Mutation

Research/Reviews in Mutation Research 759, 27–39. https://doi.org/10.1016/j.mrrev.2013.10.001
27. Comabella, M., Craig, D.W., Morcillo-Suárez, C., Río, J., Navarro, A., Fernández, M., Martin, R., Montalban, X., 2009. Genome-wide scan of 500,000 single-nucleotide polymorphisms among responders and nonresponders to interferon beta therapy in multiple sclerosis. Arch Neurol 66, 972–978. https://doi.org/10.1001/archneurol.2009.150
28. Correa-Aragunde, N., Foresi, N., Del Castello, F., Lamattina, L., 2018. A singular nitric oxide synthase with a globin domain found in Synechococcus PCC 7335 mobilizes N from arginine to nitrate. Sci Rep 8, 12505. https://doi.org/10.1038/s41598-018-30889-6
29. Coyle, P.K., 2021. What Can We Learn from Sex Differences in MS? J Pers Med 11, 1006. https://doi.org/10.3390/jpm11101006
30. Crisp, R.L., Maltaneri, R.E., Vittori, D.C., Solari, L., Gammella, D., Schvartzman, G., García, E., Rapetti, M.C., Donato, H., Nesse, A., 2016. Red blood cell aquaporin-1 expression is decreased in hereditary spherocytosis. Ann Hematol 95, 1595–1601. https://doi.org/10.1007/s00277-016-2757-0
31. De Vos, M., Schreiber, V., Dantzer, F., 2012. The diverse roles and clinical relevance of PARPs in DNA damage repair: current state of the art. Biochem Pharmacol 84, 137–146. https://doi.org/10.1016/j.bcp.2012.03.018
32. Djansugurova, L., Altynova, N., Cherednichenko, O., Khussainova, E., Dubrova, Y.E., 2020. The effects of DNA repair polymorphisms on chromosome aberrations in the population of Kazakhstan. Int J Radiat Biol 96, 614–621. https://doi.org/10.1080/09553002.2020.1711460
33. Dodson, M., Castro-Portuguez, R., Zhang, D.D., 2019. NRF2 plays a critical role in mitigating lipid peroxidation and ferroptosis. Redox Biol 23, 101107. https://doi.org/10.1016/j.redox.2019.101107
34. Dong, K., Gao, Z.-W., Zhang, H.-Z., 2016. The role of adenosinergic pathway in human autoimmune diseases. Immunol Res 64, 1133–1141. https://doi.org/10.1007/s12026-016-8870-2
35. Duffy, S.S., Lees, J.G., Moalem-Taylor, G., 2014. The contribution of immune and glial cell types in experimental autoimmune encephalomyelitis and multiple sclerosis. Mult Scler Int 2014, 285245. https://doi.org/10.1155/2014/285245
36. Eleazer, R., Fondufe-Mittendorf, Y.N., 2021. The multifaceted role of PARP1 in RNA biogenesis. Wiley Interdiscip Rev RNA 12, e1617. https://doi.org/10.1002/wrna.1617
37. Fadda, E., 2016. Role of the XPA protein in the NER pathway: A perspective on the function of structural disorder in macromolecular assembly. Comput Struct Biotechnol J 14, 78–85. https://doi.org/10.1016/j.csbj.2015.11.007
38. Fairless, R., Bading, H., Diem, R., 2021. Pathophysiological Ionotropic Glutamate Signalling in Neuroinflammatory Disease as a Therapeutic Target. Front Neurosci 15, 741280. https://doi.org/10.3389/fnins.2021.741280
39. Fang, Y., Tang, S., Li, X., 2019. Sirtuins in metabolic and epigenetic regulation of stem cells. Trends Endocrinol Metab 30, 177–188. https://doi.org/10.1016/j.tem.2018.12.002
40. Fominykh, V., Onufriev, M.V., Vorobyeva, A., Brylev, L., Yakovlev, A.A., Zakharova, M.N., Gulyaeva, N.V., 2016. Increased S-nitrosothiols are associated with spinal cord injury in multiple sclerosis. J Clin Neurosci 28, 38–42. https://doi.org/10.1016/j.jocn.2015.09.017

41. Fontana, P., Ginevrino, M., Bejo, K., Cantalupo, G., Ciavarella, M., Lombardi, C., Maioli, M., Scarano, F., Costabile, C., Novelli, A., Lonardo, F., 2021. A ZFHX4 mutation associated with a recognizable neuropsychological and facial phenotype. Eur J Med Genet 64, 104321. https://doi.org/10.1016/j.ejmg.2021.104321
42. Forrester, S.J., Kikuchi, D.S., Hernandes, M.S., Xu, Q., Griendling, K.K., 2018. Reactive Oxygen Species in Metabolic and Inflammatory Signaling. Circ Res 122, 877–902. https://doi.org/10.1161/CIRCRESAHA.117.311401
43. Gandhi, R., Laroni, A., Weiner, H.L., 2010. Role of the innate immune system in the pathogenesis of multiple sclerosis. J Neuroimmunol 221, 7–14. https://doi.org/10.1016/j.jneuroim.2009.10.015
44. Garcia, S.C., Grotto, D., Bulcão, R.P., Moro, A.M., Roehrs, M., Valentini, J., de Freitas, F.A., Paniz, C., Bubols, G.B., Charão, M.F., 2013. Evaluation of lipid damage related to pathological and physiological conditions. Drug Chem Toxicol 36, 306–312. https://doi.org/10.3109/01480545.2012.720989
45. Garcia-Venzor, A., Toiber, D., 2021. SIRT6 Through the Brain Evolution, Development, and Aging. Front Aging Neurosci 13, 747989. https://doi.org/10.3389/fnagi.2021.747989
46. Garg, N., Smith, T.W., 2015. An update on immunopathogenesis, diagnosis, and treatment of multiple sclerosis. Brain Behav 5, e00362. https://doi.org/10.1002/brb3.362
47. Gaschler, M.M., Stockwell, B.R., 2017. Lipid peroxidation in cell death. Biochem Biophys Res Commun 482, 419–425. https://doi.org/10.1016/j.bbrc.2016.10.086
48. Geiger, M., Hayter, E., Martin, R.S., Spence, D., 2022. Red blood cells in type 1 diabetes and multiple sclerosis and technologies to measure their emerging roles. J Transl Autoimmun 5, 100161. https://doi.org/10.1016/j.jtauto.2022.100161
49. Gene: ATM (ENSG00000149311) - Summary - Homo_sapiens - Ensembl genome browser 107 [WWW Document], n.d. URL https://www.ensembl.org/Homo_sapiens/Gene/Summary?g=ENSG00000149311;r=11:108223044-108369102 (accessed 9.6.22).
50. Gene: PARP1 (ENSG00000143799) - Summary - Homo_sapiens - GRCh37 Archive browser 107 [WWW Document], n.d. URL https://grch37.ensembl.org/Homo_sapiens/Gene/Summary?g=ENSG00000143799;r=1:226548392-226595780 (accessed 9.6.22).
51. Gene: XPA (ENSG00000136936) - Summary - Homo_sapiens - GRCh37 Archive browser 107 [WWW Document], n.d. URL https://grch37.ensembl.org/Homo_sapiens/Gene/Summary?g=ENSG00000136936;r=9:100437191-100459639 (accessed 9.6.22).
52. Gene: XPC (ENSG00000154767) - Summary - Homo_sapiens - GRCh37 Archive browser 107 [WWW Document], n.d. URL https://grch37.ensembl.org/Homo_sapiens/Gene/Summary?g=ENSG00000154767;r=3:14186647-14220283 (accessed 9.6.22).
53. Gene: XRCC1 (ENSG00000073050) - Summary - Homo_sapiens - GRCh37 Archive browser 107 [WWW Document], n.d. URL https://grch37.ensembl.org/Homo_sapiens/Gene/Summary?g=ENSG00000073050;r=19:44047192-44084625 (accessed 9.6.22).
54. Ghasemi, N., Razavi, S., Nikzad, E., 2017. Multiple Sclerosis: Pathogenesis, Symptoms, Diagnoses and Cell-Based Therapy. Cell J 19, 1–10.

55. Giera, M., Lingeman, H., Niessen, W.M.A., 2012. Recent Advancements in the LC- and GC-Based Analysis of Malondialdehyde (MDA): A Brief Overview. Chromatographia 75, 433–440. https://doi.org/10.1007/s10337-012-2237-1
56. Gong, L., Luo, M., Sun, R., Qiu, L., Chen, C., Luo, Z., 2021. Significant Association Between XRCC1 Expression and Its rs25487 Polymorphism and Radiotherapy-Related Cancer Prognosis. Front Oncol 11, 654784. https://doi.org/10.3389/fonc.2021.654784
57. Grabowska, W., Sikora, E., Bielak-Zmijewska, A., 2017. Sirtuins, a promising target in slowing down the ageing process. Biogerontology 18, 447–476. https://doi.org/10.1007/s10522-017-9685-9
58. Greenberg, M.M., 2016. Reactivity of Nucleic Acid Radicals. Adv Phys Org Chem 50, 119–202. https://doi.org/10.1016/bs.apoc.2016.02.001
59. Haghikia, Aiden, Kayacelebi, A.A., Beckmann, B., Hanff, E., Gold, R., Haghikia, Arash, Tsikas, D., 2015. Serum and cerebrospinal fluid concentrations of homoarginine, arginine, asymmetric and symmetric dimethylarginine, nitrite and nitrate in patients with multiple sclerosis and neuromyelitis optica. Amino Acids 47, 1837–1845. https://doi.org/10.1007/s00726-015-2015-0
60. Hancock, D.B., Martin, E.R., Fujiwara, K., Stacy, M.A., Scott, B.L., Stajich, J.M., Jewett, R., Li, Y.-J., Hauser, M.A., Vance, J.M., Scott, W.K., 2006. NOS2A and the modulating effect of cigarette smoking in Parkinson's disease. Ann Neurol 60, 366–373. https://doi.org/10.1002/ana.20915
61. Hancock, D.B., Martin, E.R., Vance, J.M., Scott, W.K., 2008. Nitric oxide synthase genes and their interactions with environmental factors in Parkinson's disease. Neurogenetics 9, 249–262. https://doi.org/10.1007/s10048-008-0137-1
62. Handel, A.E., Handunnetthi, L., Ebers, G.C., Ramagopalan, S.V., 2009. Type 1 diabetes mellitus and multiple sclerosis: common etiological features. Nat Rev Endocrinol 5, 655–664. https://doi.org/10.1038/nrendo.2009.216
63. Harding, B.N., Moccia, A., Drunat, S., Soukarieh, O., Tubeuf, H., Chitty, L.S., Verloes, A., Gressens, P., El Ghouzzi, V., Joriot, S., Di Cunto, F., Martins, A., Passemard, S., Bielas, S.L., 2016. Mutations in Citron Kinase Cause Recessive Microlissencephaly with Multinucleated Neurons. Am J Hum Genet 99, 511–520. https://doi.org/10.1016/j.ajhg.2016.07.003
64. He, X., Wang, P., Li, Y., Shen, N., 2019. ATM rs189037 significantly increases the risk of cancer in non-smokers rather than smokers: an updated meta-analysis. Biosci Rep 39, BSR20191298. https://doi.org/10.1042/BSR20191298
65. Heiss, C., Rodriguez-Mateos, A., Kelm, M., 2015. Central Role of eNOS in the Maintenance of Endothelial Homeostasis. Antioxid Redox Signal 22, 1230–1242. https://doi.org/10.1089/ars.2014.6158
66. Huang, W.-J., Chen, W.-W., Zhang, X., 2017. Multiple sclerosis: Pathology, diagnosis and treatments. Exp Ther Med 13, 3163–3166. https://doi.org/10.3892/etm.2017.4410
67. Ingwersen, J., Wingerath, B., Graf, J., Lepka, K., Hofrichter, M., Schröter, F., Wedekind, F., Bauer, A., Schrader, J., Hartung, H.-P., Prozorovski, T., Aktas, O., 2016. Dual roles of the adenosine A2a receptor in autoimmune neuroinflammation. J Neuroinflammation 13, 48. https://doi.org/10.1186/s12974-016-0512-z
68. International Multiple Sclerosis Genetics Consortium, 2019. Multiple sclerosis genomic map implicates peripheral immune cells and microglia in susceptibility. Science 365, eaav7188. https://doi.org/10.1126/science.aav7188

69. Ishikura, S., Nagai, M., Tsunoda, T., Nishi, K., Tanaka, Y., Koyanagi, M., Shirasawa, S., 2021. The transcriptional regulator Zfat is essential for maintenance and differentiation of the adipocytes. J Cell Biochem 122, 626–638. https://doi.org/10.1002/jcb.29890
70. Ito, F., Sono, Y., Ito, T., 2019. Measurement and Clinical Significance of Lipid Peroxidation as a Biomarker of Oxidative Stress: Oxidative Stress in Diabetes, Atherosclerosis, and Chronic Inflammation. Antioxidants (Basel) 8, 72. https://doi.org/10.3390/antiox8030072
71. Jaiswal, M., LaRusso, N.F., Shapiro, R.A., Billiar, T.R., Gores, G.J., 2001. Nitric oxide–mediated inhibition of DNA repair potentiates oxidative DNA damage in cholangiocytes. Gastroenterology 120, 190–199. https://doi.org/10.1053/gast.2001.20875
72. Janků, M., Luhová, L., Petřivalský, M., 2019. On the Origin and Fate of Reactive Oxygen Species in Plant Cell Compartments. Antioxidants (Basel) 8, 105. https://doi.org/10.3390/antiox8040105
73. Jazireian, P., Sasani, S.T., Assarzadegan, F., Azimian, M., 2020. TRAILR1 (rs20576) and GRIA3 (rs12557782) are not associated with interferon-β response in multiple sclerosis patients. Mol Biol Rep 47, 9659–9665. https://doi.org/10.1007/s11033-020-06026-w
74. Kallaur, A.P., Reiche, E.M.V., Oliveira, S.R., Simão, A.N.C., Pereira, W.L. de C.J., Alfieri, D.F., Flauzino, T., Proença, C. de M., Lozovoy, M.A.B., Kaimen-Maciel, D.R., Maes, M., 2017. Genetic, Immune-Inflammatory, and Oxidative Stress Biomarkers as Predictors for Disability and Disease Progression in Multiple Sclerosis. Mol Neurobiol 54, 31–44. https://doi.org/10.1007/s12035-015-9648-6
75. Kasper, L.H., Shoemaker, J., 2010. Multiple sclerosis immunology: The healthy immune system vs the MS immune system. Neurology 74 Suppl 1, S2-8. https://doi.org/10.1212/WNL.0b013e3181c97c8f
76. Kaur, K., Kaur, R., 2020. Polymorphisms in XPC and XPD genes modulate DNA damage in pesticide-exposed agricultural workers of Punjab, North-West India. Mol Biol Rep 47, 5253–5262. https://doi.org/10.1007/s11033-020-05600-6
77. Kay, J., Thadhani, E., Samson, L., Engelward, B., 2019. Inflammation-Induced DNA Damage, Mutations and Cancer. DNA Repair (Amst) 83, 102673. https://doi.org/10.1016/j.dnarep.2019.102673
78. Ke, Y., Zhang, J., Lv, X., Zeng, X., Ba, X., 2019. Novel insights into PARPs in gene expression: regulation of RNA metabolism. Cell. Mol. Life Sci. 76, 3283–3299. https://doi.org/10.1007/s00018-019-03120-6
79. Khoury, N., Koronowski, K.B., Young, J.I., Perez-Pinzon, M.A., 2018. The NAD+-Dependent Family of Sirtuins in Cerebral Ischemia and Preconditioning. Antioxid Redox Signal 28, 691–710. https://doi.org/10.1089/ars.2017.7258
80. Kim, M., Kim, H.-S., D'Souza, A., Gallagher, K., Jeong, E., Topolska-Wós, A., Ogorodnik Le Meur, K., Tsai, C.-L., Tsai, M.-S., Kee, M., Tainer, J.A., Yeo, J.-E., Chazin, W.J., Schärer, O.D., 2022. Two interaction surfaces between XPA and RPA organize the preincision complex in nucleotide excision repair. Proc Natl Acad Sci U S A 119, e2207408119. https://doi.org/10.1073/pnas.2207408119
81. Kim, M.Y., 2017. Intracellular and extracellular factors influencing the genotoxicity of nitric oxide and reactive oxygen species. Oncology Letters 13, 1417–1424. https://doi.org/10.3892/ol.2017.5584

82. Klein, M.A., Denu, J.M., 2020. Biological and catalytic functions of sirtuin 6 as targets for small-molecule modulators. J Biol Chem 295, 11021–11041. https://doi.org/10.1074/jbc.REV120.011438
83. Knott, A.B., Bossy-Wetzel, E., 2010. IMPACT OF NITRIC OXIDE ON METABOLISM IN HEALTH AND AGE-RELATED DISEASE. Diabetes Obes Metab 12, 126–133. https://doi.org/10.1111/j.1463-1326.2010.01267.x
84. Koleck, T.A., Bender, C.M., Sereika, S.M., Brufsky, A.M., Lembersky, B.C., McAuliffe, P.F., Puhalla, S.L., Rastogi, P., Conley, Y.P., 2016. Polymorphisms in DNA repair and oxidative stress genes associated with pre-treatment cognitive function in breast cancer survivors: an exploratory study. Springerplus 5, 422. https://doi.org/10.1186/s40064-016-2061-4
85. Kosciuk, T., Wang, M., Hong, J.Y., Lin, H., 2019. Updates on the Epigenetic Roles of Sirtuins. Curr Opin Chem Biol 51, 18–29. https://doi.org/10.1016/j.cbpa.2019.01.023
86. Kratz, E.M., Sołkiewicz, K., Kubis-Kubiak, A., Piwowar, A., 2021. Sirtuins as Important Factors in Pathological States and the Role of Their Molecular Activity Modulators. Int J Mol Sci 22, 630. https://doi.org/10.3390/ijms22020630
87. Lan, M., Tang, X., Zhang, J., Yao, Z., 2018. Insights in pathogenesis of multiple sclerosis: nitric oxide may induce mitochondrial dysfunction of oligodendrocytes. Rev Neurosci 29, 39–53. https://doi.org/10.1515/revneuro-2017-0033
88. Lane, M., Yadav, V., 2020. Multiple Sclerosis. Textbook of Natural Medicine 1587-1599.e3. https://doi.org/10.1016/B978-0-323-43044-9.00199-0
89. Lee, I.H., 2019. Mechanisms and disease implications of sirtuin-mediated autophagic regulation. Exp Mol Med 51, 102. https://doi.org/10.1038/s12276-019-0302-7
90. Li, G., Chen, Y., Hu, H., Liu, L., Hu, X., Wang, J., Shi, W., Yin, D., 2012. Association between age-related decline of kidney function and plasma malondialdehyde. Rejuvenation Res 15, 257–264. https://doi.org/10.1089/rej.2011.1259
91. Ljubisavljevic, S., Stojanovic, I., Pavlovic, R., Pavlovic, D., 2014. The importance of nitric oxide and arginase in the pathogenesis of acute neuroinflammation: are those contra players with the same direction? Neurotox Res 26, 392–399. https://doi.org/10.1007/s12640-014-9470-3
92. Longo, V.D., Kennedy, B.K., 2006. Sirtuins in aging and age-related disease. Cell 126, 257–268. https://doi.org/10.1016/j.cell.2006.07.002
93. Lubina-Dąbrowska, N., Stepień, A., Sulkowski, G., Dąbrowska-Bouta, B., Langfort, J., Chalimoniuk, M., 2017. Effects of IFN-β1a and IFN-β1b treatment on the expression of cytokines, inducible NOS (NOS type II), and myelin proteins in animal model of multiple sclerosis. Arch Immunol Ther Exp (Warsz) 65, 325–338. https://doi.org/10.1007/s00005-017-0458-6
94. Luo, Y., Hong, S., 2020. The Role of Ataxia Telangiectasia Mutant and Rad3-Related DNA Damage Response in Pathogenesis of Human Papillomavirus. Pathogens 9, 506. https://doi.org/10.3390/pathogens9060506
95. Ma, W.-T., Gao, F., Gu, K., Chen, D.-K., 2019. The Role of Monocytes and Macrophages in Autoimmune Diseases: A Comprehensive Review. Front Immunol 10, 1140. https://doi.org/10.3389/fimmu.2019.01140
96. Mallucci, G., Peruzzotti-Jametti, L., Bernstock, J.D., Pluchino, S., 2015. The role of immune cells, glia and neurons in white and gray matter pathology in multiple sclerosis. Prog Neurobiol 127–128, 1–22. https://doi.org/10.1016/j.pneurobio.2015.02.003

97. Mancini, A., Tantucci, M., Mazzocchetti, P., de Iure, A., Durante, V., Macchioni, L., Giampà, C., Alvino, A., Gaetani, L., Costa, C., Tozzi, A., Calabresi, P., Di Filippo, M., 2018. Microglial activation and the nitric oxide/cGMP/PKG pathway underlie enhanced neuronal vulnerability to mitochondrial dysfunction in experimental multiple sclerosis. Neurobiol Dis 113, 97–108. https://doi.org/10.1016/j.nbd.2018.01.002
98. Mas-Bargues, C., Escrivá, C., Dromant, M., Borrás, C., Viña, J., 2021. Lipid peroxidation as measured by chromatographic determination of malondialdehyde. Human plasma reference values in health and disease. Arch Biochem Biophys 709, 108941. https://doi.org/10.1016/j.abb.2021.108941
99. McGinley, M.P., Goldschmidt, C.H., Rae-Grant, A.D., 2021. Diagnosis and Treatment of Multiple Sclerosis: A Review. JAMA 325, 765–779. https://doi.org/10.1001/jama.2020.26858
100. Medrano, L.M., Berenguer, J., Jiménez-Sousa, M.A., Aldámiz-Echevarria, T., Tejerina, F., Diez, C., Vigón, L., Fernández-Rodríguez, A., Resino, S., 2017. ADAR1 polymorphisms are related to severity of liver fibrosis in HIV/HCV-coinfected patients. Sci Rep 7, 12918. https://doi.org/10.1038/s41598-017-12885-4
101. Menezes, K.M., Algarve, T.D., Flôres, F.S., Cruz, I.B.M., Copetti, F., Silveira, A.F., 2017. DNA damage and postural balance in multiple sclerosis patients. Fisioter. mov. 30, 85–91. https://doi.org/10.1590/1980-5918.030.S01.AO08
102. Milkovic, L., Cipak Gasparovic, A., Cindric, M., Mouthuy, P.-A., Zarkovic, N., 2019. Short Overview of ROS as Cell Function Regulators and Their Implications in Therapy Concepts. Cells 8, 793. https://doi.org/10.3390/cells8080793
103. Mnika, K., Pule, G.D., Dandara, C., Wonkam, A., 2016. An Expert Review of Pharmacogenomics of Sickle Cell Disease Therapeutics: Not Yet Ready for Global Precision Medicine. OMICS 20, 565–574. https://doi.org/10.1089/omi.2016.0105
104. Mou, J., Hu, T., Wang, Z., Chen, W., Wang, Y., Zhang, W., 2020. ATM gene polymorphisms are associated with poor prognosis of non-small cell lung cancer receiving radiation therapy. Aging (Albany NY) 12, 7465–7479. https://doi.org/10.18632/aging.103094
105. Nagababu, E., Rifkind, J.M., 2007. Measurement of Plasma Nitrite by Chemiluminescence without Interference of S-, N-nitroso and Nitrated Species. Free Radic Biol Med 42, 1146–1154. https://doi.org/10.1016/j.freeradbiomed.2006.12.029
106. Niedziela, N., Adamczyk-Sowa, M., Niedziela, J.T., Mazur, B., Kluczewska, E., Sowa, P., Gąsior, M., 2016. Assessment of Serum Nitrogen Species and Inflammatory Parameters in Relapsing-Remitting Multiple Sclerosis Patients Treated with Different Therapeutic Approaches. Biomed Res Int 2016, 4570351. https://doi.org/10.1155/2016/4570351
107. Nishikura, K., 2016. A-to-I editing of coding and non-coding RNAs by ADARs. Nat Rev Mol Cell Biol 17, 83–96. https://doi.org/10.1038/nrm.2015.4
108. Noroozi, S., Arababadi, M.K., Meimand, H.A.E., Asadikaram, G., 2017. The Effect of IFN-beta 1a on Biochemical Factors in Multiple Sclerosis Patients. Iranian Red Crescent Medical Journal 19, 8.
109. Özgöz, A., Hekimler Öztürk, K., Yükseltürk, A., Şamlı, H., Başkan, Z., Mutlu İçduygu, F., Bacaksız, M., 2019. Genetic Variations of DNA Repair Genes in Breast Cancer. Pathol Oncol Res 25, 107–114. https://doi.org/10.1007/s12253-017-0322-3

110. Pasqualetti, F., Gonnelli, A., Orlandi, P., Palladino, E., Giannini, N., Gadducci, G., Mattioni, R., Montrone, S., Calistri, E., Mazzanti, C.M., Franceschi, S., Ortenzi, V., Scatena, C., Zavaglia, K., Fanelli, G.N., Morganti, R., Santonocito, O., Bocci, G., Naccarato, G.A., Paiar, F., 2021. Association of XRCC3 rs1799794 polymorphism with survival of glioblastoma multiforme patients treated with combined radio-chemotherapy. Invest New Drugs 39, 1159–1165. https://doi.org/10.1007/s10637-021-01075-9
111. Patsopoulos, N.A., 2018. Genetics of Multiple Sclerosis: An Overview and New Directions. Cold Spring Harb Perspect Med 8, a028951. https://doi.org/10.1101/cshperspect.a028951
112. Paul, K.C., Sinsheimer, J.S., Rhodes, S.L., Cockburn, M., Bronstein, J., Ritz, B., 2016. Organophosphate Pesticide Exposures, Nitric Oxide Synthase Gene Variants, and Gene-Pesticide Interactions in a Case-Control Study of Parkinson's Disease, California (USA). Environ Health Perspect 124, 570–577. https://doi.org/10.1289/ehp.1408976
113. Perrone, S., Lotti, F., Geronzi, U., Guidoni, E., Longini, M., Buonocore, G., 2016. Oxidative Stress in Cancer-Prone Genetic Diseases in Pediatric Age: The Role of Mitochondrial Dysfunction. Oxid Med Cell Longev 2016, 4782426. https://doi.org/10.1155/2016/4782426
114. Pessina, F., Gioia, U., Brandi, O., Farina, S., Ceccon, M., Francia, S., d'Adda di Fagagna, F., 2021. DNA Damage Triggers a New Phase in Neurodegeneration. Trends in Genetics 37, 337–354. https://doi.org/10.1016/j.tig.2020.09.006
115. Polachini, C.R.N., Spanevello, R.M., Zanini, D., Baldissarelli, J., Pereira, L.B., Schetinger, M.R.C., da Cruz, I.B.M., Assmann, C.E., Bagatini, M.D., Morsch, V.M., 2016. Evaluation of Delta-Aminolevulinic Dehydratase Activity, Oxidative Stress Biomarkers, and Vitamin D Levels in Patients with Multiple Sclerosis. Neurotox Res 29, 230–242. https://doi.org/10.1007/s12640-015-9584-2
116. Polito, L., Greco, A., Seripa, D., 2016. Genetic Profile, Environmental Exposure, and Their Interaction in Parkinson's Disease. Parkinsons Dis 2016, 6465793. https://doi.org/10.1155/2016/6465793
117. Potenski, C.J., Klein, H.L., 2014. How the misincorporation of ribonucleotides into genomic DNA can be both harmful and helpful to cells. Nucleic Acids Res 42, 10226–10234. https://doi.org/10.1093/nar/gku773
118. Poulose, N., Raju, R., 2015. SIRTUIN REGULATION IN AGING AND INJURY. Biochim Biophys Acta 1852, 2442–2455. https://doi.org/10.1016/j.bbadis.2015.08.017
119. Pozzilli, V., Grasso, E.A., Tomassini, V., 2022. Similarities and differences between multiple sclerosis and type 1 diabetes. Diabetes/Metabolism Research and Reviews 38, e3505. https://doi.org/10.1002/dmrr.3505
120. Ravanat, J.-L., Cadet, J., Douki, T., 2012. Oxidatively generated DNA lesions as potential biomarkers of in vivo oxidative stress. Curr Mol Med 12, 655–671. https://doi.org/10.2174/156652412800792651
121. Ray Chaudhuri, A., Nussenzweig, A., 2017. The multifaceted roles of PARP1 in DNA repair and chromatin remodelling. Nat Rev Mol Cell Biol 18, 610–621. https://doi.org/10.1038/nrm.2017.53
122. Redenšek, S., Flisar, D., Kojović, M., Kramberger, M.G., Georgiev, D., Pirtošek, Z., Trošt, M., Dolžan, V., 2019. Genetic variability of inflammation and oxidative stress genes does not play a major role in the occurrence of adverse events of dopaminergic

treatment in Parkinson's disease. J Neuroinflammation 16, 50. https://doi.org/10.1186/s12974-019-1439-y
123. Reich, D.S., Lucchinetti, C.F., Calabresi, P.A., 2018. Multiple Sclerosis. N Engl J Med 378, 169–180. https://doi.org/10.1056/NEJMra1401483
124. Rostoka, E., Salna, I., Dekante, A., Pahirko, L., Borisovs, V., Celma, L., Valeinis, J., Sjakste, N., Sokolovska, J., 2021. DNA damage in leukocytes and serum nitrite concentration are negatively associated in type 1 diabetes. Mutagenesis 36, 213–222. https://doi.org/10.1093/mutage/geab015
125. Saieva, C., Peluso, M., Palli, D., Cellai, F., Ceroti, M., Selvi, V., Bendinelli, B., Assedi, M., Munnia, A., Masala, G., 2016. Dietary and lifestyle determinants of malondialdehyde DNA adducts in a representative sample of the Florence City population. Mutagenesis 31, 475–480. https://doi.org/10.1093/mutage/gew012
126. Saif Eldeen, E.M.S., El Sharkawy, R., Abd El Azim, G., Mohamed, N., Abd Elmajed, M., 2019. Role of nitric oxide and malondialdehyde biomarkers in relapsing-remitting multiple sclerosis. Sci J Al-Azhar Med Fac Girls 3, 544. https://doi.org/10.4103/sjamf.sjamf_59_19
127. Samarajiwa, S.A., Mangan, N.E., Hardy, M.P., Najdovska, M., Dubach, D., Braniff, S.-J., Owczarek, C.M., Hertzog, P.J., 2014. Soluble IFN receptor potentiates in vivo type I IFN signaling and exacerbates TLR4-mediated septic shock. J Immunol 192, 4425–4435. https://doi.org/10.4049/jimmunol.1302388
128. Santos-Lobato, B.L., Borges, V., Ferraz, H.B., Mata, I.F., Zabetian, C.P., Tumas, V., 2018. Association of a neuronal nitric oxide synthase gene polymorphism with levodopa-induced dyskinesia in Parkinson's disease. Nitric Oxide 74, 86–90. https://doi.org/10.1016/j.niox.2017.06.004
129. Shall, S., de Murcia, G., 2000. Poly(ADP-ribose) polymerase-1: what have we learned from the deficient mouse model? Mutat Res 460, 1–15. https://doi.org/10.1016/s0921-8777(00)00016-1
130. Simon, M., Yang, J., Gigas, J., Earley, E.J., Schaff, T.M., Zhang, L., Zagorulya, M., Tombline, G., Gilbert, M., Yuen, S.L., Pope, A., Meter, M.V., Emmrich, S., Han, J., Ryu, S., Tare, A., Zhu, Y., Hudgins, A., Atzmon, G., Barzilai, N., Wolfe, A., Moody, K., Garcia, B.A., Thomas, D.D., Robbins, P.D., Vijg, J., Seluanov, A., Suh, Y., Gorbunova, V., 2021. A rare human centenarian variant of SIRT6 enhances genome stability and interaction with Lamin A. https://doi.org/10.1101/2021.12.13.472381
131. Singh, A., Kukreti, R., Saso, L., Kukreti, S., 2019. Oxidative Stress: A Key Modulator in Neurodegenerative Diseases. Molecules 24, 1583. https://doi.org/10.3390/molecules24081583
132. SIRT6 sirtuin 6 [Homo sapiens (human)] - Gene - NCBI [WWW Document], n.d. URL https://www.ncbi.nlm.nih.gov/gene/51548#summary (accessed 9.13.22).
133. Slotkin, W., Nishikura, K., 2013. Adenosine-to-inosine RNA editing and human disease. Genome Med 5, 105. https://doi.org/10.1186/gm508
134. Sokolovska, J., Dekante, A., Baumane, L., Pahirko, L., Valeinis, J., Dislere, K., Rovite, V., Pirags, V., Sjakste, N., 2020. Nitric oxide metabolism is impaired by type 1 diabetes and diabetic nephropathy. Biomed Rep 12, 251–258. https://doi.org/10.3892/br.2020.1288

135. Song, B., Shiromoto, Y., Minakuchi, M., Nishikura, K., 2022. The role of RNA editing enzyme ADAR1 in human disease. Wiley Interdiscip Rev RNA 13, e1665. https://doi.org/10.1002/wrna.1665
136. Souliotis, V.L., Vlachogiannis, N.I., Pappa, M., Argyriou, A., Ntouros, P.A., Sfikakis, P.P., 2019. DNA Damage Response and Oxidative Stress in Systemic Autoimmunity. Int J Mol Sci 21, E55. https://doi.org/10.3390/ijms21010055
137. Soydinç, S., Çelik, A., Demiryürek, S., Davutoğlu, V., Tarakçıoğlu, M., Aksoy, M., 2007. THE RELATIONSHIP BETWEEN OXIDATIVE STRESS, NITRIC OXIDE, AND CORONARY ARTERY DISEASE. ELECTRON J GEN MED 4, 62–66. https://doi.org/10.29333/ejgm/82487
138. Spiegel, J.O., Van Houten, B., Durrant, J.D., 2021. PARP1: Structural Insights and Pharmacological Targets for Inhibition. DNA Repair (Amst) 103, 103125. https://doi.org/10.1016/j.dnarep.2021.103125
139. Stratigopoulou, M., van Dam, T.P., Guikema, J.E.J., 2020. Base Excision Repair in the Immune System: Small DNA Lesions With Big Consequences. Frontiers in Immunology 11.
140. Sugitani, N., Sivley, R.M., Perry, K.E., Capra, J.A., Chazin, W.J., 2016. XPA: A key scaffold for human nucleotide excision repair. DNA Repair (Amst) 44, 123–135. https://doi.org/10.1016/j.dnarep.2016.05.018
141. Sun, Q., Sha, W., Liu, H.-P., Wang, P., Liu, Z.-B., Sun, W.-W., Xiao, H.-P., 2020. Genetic Polymorphisms in Antioxidant Enzymes Modulate the Susceptibility of Idiosyncratic Antituberculous Drug-Induced Liver Injury and Treatment Outcomes in Patients with Tuberculosis. Pharmacotherapy 40, 4–16. https://doi.org/10.1002/phar.2349
142. Sun, Y., Lu, Y., Saredy, J., Wang, X., Drummer IV, C., Shao, Y., Saaoud, F., Xu, K., Liu, M., Yang, W.Y., Jiang, X., Wang, H., Yang, X., 2020. ROS systems are a new integrated network for sensing homeostasis and alarming stresses in organelle metabolic processes. Redox Biology 37, 101696. https://doi.org/10.1016/j.redox.2020.101696
143. Tafti, D., Ehsan, M., Xixis, K.L., 2022. Multiple Sclerosis, in: StatPearls. StatPearls Publishing, Treasure Island (FL).
144. Tavassolifar, M. javad, Vodjgani, M., Salehi, Z., Izad, M., 2020. The Influence of Reactive Oxygen Species in the Immune System and Pathogenesis of Multiple Sclerosis. Autoimmune Dis 2020, 5793817. https://doi.org/10.1155/2020/5793817
145. Tettey, P., Simpson, S., Taylor, B.V., Mei, I.A.F. van der, 2015. The co-occurrence of multiple sclerosis and type 1 diabetes: Shared aetiologic features and clinical implication for MS aetiology. Journal of the Neurological Sciences 348, 126–131. https://doi.org/10.1016/j.jns.2014.11.019
146. Tropp, B.E., 2012. Molecular Biology: Genes to Proteins. Jones & Bartlett Publishers.
147. Tsikas, D., 2017. Assessment of lipid peroxidation by measuring malondialdehyde (MDA) and relatives in biological samples: Analytical and biological challenges. Anal Biochem 524, 13–30. https://doi.org/10.1016/j.ab.2016.10.021
148. Tsikas, D., 2012. Measurement of nitrite in plasma and serum: still a challenging analytical task. Clinical Chemistry and Laboratory Medicine (CCLM) 50. https://doi.org/10.1515/cclm-2011-0946
149. Tsunoda, T., Shirasawa, S., 2013. Roles of ZFAT in haematopoiesis, angiogenesis and cancer development. Anticancer Res 33, 2833–2837.

150. Vaisman, A., Woodgate, R., 2017. Translesion DNA polymerases in eukaryotes: what makes them tick? Crit Rev Biochem Mol Biol 52, 274–303. https://doi.org/10.1080/10409238.2017.1291576
151. Violi, F., Marino, R., Milite, M. t., Loffredo, L., 1999. Nitric oxide and its role in lipid peroxidation. Diabetes/Metabolism Research and Reviews 15, 283–288. https://doi.org/10.1002/(SICI)1520-7560(199907/08)15:4<283::AID-DMRR42>3.0.CO;2-U
152. Wang, H., Wang, L., Xie, Z., Zhou, S., Li, Y., Zhou, Y., Sun, M., 2020. Nitric Oxide (NO) and NO Synthases (NOS)-Based Targeted Therapy for Colon Cancer. Cancers (Basel) 12, 1881. https://doi.org/10.3390/cancers12071881
153. Wu, A., Duan, T., Tang, D., Xu, Y., Feng, L., Zheng, Z., Zhu, J., Wang, R., Zhu, Q., 2013. Determination of Nitric Oxide-Derived Nitrite and Nitrate in Biological Samples by HPLC Coupled to Nitrite Oxidation. Chromatographia 76, 1649–1655. https://doi.org/10.1007/s10337-013-2529-0
154. Xie, C., Zhao, J., Hua, W., Tan, P., Chen, Y., Rui, J., Sun, X., Fan, J., Wei, X., Xu, X., Yang, X., 2019. Effect of XPC polymorphisms on the response to platinum-based chemotherapy: a meta-analysis. Onco Targets Ther 12, 3839–3848. https://doi.org/10.2147/OTT.S202617
155. Xie, X., Lin, S.H., Welsh, J.W., Wei, X., Jin, H., Mohan, R., Liao, Z., Xu, T., 2021. Radiation-induced lymphopenia during chemoradiation therapy for non-small cell lung cancer is linked with age, lung V5, and XRCC1 rs25487 genotypes in lymphocytes. Radiother Oncol 154, 187–193. https://doi.org/10.1016/j.radonc.2020.09.002
156. XPA XPA, DNA damage recognition and repair factor [Homo sapiens (human)] - Gene - NCBI [WWW Document], n.d. URL https://www.ncbi.nlm.nih.gov/gene/7507#summary (accessed 9.6.22).
157. XPC XPC complex subunit, DNA damage recognition and repair factor [Homo sapiens (human)] - Gene - NCBI [WWW Document], n.d. URL https://www.ncbi.nlm.nih.gov/gene/7508#summary (accessed 9.6.22).
158. XRCC1 X-ray repair cross complementing 1 [Homo sapiens (human)] - Gene - NCBI [WWW Document], n.d. URL https://www.ncbi.nlm.nih.gov/gene/7515#summary (accessed 9.6.22).
159. Yeo, C.T., Stancill, J.S., Oleson, B.J., Schnuck, J.K., Stafford, J.D., Naatz, A., Hansen, P.A., Corbett, J.A., 2021. Regulation of ATR-dependent DNA damage response by nitric oxide. Journal of Biological Chemistry 296. https://doi.org/10.1016/j.jbc.2021.100388
160. Yi, Y., El Khoudary, S.R., Buchanich, J.M., Miller, R.G., Rubinstein, D., Matthews, K., Orchard, T.J., Costacou, T., 2021. Women with Type 1 diabetes (T1D) experience a shorter reproductive period compared with nondiabetic women: the Pittsburgh Epidemiology of Diabetes Complications (EDC) study and the Study of Women's Health Across the Nation (SWAN). Menopause 28, 634–641. https://doi.org/10.1097/GME.0000000000001758
161. Yu, T., Xia, L., Bi, D., Wang, Yangong, Shang, Q., Zhu, D., Song, J., Wang, Yong, Wang, X., Zhu, C., Xing, Q., 2018. Association of NOS1 gene polymorphisms with cerebral palsy in a Han Chinese population: a case-control study. BMC Med Genomics 11, 56. https://doi.org/10.1186/s12920-018-0374-6

162. Yuan, M., Yu, C., Yu, K., 2020. Association of human XPA rs1800975 polymorphism and cancer susceptibility: an integrative analysis of 71 case-control studies. Cancer Cell Int 20, 164. https://doi.org/10.1186/s12935-020-01244-5
163. Zacca, E.R., Amezcua Vesely, M.C., Ferrero, P.V., Acosta, C.D.V., Ponce, N.E., Bossio, S.N., Mussano, E., Onetti, L., Cadile, I., Acosta Rodríguez, E.V., Montes, C.L., Gruppi, A., 2021. B cells from Patients with Rheumatoid Arthritis Show Conserved CD39-Mediated Regulatory Function and increased CD39 Expression After Positive Response to Therapy. J Mol Biol 433, 166687. https://doi.org/10.1016/j.jmb.2020.10.021
164. Zhang, G.-H., Ren, J.-C., Luo, M., Cui, J., Du, Y., Yang, D., Cui, S., Wang, X., Wu, W., Cao, J., Xia, Z.-L., 2019. Association of BER and NER pathway polymorphism haplotypes and micronucleus frequencies with global DNA methylation in benzene-exposed workers of China: Effects of DNA repair genes polymorphisms on genetic damage. Mutat Res Genet Toxicol Environ Mutagen 839, 13–20. https://doi.org/10.1016/j.mrgentox.2019.01.006
165. Zhao, J., Wu, J., Zuo, W., Kang, S., Li, Y., 2020. A functional polymorphism in the poly(ADP-ribose) polymerase-1 gene is associated with platinum-based chemotherapeutic response and prognosis in epithelial ovarian cancer patients. Eur J Obstet Gynecol Reprod Biol 255, 183–189. https://doi.org/10.1016/j.ejogrb.2020.10.021
166. Zhao, Z., 2019. Iron and oxidizing species in oxidative stress and Alzheimer's disease. Aging Med (Milton) 2, 82–87. https://doi.org/10.1002/agm2.12074
167. Zhou, R., Li, Y., Wang, N., Niu, C., Huang, X., Cao, S., Huo, X., 2021. PARP1 rs1136410 C/C genotype associated with an increased risk of esophageal cancer in smokers. Mol Biol Rep 48, 1485–1491. https://doi.org/10.1007/s11033-021-06169-4

APPENDIX A

Table A-1. MS patient gender associated with biochemical markers

Descriptor	Gender		Statistics	
	Female	**Male**	**P_T or MW***	**η**
DNA damage levels				
Lymphocytes				
Mean ± SD	70.78 ± 28.54	84.63 ± 15.33		
Interval (Min … max)	11 .. 132	60 .. 111		
CI 95% mean	56.59 .. 84.97	71.81 .. 97.44	0.38	0.18
Median with IQR	73 and 26.25	87.5 and 18.25		
Normal distribution	>0.05	>0.05		
Levels of NO				
Mean ± SD	70.78 ± 28.54	84.63 ± 15.33		
Interval (Min … max)	11 .. 132	60 .. 111		
CI 95% mean	56.59 .. 84.97	71.81 .. 97.44	0.17	0.35
Median with IQR	73 and 26.25	87.5 and 18.25		
Normal distribution	>0.05	>0.05		
Nitrate levels				
Plasma				
Mean ± SD	33.77 ± 17.59	33.47 ± 6.89		
Interval (Min … max)	11.04 .. 77.87	24.05 .. 44.73		
CI 95% mean	24.72 .. 42.81	27.71 .. 39.23	0.96	0.01
Median with IQR	27.26 and 22.17	33.01 and 10.95		
Normal distribution	>0.05	>0.05		
Serum				
Mean ± SD	35.42 ± 21.1	38.18 ± 14.74		
Interval (Min … max)	9.95 .. 72.11	19.54 .. 57.16		
CI 95% mean	24.57 .. 46.27	25.86 .. 50.51	0.74	0.07
Median with IQR	30.27 and 38.46	42.97 and 28.49		
Normal distribution	>0.05	>0.05		
Nitrite levels				
Plasma				
Mean ± SD	1.20 ± 0.29	1.00 ± 0.09		
Interval (Min … max)	0.89 .. 1.78	0.92 .. 1.14		
CI 95% mean	1.05 .. 1.34	0.93 .. 1.08	0.18	0.36
Median with IQR	1.06 and 0.48	0.97 and 0.18		

Normal distribution	<0.05	>0.05		
Serum				
Mean ± SD	0.88 ± 0.31	0.60 ± 0.13		
Interval (Min … max)	0.47 .. 1.5	0.5 .. 0.89		
CI 95% mean	0.72 .. 1.04	0.49 .. 0.71	**2.66×10^{-2}**	**0.46**
Median with IQR	0.93 and 0.51	0.56 and 0.14		
Normal distribution	>0.05	<0.05		
MDA levels				
Plasma				
Mean ± SD	3.95 ± 1.41	3.53 ± 1.51		
Interval (Min … max)	1.73 .. 6.47	1.85 .. 6.81		
CI 95% mean	3.05 .. 4.85	2.26 .. 4.79	0.53	0.15
Median with IQR	3.81 and 1.63	3.43 and 1.48		
Normal distribution	>0.05	>0.05		
Serum				
Mean ± SD	5.06 ± 1.19	4.78 ± 0.83		
Interval (Min … max)	3.35 .. 6.86	3.43 .. 5.61		
CI 95% mean	4.31 .. 5.82	4.09 .. 5.47	0.57	0.14
Median with IQR	4.88 and 2.27	4.96 and 1.56		
Normal distribution	>0.05	>0.05		

In gray – Mann-Whitney non-parametric test

Table A-2. MS patient age associated with biochemical markers

Parameter		Correlation statistics	
		ρ or r*	P_r
DNA damage	Lymphocytes	-0.12	0.55
Levels of NO		-0.26	0.23
Nitrate levels	Plasma	0.08	0.71
	Serum	*-0.37*	*0.066*
Nitrite levels	Plasma	-0.25	0.23
	Serum	-0.01	0.98
MDA levels	Plasma	0.26	0.27
	Serum	0.05	0.85

In gray – Spearman correlation test

Table A-3. Biochemical marker association with MS type

Descriptor	Disease type		Statistics	
	RR	**SP**	**P_T vai MW**	**η**
DNA damage levels				
Limfocītos				
Mean ± SD	62.25 ± 34.63	69.93 ± 36.43	0.59	0.11
Interval (Min … max)	8 .. 105	13 .. 134		
CI 95% mean	40.25 .. 84.25	48.89 .. 90.97		
Median with IQR	68.5 and 62	71 and 50.75		
Normal distribution	>0.05	>0.05		
Levels of NO				
Mean ± SD	33.07 ± 5.29	33.58 ± 6.23	0.84	0.05
Interval (Min … max)	27 .. 41.3	22.6 .. 46.3		
CI 95% mean	29 .. 37.13	29.81 .. 37.34		
Median with IQR	33.9 and 9.75	34.4 and 8.9		
Normal distribution	>0.05	>0.05		
Nitrate levels				
Plasma				
Mean ± SD	32.83 ± 17.76	34.33 ± 12.76	0.44	0.51
Interval (Min … max)	15.44 .. 77.87	11.04 .. 61.07		
CI 95% mean	20.9 .. 44.77	26.96 .. 41.69		
Median with IQR	27.26 and 18.71	32 and 17.26		
Normal distribution	<0.05	>0.05		
Serum				
Mean ± SD	34.82 ± 18.77	37.47 ± 19.84	0.74	0.07
Interval (Min … max)	11.82 .. 71.29	9.95 .. 72.11		
CI 95% mean	22.2 .. 47.43	26.02 .. 48.93		
Median with IQR	30.27 and 32.41	41.59 and 32.9		
Normal distribution	>0.05	>0.05		
Nitrite levels				
Plasma				
Mean ± SD	1.16 ± 0.3	1.11 ± 0.23	0.7	0.09
Interval (Min … max)	0.92 .. 1.78	0.89 .. 1.6		
CI 95% mean	0.96 .. 1.36	0.98 .. 1.25		
Median with IQR	1.01 and 0.42	1.03 and 0.38		
Normal distribution	<0.05	<0.05		
Serum				
Mean ± SD	0.89 ± 0.35	0.72 ± 0.24	0.25	0.29
Interval (Min … max)	0.47 .. 1.5	0.47 .. 1.15		

CI 95% mean	0.65 .. 1.12	0.58 .. 0.86		
Median with IQR	0.92 and 0.6	0.64 and 0.45		
Normal distribution	>0.05	<0.05		
MDA levels				
Plasma				
Mean ± SD	3.47 ± 1.48	3.99 ± 1.42		
Interval (Min … max)	1.73 .. 5.57	1.85 .. 6.81		
CI 95% mean	2.24 .. 4.71	3.08 .. 4.89	0.44	0.18
Median with IQR	3.37 and 3.05	3.49 and 1.04		
Normal distribution	>0.05	>0.05		
Serum				
Mean ± SD	4.56 ± 0.88	5.21 ± 1.1		
Interval (Min … max)	3.35 .. 5.61	3.43 .. 6.86		
CI 95% mean	3.82 .. 5.3	4.51 .. 5.91	0.18	0.31
Median with IQR	4.39 and 1.7	5.09 and 1.62		
Normal distribution	>0.05	>0.05		

In gray – Mann-Whitney non-parametric test

Table A-4. Biochemical marker association with disease duration

Parameter		Correlation statistics	
		ρ	P_r
DNA damage	Lymphocytes	0.24	0.24
Levels of NO		-0.01	0.97
Nitrate levels	Plasma	0.13	0.55
	Serum	-0.1	0.64
Nitrite levels	Plasma	-0.12	0.56
	Serum	-0.16	0.45
MDA levels	Plasma	0.11	0.63
	Serum	0.09	0.7

Table A-4. Biochemical marker association with MS patient EDSS score

Parameter		Correlation statistics	
		ρ or r*	P_r
DNA damage	Lymphocytes	0	0.99
Levels of NO		0.07	0.75
Nitrate levels	Plasma	0.31	0.13
	Serum	0.25	0.22
Nitrite levels	Plasma	-0.19	0.36
	Serum	**-0.41**	**4.45 x10^{-2}**
MDA levels	Plasma	0.12	0.61
	Serum	0.34	0.15

In gray – Spearman correlation test

Table A-5. Biochemical marker association with DMTs

Descriptor	**DMT in 2018**		**Statistics**	
	Yes	**No**	**$P_{T\ vai\ MV}$***	**η**
DNA damage levels				
Lymphocytes				
Mean ± SD	68.25 ± 30.07	65.56 ± 37.93		
Interval (Min … max)	22 .. 105	8 .. 134		
CI 95% mean	43.11 .. 93.39	46.69 .. 84.42	0.86	0.04
Median with IQR	61.5 and 52.5	80 and 53.75		
Normal distribution	>0.05	>0.05		
Levels of NO				
Mean ± SD	32.26 ± 6.51	33.69 ± 5.66		
Interval (Min … max)	22.6 .. 39.7	27 .. 46.3		
CI 95% mean	24.17 .. 40.35	30.78 .. 36.61	0.64	0.11
Median with IQR	34.7 and 11.3	33.9 and 9.45		
Normal distribution	>0.05	>0.05		
Nitrate levels				
Plasma				
Mean ± SD	37.99 ± 12.38	31.99 ± 15.69		
Interval (Min … max)	21.48 .. 61.07	11.04 .. 77.87	0.23	0.19
CI 95% mean	26.54 .. 49.44	24.19 .. 39.79		

Median with IQR	36.15 and 13.12	27.2 and 17.9		
Normal distribution	>0.05	<0.05		
Serum				
Mean ± SD	30.87 ± 19.07	38.42 ± 19.12		
Interval (Min … max)	9.95 .. 64.13	11.82 .. 72.11		
CI 95% mean	13.24 .. 48.51	28.91 .. 47.93	0.38	0.18
Median with IQR	25.12 and 31.58	35.95 and 33.71		
Normal distribution	>0.05	>0.05		
Nitrite levels				
Plasma				
Mean ± SD	1.07 ± 0.23	1.16 ± 0.27		
Interval (Min … max)	0.89 .. 1.4	0.92 .. 1.78		
CI 95% mean	0.86 .. 1.28	1.02 .. 1.29	0.15	0.15
Median with IQR	0.92 and 0.47	1.04 and 0.36		
Normal distribution	<0.05	<0.05		
Serum				
Mean ± SD	0.7 ± 0.25	0.83 ± 0.31		
Interval (Min … max)	0.47 .. 1.15	0.47 .. 1.5		
CI 95% mean	0.47 .. 0.94	0.67 .. 0.98	0.36	0.19
Median with IQR	0.64 and 0.43	0.81 and 0.52		
Normal distribution	>0.05	>0.05		
MDA levels				
Plasma				
Mean ± SD	3.7 ± 1.78	3.81 ± 1.36		
Interval (Min … max)	1.75 .. 6.47	1.73 .. 6.81		
CI 95% mean	1.49 .. 5.91	3.05 .. 4.56	0.88	0.04
Median with IQR	3.46 and 3.05	3.44 and 1.21		
Normal distribution	>0.05	>0.05		
Serum				
Mean ± SD	4.86 ± 1.26	4.98 ± 1.01		
Interval (Min … max)	3.63 .. 6.74	3.35 .. 6.86		
CI 95% mean	3.3 .. 6.42	4.42 .. 5.54	0.84	0.05
Median with IQR	5.04 and 2.23	4.87 and 1.31		
Normal distribution	>0.05	>0.05		

In gray – Mann-Whitney non-parametric test

APPENDIX B

Table B-1. DNA damage in lymphocytes association with SNP genotypes

SNP genotypes	N (%)	Parameters									Statistics
		Mean	SD	Min	Max	CI 95%		Median	IQR	P_N^	P*/ η&
*ATM rs189037 G>**A***											
AA	9 (34.62)	68.11	35.5	13	134	40.81	95.42	61	46.5	>0.05	
AG	10 (38.46)	65.1	41.3	8	130	35.53	94.67	65.5	78.8	>0.05	0.99
GG	7 (26.92)	66	29.8	12	90	38.47	93.53	82	48	>0.05	
*PARP1 rs1136410 **A**>G*											
AA	17 (65.38)	71	38.3	8	134	51.29	90.71	82	56.5	>0.05	
AG	7 (26.92)	52.43	28.9	13	81	25.7	79.16	51	59	>0.05	0.31
GG	2 (7.69)	76	19.8	62	90	-101.9	253.9	76	0	<0.05	
PARP1 rs3219090 C>T											
CC	9 (34.62)	52.56	45.7	8	130	17.45	87.66	41	87	>0.05	
CT	11 (42.31)	67	25.6	21	105	49.82	84.18	80	40	>0.05	0.2
TT	6 (23.08)	86	26.7	61	134	57.97	114	84.5	39.3	>0.05	
*XPA rs1800975 T>**C***											
CC	14 (53.85)	58.64	38.1	8	134	36.67	80.62	55	68	>0.05	
CT	10 (38.46)	72.5	32.4	22	130	49.29	95.71	71.5	44.8	>0.05	0.37
TT	2 (7.69)	90	14.1	80	100	-37.06	217.1	90	0	<0.05	
*XPC rs2228001 G>**T***											
TT	8 (30.77)	73.88	42.8	8	134	38.12	109.6	83	73.3	>0.05	
TG	14 (53.85)	67.86	34.9	12	130	47.69	88.03	80.5	53.3	>0.05	0.44
GG	4 (15.38)	46.25	4.65	40	51	38.86	53.64	47	8.75	>0.05	
XRCC1 rs1799782 G>A											
GG	21 (80.77)	66.19	38	8	134	48.91	83.47	62	63	>0.05	
GA	5 (19.23)	67.2	22.5	40	89	39.31	95.09	80	42	>0.05	0.96
AA											
*XRCC1 rs25487 T>**C***											
CC	4 (15.38)	52	24.9	21	80	12.36	91.64	53.5	48	>0.05	
CT	15 (57.69)	54.93	31.8	8	99	37.34	72.53	51	64	>0.05	**9.28×10^{-3} / 0.50**
TT	7 (26.92)	99.14	27.5	56	134	73.72	124.6	100	50	>0.05	

In gray – data not following normal distribution, thus Kruskal-Wallis test was used

Table B-2. Levels of NO association with SNP genotypes

SNP genotypes	N (%)	Parameters									Statistics
		Mean	SD	Min	Max	CI 95%		Median	IQR	P_N^	P*/ η&
*ATM rs189037 G>**A***											
AA	8 (36.36)	30.84	7.29	23	46.3	24.74	36.93	28.55	7.28	>0.05	
AG	7 (31.82)	35.41	4.52	29	39.7	31.23	39.6	37.2	9.5	>0.05	0.27
GG	7 (31.82)	34.21	4.29	28	41.3	30.25	38.18	34.4	6.4	>0.05	
*PARP1 rs1136410 **A**>G*											
AA	15 (68.18)	33.62	5.53	23	41.3	30.56	36.68	34.9	10	>0.05	
AG	5 (22.73)	33.42	7.61	28	46.3	23.97	42.87	29.3	11.8	>0.05	0.64
GG	2 (9.09)	31.35	4.74	28	34.7	-11.22	73.92	31.35	0	<0.05	
PARP1 rs3219090 C>T											
CC	7 (31.82)	35.64	4.99	29	41.3	31.03	40.26	37.2	10.4	>0.05	
CT	9 (40.91)	32.79	6.09	27	46.3	28.1	37.47	30.4	7.65	>0.05	0.43
TT	6 (27.27)	31.58	6.09	23	38.9	25.19	37.98	31.85	10.3	>0.05	
*XPA rs1800975 T>**C***											
CC	13 (61.9)	34.76	5.83	28	46.3	31.24	38.28	34.7	10.2	>0.05	
CT	8 (38.1)	31.65	5.55	23	38.9	27.01	36.29	32.15	9.3	>0.05	0.24
TT											
*XPC rs2228001 G>**T***											
TT	6 (27.27)	33.8	4.71	27	38.8	28.86	38.74	35.6	8.8	>0.05	
TG	13 (59.09)	34.22	6.5	23	46.3	30.29	38.14	34.4	10.6	>0.05	0.35
GG	3 (13.64)	28.83	0.55	28	29.4	27.47	30.2	28.8	0	>0.05	
XRCC1 rs1799782 G>A											
GG	17 (77.27)	33.42	5.33	23	41.3	30.68	36.16	34.7	9.1	>0.05	
GA	5 (22.73)	33.2	7.69	28	46.3	23.65	42.75	29.4	11.9	<0.05	0.86
AA											
*XRCC1 rs25487 T>**C***											
CC	3 (13.64)	27	3.82	23	29.4	17.52	36.48	29	0	>0.05	
CT	13 (59.09)	33.65	5.04	28	41.3	30.61	36.7	34.4	10.3	>0.05	*0.079 / 0.58*
TT	6 (27.27)	35.93	6.23	27	46.3	29.39	42.47	35.6	7.3	>0.05	

In gray – data not following normal distribution, thus Kruskal-Wallis test was used

Table B-3. SNP genotype association with plasma nitrate levels

SNP genotypes	N (%)	Parameters									Statistics
		Mean	SD	Min	Max	CI 95%		Median	IQR	P_N^	P*/ η&
*ATM rs189037 G>**A***											
AA	8 (32)	28.38	9.32	15	44.7	20.58	36.17	25.6	13	>0.05	
AG	10 (40)	35.25	15.8	11	61.1	23.96	46.55	35.09	26.1	>0.05	0.44
GG	7 (28)	37.46	18.6	24	77.9	20.23	54.69	30.06	12.8	<0.05	
*PARP1 rs1136410 **A**>G*											
AA	16 (64)	32.49	11.6	19	61.1	26.28	38.69	29.98	15.3	>0.05	
AG	7 (28)	29.71	13.9	11	45.1	16.86	42.56	27.14	29.3	>0.05	0.27
GG	2 (8)	57.01	29.5	36	77.9	-208	322.1	57.01	0	<0.05	
PARP1 rs3219090 C>T											
CC	8 (32)	35.17	15.5	19	61.1	22.24	48.1	28.61	26.7	>0.05	
CT	11 (44)	31.57	9.83	15	45.1	24.97	38.18	30.06	17.9	>0.05	0.83
TT	6 (24)	35.52	22.6	11	77.9	11.78	59.25	32	25.8	>0.05	
*XPA rs1800975 T>**C***											
CC	14 (58.33)	33.36	15.8	15	77.9	24.22	42.5	28.61	19.6	<0.05	
CT	10 (41.67)	36.37	12.7	21	61.1	27.32	45.42	35.02	17.5	>0.05	0.52
TT											
*XPC rs2228001 G>**T***											
TT	7 (28)	26.94	16.1	11	61.1	12.04	41.84	22.32	11.5	<0.05	
TG	14 (56)	36.47	15.3	15	77.9	27.62	45.32	32	17.7	>0.05	0.14
GG	4 (16)	35.65	8.73	23	43.1	21.75	49.54	38.11	15.9	>0.05	
*XRCC1 rs1799782 **G**>A*											
GG	20 (80)	34.02	15.9	11	77.9	26.6	41.44	29.98	20.1	<0.05	
GA	5 (20)	32.27	11.1	15	43.1	18.45	46.09	36.03	20.1	>0.05	*0.062 / 0.048*
AA											
*XRCC1 rs25487 T>**C***											
CC	4 (16)	33.29	15.6	11	45.1	8.48	58.11	38.54	27.8	>0.05	
CT	15 (60)	34.79	16.4	15	77.9	25.73	43.84	29.99	15.8	<0.05	0.75
TT	6 (24)	31.13	12.3	21	52.1	18.27	43.99	25.6	20.7	>0.05	

In gray – data not following normal distribution, thus Kruskal-Wallis test was used

Table B-4. SNP genotype association with serum nitrate levels

SNP genotypes	N (%)	Parameters									Statistics
		Mean	SD	Min	Max	CI 95%		Median	IQR	P_N^	P*/ η&
*ATM rs189037 G>**A***											
AA	8 (32)	28.04	17.2	12	57.2	13.7	42.39	19.54	29.9	>0.05	
AG	10 (40)	35.87	15.5	10	64.1	24.81	46.93	33.49	22.3	>0.05	0.18
GG	7 (28)	46.36	23.2	17	72.1	24.95	67.78	51.95	49.7	>0.05	
*PARP1 rs1136410 **A**>G*											
AA	16 (64)	32.82	17.5	10	64.1	23.48	42.17	31.06	31.2	>0.05	
AG	7 (28)	41.37	19.4	16	72.1	23.42	59.31	43.12	32	>0.05	0.52
GG	2 (8)	46.43	35.2	22	71.3	-269.5	362.3	46.43	0	<0.05	
PARP1 rs3219090 C>T											
CC	8 (32)	44.03	19.3	12	72.1	27.88	60.18	45.97	30	>0.05	
CT	11 (44)	32.93	17.5	10	60	21.21	44.66	30.13	34.6	>0.05	0.39
TT	6 (24)	32.18	21.5	14	71.3	9.57	54.79	22.41	31.9	>0.05	
*XPA rs1800975 T>**C***											
CC	14 (58.33)	37.39	21.4	10	72.1	25.01	49.77	31.06	39.3	>0.05	
CT	10 (41.67)	34.1	17	14	64.1	21.94	46.25	30.13	31.6	>0.05	0.69
TT											
*XPC rs2228001 G>**T***											
TT	7 (28)	39.04	17.9	20	64.1	22.53	55.56	35.13	40.5	>0.05	
TG	14 (56)	39.1	20	14	72.1	27.57	50.62	38.08	32.7	>0.05	0.26
GG	4 (16)	21.74	14	10	40.1	-0.47	43.94	18.47	25.9	>0.05	
XRCC1 rs1799782 G>A											
GG	20 (80)	36.63	19	12	72.1	27.72	45.53	31.06	29.1	>0.05	
GA	5 (20)	35	21.2	10	57.2	8.68	61.32	40.05	41.6	>0.05	0.87
AA											
*XRCC1 rs25487 T>**C***											
CC	4 (16)	24.38	15.2	10	43.1	0.18	48.58	22.22	28.8	>0.05	
CT	15 (60)	38.44	20.6	12	72.1	27.05	49.83	31.84	38.4	>0.05	0.41
TT	6 (24)	38.91	16.7	20	57.2	21.39	56.43	42.63	33.7	>0.05	

Table B-5. SNP genotype association with plasma nitrite levels

SNP genotypes	N (%)	Parameters									Statistics
		Mean	SD	Min	Max	CI 95%		Median	IQR	P_N^	P*/ η&
*ATM rs189037 G>**A***											
AA	8 (32)	1.08	0.29	0.9	1.78	0.84	1.33	0.99	0.18	<0.05	
AG	10 (40)	1.16	0.25	0.9	1.6	0.99	1.34	1.12	0.47	>0.05	0.77
GG	7 (28)	1.15	0.27	0.9	1.6	0.9	1.4	1.06	0.53	<0.05	
*PARP1 rs1136410 **A**>G*											
AA	16 (64)	1.06	0.24	0.9	1.78	0.93	1.19	0.96	0.19	<0.05	
AG	7 (28)	1.24	0.24	1	1.6	1.02	1.47	1.14	0.47	>0.05	**4.58 x10^{-2} / 0.40**
GG	2 (8)	1.33	0.38	1.1	1.6	0	4.76	1.33	0	<0.05	
PARP1 rs3219090 C>T											
CC	8 (32)	1.15	0.21	0.9	1.47	0.97	1.32	1.08	0.38	>0.05	
CT	11 (44)	1.09	0.27	0.9	1.78	0.9	1.27	0.98	0.2	<0.05	0.48
TT	6 (24)	1.21	0.32	0.9	1.6	0.87	1.54	1.09	0.67	>0.05	
*XPA rs1800975 T>**C***											
CC	14 (58.33)	1.08	0.21	0.9	1.6	0.96	1.2	1.01	0.16	<0.05	
CT	10 (41.67)	1.16	0.3	0.9	1.78	0.95	1.37	1.03	0.47	<0.05	0.98
TT											
*XPC rs2228001 G>**T***											
TT	7 (28)	1.24	0.35	0.9	1.78	0.91	1.56	1.06	0.67	>0.05	
TG	14 (56)	1.11	0.21	0.9	1.6	0.98	1.23	1.04	0.24	<0.05	0.58
GG	4 (16)	1.05	0.24	0.9	1.4	0.68	1.43	0.96	0.4	>0.05	
XRCC1 rs1799782 G>A											
GG	20 (80)	1.18	0.27	0.9	1.78	1.06	1.31	1.09	0.45	<0.05	
GA	5 (20)	0.94	0.05	0.9	1	0.89	1	0.93	0.09	>0.05	0.6
AA											
*XRCC1 rs25487 T>**C***											
CC	4 (16)	1.13	0.33	0.9	1.6	0.61	1.65	1.02	0.58	>0.05	
CT	15 (60)	1.13	0.22	0.9	1.6	1.01	1.26	1.06	0.41	<0.05	0.67
TT	6 (24)	1.14	0.34	0.9	1.78	0.78	1.5	0.97	0.49	<0.05	

In gray – data not following normal distribution, thus Kruskal-Wallis test was used

Table B-6. SNP genotype association with serum nitrite levels

SNP genotypes	N (%)	Parameters								Statistics	
		Mean	SD	Min	Max	CI 95%		Median	IQR	P_N^	P*/ η&
*ATM rs189037 G>**A***											
AA	8 (32)	0.91	0.4	0.5	1.5	0.58	1.24	0.81	0.8	>0.05	
AG	10 (40)	0.75	0.24	0.5	1.11	0.58	0.92	0.68	0.48	>0.05	0.42
GG	7 (28)	0.72	0.24	0.5	1.05	0.5	0.94	0.64	0.42	>0.05	
*PARP1 rs1136410 **A**>G*											
AA	16 (64)	0.79	0.3	0.5	1.5	0.63	0.95	0.68	0.51	>0.05	
AG	7 (28)	0.8	0.35	0.5	1.39	0.48	1.12	0.72	0.52	>0.05	0.97
GG	2 (8)	0.78	0.2	0.6	0.92	-1	2.56	0.78	0	<0.05	
PARP1 rs3219090 C>T											
CC	8 (32)	0.72	0.38	0.5	1.5	0.4	1.04	0.52	0.49	<0.05	
CT	11 (44)	0.8	0.29	0.5	1.39	0.61	0.99	0.72	0.48	>0.05	0.33
TT	6 (24)	0.88	0.2	0.6	1.15	0.66	1.09	0.91	0.41	>0.05	
*XPA rs1800975 T>**C***											
CC	14 (58.33)	0.84	0.34	0.5	1.5	0.65	1.04	0.91	0.51	>0.05	
CT	10 (41.67)	0.7	0.23	0.5	1.15	0.54	0.86	0.64	0.29	<0.05	0.56
TT											
*XPC rs2228001 G>**T***											
TT	7 (28)	0.81	0.25	0.5	1.11	0.58	1.04	0.89	0.5	>0.05	
TG	14 (56)	0.74	0.3	0.5	1.39	0.57	0.92	0.64	0.5	<0.05	0.5
GG	4 (16)	0.94	0.4	0.6	1.5	0.3	1.57	0.83	0.73	>0.05	
XRCC1 rs1799782 G>A											
GG	20 (80)	0.79	0.28	0.5	1.5	0.66	0.93	0.72	0.5	>0.05	
GA	5 (20)	0.79	0.38	0.5	1.39	0.31	1.26	0.6	0.66	>0.05	0.96
AA											
*XRCC1 rs25487 T>**C***											
CC	4 (16)	1.02	0.09	0.9	1.15	0.87	1.17	1.01	0.17	>0.05	
CT	15 (60)	0.8	0.33	0.5	1.5	0.62	0.99	0.64	0.54	<0.05	**4.95×10^{-2} / 0.43**
TT	6 (24)	0.62	0.16	0.5	0.89	0.45	0.79	0.57	0.27	>0.05	

In gray – data not following normal distribution, thus Kruskal-Wallis test was used

Table B-7. SNP genotype association with plasma MDA levels

SNP genotypes	N (%)	Parameters									Statistics
		Mean	SD	Min	Max	CI 95%		Median	IQR	P_N^	P*/ η&
*ATM rs189037 G>**A***											
AA	8 (40)	4.32	1.7	1.9	6.81	2.9	5.74	3.78	2.78	>0.05	
AG	6 (30)	3.32	0.98	1.8	4.45	2.3	4.35	3.47	1.71	>0.05	0.4
GG	6 (30)	3.52	1.4	1.7	5.57	2.05	4.98	3.43	2.57	>0.05	
*PARP1 rs1136410 **A**>G*											
AA	14 (73.68)	3.99	1.61	1.7	6.81	3.06	4.92	3.77	2.61	>0.05	
AG	5 (26.32)	3.26	0.84	1.9	4.12	2.21	4.3	3.4	1.2	>0.05	0.35
GG											
PARP1 rs3219090 C>T											
CC	6 (30)	3.59	1.24	1.7	5.13	2.29	4.89	3.76	2.16	>0.05	
CT	9 (45)	3.75	1.7	1.8	6.81	2.44	5.06	3.4	2.94	>0.05	0.76
TT	5 (25)	4.06	1.35	3.4	6.47	2.39	5.73	3.46	1.57	<0.05	
*XPA rs1800975 T>**C***											
CC	12 (63.16)	3.61	1.17	1.7	5.57	2.87	4.35	3.45	1.49	>0.05	
CT	7 (36.84)	4.1	1.94	1.8	6.81	2.31	5.9	3.41	4.07	>0.05	0.5
TT											
*XPC rs2228001 G>**T***											
TT	6 (30)	3.68	1.27	1.8	5.57	2.34	5.01	3.48	1.79	>0.05	
TG	11 (55)	3.41	1.34	1.7	6.47	2.51	4.31	3.4	1.72	>0.05	0.11
GG	3 (15)	5.34	1.37	4.1	6.81	1.93	8.75	5.13	0	>0.05	
XRCC1 rs1799782 G>A											
GG	15 (75)	3.8	1.3	1.7	6.47	3.08	4.52	3.46	1.21	>0.05	
GA	5 (25)	3.71	1.94	1.9	6.81	1.3	6.12	3.4	3.33	>0.05	0.9
AA											
*XRCC1 rs25487 T>**C***											
CC	3 (15)	4.69	1.56	3.5	6.47	0.81	8.58	4.09	0	>0.05	
CT	12 (60)	4.06	1.36	1.7	6.81	3.2	4.92	3.79	1.59	>0.05	*0.059 / 0.53*
TT	5 (25)	2.56	0.8	1.8	3.44	1.56	3.55	2.4	1.59	>0.05	

In gray – data not following normal distribution, thus Kruskal-Wallis test was used

Table B-8. SNP genotype association with serum MDA levels

SNP genotypes	N (%)	Parameters									Statistics
		Mean	SD	Min	Max	CI 95%		Median	IQR	$P_N^{\wedge}$	P*/ η&
*ATM rs189037 G>**A***											
AA	8 (40)	4.73	0.7	3.4	5.54	4.14	5.31	4.85	0.97	>0.05	
AG	6 (30)	4.68	1.53	3.4	6.74	3.07	6.28	3.87	3.01	<0.05	0.19
GG	6 (30)	5.53	0.75	4.6	6.86	4.74	6.32	5.52	0.99	>0.05	
*PARP1 rs1136410 **A**>G*											
AA	14 (73.68)	4.71	1	3.4	6.74	4.14	5.29	4.75	1.77	>0.05	
AG	5 (26.32)	5.6	1.11	4.2	6.86	4.22	6.98	5.54	2.18	>0.05	0.12
GG											
PARP1 rs3219090 C>T											
CC	6 (30)	4.69	1.33	3.4	6.86	3.29	6.08	4.39	2.28	>0.05	
CT	9 (45)	5.1	0.9	3.8	6.74	4.41	5.79	5.32	1.19	>0.05	0.77
TT	5 (25)	5	1.1	3.4	6.54	3.63	6.37	5.04	1.69	>0.05	
*XPA rs1800975 T>**C***											
CC	12 (63.16)	5.01	1.11	3.4	6.86	4.3	5.71	4.96	1.52	>0.05	
CT	7 (36.84)	4.63	0.8	3.4	5.61	3.89	5.37	4.62	1.54	>0.05	0.45
TT											
*XPC rs2228001 G>**T***											
TT	6 (30)	4.87	1.04	3.8	6.54	3.78	5.96	4.71	1.88	>0.05	
TG	11 (55)	4.95	0.97	3.4	6.86	4.29	5.6	5.04	1.31	>0.05	0.94
GG	3 (15)	5.14	1.7	3.4	6.74	0.91	9.37	5.32	0	>0.05	
XRCC1 rs1799782 G>A											
GG	15 (75)	4.77	1.06	3.4	6.86	4.19	5.36	4.82	1.72	>0.05	
GA	5 (25)	5.49	0.89	4.2	6.74	4.38	6.6	5.54	1.4	>0.05	0.19
AA											
*XRCC1 rs25487 T>**C***											
CC	3 (15)	6.14	0.88	5.1	6.74	3.96	8.32	6.54	0	>0.05	*0.093 / 0.49*
CT	12 (60)	4.69	1.04	3.4	6.86	4.03	5.35	4.72	1.75	>0.05	
TT	5 (25)	4.87	0.76	3.8	5.61	3.93	5.81	4.87	1.42	>0.05	

In gray – data not following normal distribution, thus Kruskal-Wallis test was used